Investigating excitatory GABAergic signalling & benzodiazepine resistance in an *in vitro* model of status epilepticus

Richard J. Burman

BRMRIC001

A thesis presented for the degree of

Masters of Medical Science in Medical Biochemistry

Supervisor:

Dr Joseph V. Raimondo

Department of Human Biology

Co-supervisor:

Professor Arieh A. Katz

Department of Integrated Biomedical Sciences

November 2017

Plagiarism declaration

I, **Richard Joseph Burman**, hereby declare that the work in this thesis is my original work (except where acknowledgements indicate otherwise). I know what plagiarism entails and that it is a punishable offence because it constitutes theft. I understand the plagiarism policy of the University of Cape Town and the consequences if I am seen to plagiarise any part of this thesis.

I declare, therefore, that all work presented by me in this thesis is my own, and where I have made use of another's work, I have referenced accordingly using the **Harvard** referencing convention.

Signed by candidate

signature removed

3 November 2017

Signature **Date**

Abstract

Status epilepticus (SE) describes a state of persistent seizures which are unrelenting. First-line treatment for status epilepticus uses a group of drugs, the benzodiazepines, that promote the action of the major inhibitory neurotransmitter within the brain, gamma (γ)-aminobutyric acid (GABA). In a subset of patients however, benzodiazepines prove to be ineffective in terminating SE.

Previous data from *in vitro* models has demonstrated that during single seizures, instead of being inhibitory, activation of the $GABA_A$ receptor can have an excitatory effect on neurons. To date, it is unknown whether this shift in GABAergic function contributes to SE, nor how it may modulate the anticonvulsant properties of benzodiazepines. In this thesis I explore the role of excitatory GABAergic signaling in an *in vitro* model of SE and how this may affect the anticonvulsant efficacy of the benzodiazepine, diazepam.

Firstly, I confirm that benzodiazepine-resistant SE is prevalent in a South African paediatric population. Secondly, consistent with its established mechanism of action, I show that diazepam enhances $GABA_AR$ synaptic currents. Thirdly, using the *in vitro* 0 Mg^{2+} model of status epilepticus I show that whilst early application of diazepam has anticonvulsant properties, this is lost when the drug is applied during prolonged epileptiform activity. Fourthly, to investigate this phenomenon I use optogenetic activation of GABAergic interneurons to show that interneurons can drive epileptiform discharges during SE-like activity *in vitro*. Finally, I confirm that during seizure-like events there is a transient shift in GABAergic signaling that is caused by activity driven changes in the transmembrane Cl^- gradient.

This thesis provides insight into how excitatory GABAergic signaling during prolonged seizures may contribute towards benzodiazepine resistance in SE. I believe that these results are relevant for understanding of the pathophysiology of SE and may help inform optimal treatment protocols for this condition.

Acknowledgements

To my supervisor, Joe Raimondo, you have been incredible. Thank you for sharing your passion for neuroscience with me, for always having an open door and above all, for believing in me. You have enriched my life in so many wonderful ways and through it all you have been a constant source of inspiration. Thank you.

To my co-supervisor, Arieh Katz, thank you for your selfless work in creating a platform for medical students to engage with science. Your dedication to students is unparalleled.

To my mentors, Jo Wilmshurst and Graham Fieggen, thank you for being so generous with your time and for always being there to support me.

To Andy Trevelyan and Colin Akerman, thank you for your invaluable input into this project over the years.

To my fellow Raimondo Lab minions, thank you for always making the lab such a happy place.

To Hayley, it has been such a privilege sharing this adventure with you right from the start. Thank you for being the loving person that you are.

To my dear friends, thank you all for being such wonderful cheerleaders.

To my clinical partner, Dave, thank you for your patience and for always having my back. It has been a pleasure spending my clinical years with you.

Für meine liebe Anna. Auch wenn du erst gegen Ende zu mir gestossen bist, warst du umso wichtiger, um mich über diese Ziellinie zu bringen.

And finally to my beloved family. Mum, Dad and Greg, you have each played such a significant part in this journey. None of what I have been able to achieve would have been possible without you. I love you all very much.

Mum,

I dedicate this to you.

Contents

List of Figures

Chapter 1

Introduction

1.1 GABAergic signalling: the principal player in fast synaptic inhibition

1.1.1 Normal neuronal signalling: a balance between excitation and inhibition

The sophisticated processing ability of the brain depends on the coordinated electrical activity of neurons. Communication between neurons is made possible by a tightly regulated ionic environment that produces the necessary electrochemical gradients to facilitate synaptic signalling (Johnston and Wu, 1995).

Communication between different brain cells largely, but not exclusively, occurs at the synaptic junction (Shepherd, 2003). Here, the interaction between neurotransmitters and their specific receptors directs the flow of electrical charge. These seceptors on the postsynaptic membrane are linked to specific ion channels. When activated, these channels open and permit a movement of charge that causes both positive and negative shifts in the neuronal membrane potential.

Signals that precipitate membrane depolarisation, bringing it closer to the action potential threshold, are termed excitatory. These are matched by inhibitory synaptic inputs that cause membrane hyperpolarisation and thereby impede action potential generation. A broad equilibrium between excitation and inhibition is critical to produce the asynchronous firing patterns that underlie normal network function. However, under certain conditions this state can can be disrupted. The consequence of this is either uncontrolled excitation or prolonged inactivity, which are both dysfunctional.

1.1.2 The inhibitory network

The stability of neural networks is maintained by the inhibitory action of neurons loosely termed inhibitory interneurons (Markram et al., 2004). The essential role of inhibitory interneurons is evident in both their diversity and strategic positioning throughout the brain. There is a large variety of these cells, each type with their own morphology, firing pattern and distribution of synaptic contacts onto pyramidal cells.

At inhibitory synapses, inhibition is mediated by the presynaptic release of one of two neurotransmitters: gamma (γ)-amino butyric acid (GABA) or glycine (Bowery and Smart, 2006). GABA is the principal neurotransmitter which mediates fast synaptic inhibition within the mature central nervous system (CNS) and will be the focus of my thesis (Krnjević, 1974).

1.1.3 Fast synaptic inhibition is mediated by the $GABA_A$ receptor

GABA is produced within the presynaptic terminal of what are referred to as GABAergic interneurons, the major class of inhibitory interneurons. Interestingly, GABA's biosynthesis originates from the principal excitatory neurotransmitter, glutamate, a reaction catalysed by the enzyme glutamate decarboxylase (Bak et al., 2006). The inhibitory effects of GABA are generated through its binding to either $GABA_A$, $GABA_B$ or $GABA_C$ receptors ($GABA_A$Rs, $GABA_B$Rs and $GABA_C$Rs) (Bormann, 2000). The distribution of these different GABA receptors is responsible for synaptic inhibition across various spatial and temporal contexts. Here I will specifically focus on the role of the $GABA_A$R in fast synaptic inhibition.

The $GABA_A$R is a ligand-activated, ionotropic receptor (Olsen and Sieghart, 2009). It is largely, but not exclusively, expressed on the postsynaptic membrane. Its structure consists of a pentameric channel that is formed by different permutations of constitutive subunits. The different subunits are separated into classes according to their varied amino acid composition (α, β, γ, δ, ϵ, π, θ). Furthermore, some of these can be sub-classified into different isoforms ($\alpha_{1\text{-}6}$, $\beta_{1\text{-}3}$, $\gamma_{1\text{-}3}$). It is the multiplicity of subunit classes and isoforms that ultimately determines the biophysical properties of the channel including its ligand binding capacity and conductance. The most commonly expressed form of $GABA_A$R pentamer includes the following combination: α_1-β_2-γ_2-α_1-β_2. This is further illustrated in Figure 1.1.

The $GABA_A$R is activated by the binding of GABA at sites located between the α_1 and β_2 subunits. This induces a conformational change in the pentameric channel to make it selectively permeable to Cl^- influx and, to a lesser extent, bicarbonate (HCO_3^-) efflux (Kaila and Voipio, 1987; Kaila, 1994). Cl^- and HCO_3^- efflux occur at the same time at an estimated ratio of 4:1 (Kaila and Voipio, 1987; Kaila et al., 1989; Kaila,

1994). However, Cl^- is predominant and because Cl^- moves down its transmembrane electrochemical gradient, under typical conditions there is an inward movement of negative charge. This hyperpolarises the neuronal membrane and is referred to as an inhibitory postsynaptic potential (IPSP).

The function of the $GABA_AR$ can be enhanced or impeded using various pharmacological manipulations (Krogsgaard-Larsen et al., 1994; Olsen and Sieghart, 2009). $GABA_ARs$ can be activated by agonists such as isoguvacine and muscimol. $GABA_AR$ function can also be blocked by antagonists such as bicucullin and picrotoxin. Furthermore, there are a growing selection of $GABA_AR$ positive allosteric modulators, such as the benzodiazepines, that are able to enhance the $GABA_AR$ conductance.

Figure 1.1 ***(following page)*:** The $GABA_AR$ is selectively permeable to Cl^- and HCO_3^-. **A**, The $GABA_AR$ is a pentameric channel that is expressed on the neuronal membrane. It is formed from different combinations of subunits and is selectively permeable to both Cl^- and HCO_3^- ions. The most common configuration is α_1-β_2-γ_2-α_1-β_2. The channel is activated by the binding of the neurotransmitter, γ-amino butyric acid (GABA, blue), at the junction between α_1 and β_2 subunits. The channel is then opened and allows for Cl^- (green) and HCO_3^- (orange) flux down their respective electrochemical gradients in a ratio of 4:1. The benzodiazepines (red) are a class of $GABA_AR$ allosteric modulators that bind onto the $GABA_AR$ at the junction of its γ and α subunits. Under baseline conditions there is typically a low intracellular concentration of Cl^- ($[Cl^-]_i$). **B**, When $GABA_ARs$ are activated, the predominant flux of ions is Cl^- movement down its electrochemical gradient into the cell. This influx of negative charge causes a membrane hyperpolarisation. **C**, Benzodiazepines broadly increase the conductance of the $GABA_ARs$ by increasing the frequency at which the $GABA_AR$ opens. This increases the amplitude and duration of the inhibitory postsynaptic potential (IPSP).

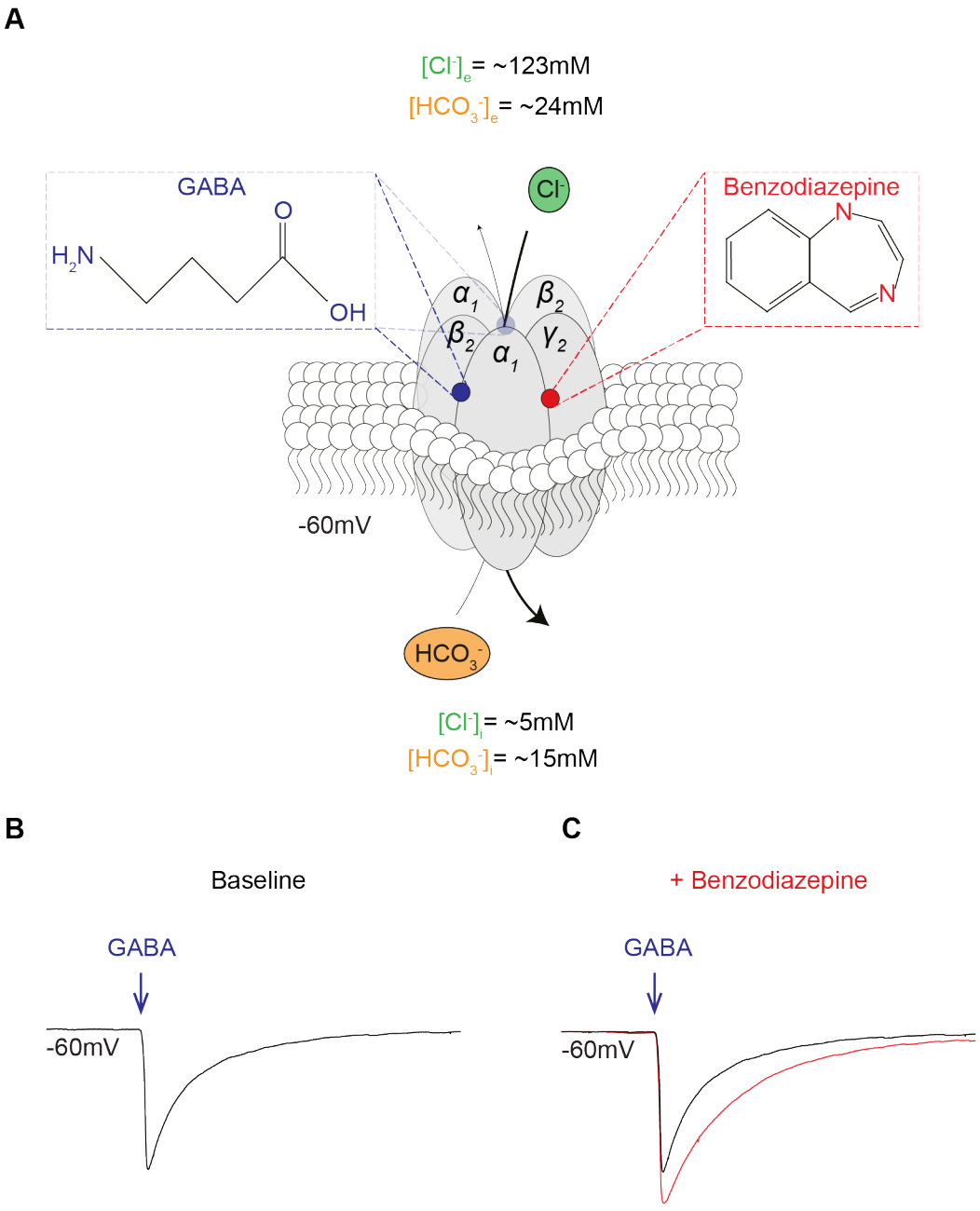
A
[Cl-]e = ~123mM
[HCO3-]e = ~24mM
GABA
O
H2N
OH
Cl-
Benzodiazepine
N
N
α1
β2
β2
α1
γ2
-60mV
HCO3-
[Cl-]i = ~5mM
[HCO3-]i = ~15mM
B
Baseline
GABA
-60mV
C
+ Benzodiazepine
GABA
-60mV

1.1.4 The benzodiazepines: a class of $GABA_AR$ allosteric modulator

Benzodiazepines are a class of synthetic compounds, formed from the union of the benzene and diazepine chemical rings (Müller and Wollert, 1973). By enhancing GABAergic signalling they have anticonvulsant, sedative, hypnotic and anxiolytic properties. The effect of benzodiazepines is determined by the different subunit configurations of the $GABA_AR$ and their relative distribution throughout the CNS. Furthermore, there are distinct pharmacological profiles for the different benzodiazepine agents including different binding affinities to the different $GABA_AR$ isoform configurations.

Benzodiazepines bind to the $GABA_AR$ between its γ and α subunits (Haefely et al., 1993). Specifically, effective benzodiazepine binding onto the α subunit requires a histidine residue (Wieland et al., 1992). This structural requirement for benzodiazepine binding is present in all isoforms of the α subunit except α_4 and α_6 (Duncalfe and Dunn, 1996).

Upon binding, benzodiazepines are able to assert their effects by enhancing the potency of GABA binding (Haefely et al., 1975). This results in an increase in the frequency of channel opening, thereby increasing the conductance of the $GABA_AR$. Under typical conditions this facilitates the influx of the negatively charged Cl^- ion and enhances membrane hyperpolarisation.

Interestingly, there exists an endogenous equivalent to benzodiazepines known as the endozepines (Costa and Guidotti, 1985; Farzampour et al., 2015). These compounds are released by astrocytes and are also able to positively modulate GABAergic signalling (Christian et al., 2013; Christian and Huguenard, 2013).

The $GABA_AR$ is primarily a Cl^- channel with the effects of its activation being determined by the state of the transmembrane Cl^- gradient. The $GABA_AR$'s inhibitory function is therefore linked to the transmembrane Cl^- gradient. However, this gradient is dependent on both time and state, fluctuating as a function of development and network activity.

1.2 Chloride dynamics in the brain

1.2.1 Establishing the transmembrane chloride gradient in mature neural tissue

Two membrane cation-chloride co-transporters (CCCs) are primarily responsible for setting the resting neuronal Cl^- gradient (Kaila et al., 2014). These include the Na^+-K^+-Cl^- cotransporter (NKCC) and the K^+-Cl^- cotransporter (KCC). While there are different configurations of these constructs, NKCC1 and KCC2 are the most prevalent in establishing Cl^- homeostasis in the brain. NKCC1 uses the Na^+ gradient to actively pump Cl^- into the cell. Opposing this is KCC2 that uses the K^+ gradient to facilitate Cl^- extrusion.

1.2.2 The state of the Cl^- gradient determines the nature of $GABA_AR$ function

To fully appreciate $GABA_AR$ function, first there needs to be an understanding of how Cl^- ions are directed through the channel (Johnston and Wu, 1995; Raimondo et al., 2017).

The current associated with $GABA_AR$ activation (I_{GABA}) is the product of channel conductance (gGABA) and driving force (DF_{GABA}) as seen here in Equation 1.1.

$$I_{\mathrm{GABA}} = g_{\mathrm{GABA}} \times DF_{\mathrm{GABA}} \tag{1.1}$$

The (DF_{GABA}) is determined by the difference between the membrane potential and the reversal potential for GABA (E_{GABA}) highlighted in Equation 1.2.

$$DF_{\mathrm{GABA}} = V_{\mathrm{m}} - E_{\mathrm{GABA}} \tag{1.2}$$

The reversal potential is defined as the membrane potential where the net ionic current is 0. At this point the movement of ions through the $GABA_AR$ due to the electric field is matched by the diffusion of ions down their concentration gradient (Raimondo et al., 2015).

During normal baseline activity, the $[Cl^-]_i$ is typically 5mM and the $[Cl^-]_e$ 123mM (Raimondo et al., 2013; Ellender et al., 2014). The intracellular concentration of HCO_3^- ($[HCO_3^-]_i$) is 15mM and the extracellular concentration of HCO_3^- ($[HCO_3^-]_e$) is 24mM (Kaila and Voipio, 1987; Kaila et al., 1989). Using these values, the E_{GABA} (-70.6mV) is calculated by combining the E_{Cl} (-80mV) and the E_{HCO3}(-13mV) in a similar ratio to their relative permeability (see Equation 1.3). As previously mentioned (see Section 1.1.3), the $GABA_AR$ is permeable to both Cl^- and HCO_3^-- in a ratio of 4:1.

$$E_{\mathrm{GABA}} = \frac{4}{5} \times \frac{RT}{zF} \ln \frac{[Cl^-]_{\mathrm{e}}}{[Cl^-]_{\mathrm{i}}} + \frac{1}{5} \times \frac{RT}{zF} \ln \frac{[HCO_3^-]_{\mathrm{e}}}{[HCO_3^-]i} \tag{1.3}$$

The state of the $[Cl^-]_i$, which may differ in space and time, sets the E_{GABA} that then determines the polarity of $GABA_AR$ signalling (Wright et al., 2011). When E_{GABA} is negative relative to the resting potential (V_m), due to a low $[Cl^-]_i$, it favours Cl^- influx and membrane hyperpolarisation. This reduces the probability of action potential generation and inhibits network excitability. If the E_{GABA} were to rise, following an increase in $[Cl^-]_i$, it can exceed V_m but still remain below the action potential threshold. In this state $GABA_AR$ remains inhibitory as the increased Cl^- conductance counterbalances the surrounding glutamate-mediated cation influx and thereby prevents further depolarisation towards the AP threshold. This is known as shunting inhibition (Staley and Mody, 1992). However, if the E_{GABA} is more positive than the action potential threshold, $GABA_AR$ activation can trigger a spike. When this occurs GABAergic signalling has become excitatory (Staley et al., 1995).

1.2.3 Studying $GABA_AR$ signalling & Cl^- dynamics

There are various experimental techniques to elicit $GABA_AR$-mediated currents. These include the use of exogenous GABA or a selective $GABA_AR$ agonist like muscimol (Forman et al., 2017). In addition, GABA-releasing interneurons can be activated to release endogenous GABA. Traditionally, this has been achieved through electrical stimulation of these GABAergic cells concurrent with glutamate receptor blockade (Ge et al., 2006). More recently however, optogenetic stimulation has allowed for the activation of interneurons either has a group or as individual interneuronal sub-groups. This is achieved by expressing channelrhodopsin (ChR2), a light-sensitive Na^+ channel, selectively in interneuronal cells (Boyden et al., 2005). When a blue light is then used to activate the opsin, the cells are depolarised and elicit action potentials that then initiates endogenous GABA release at their synaptic targets (English et al., 2012; Ledri et al., 2014).

To explore changes in $[Cl^-]_i$, a variety of different electrical and imaging tools are available. Imaging techniques include the use of Cl^--sensitive dyes (Kovalchuk and Garaschuk, 2012), or more recently, genetically encoded fluorescent reporters (Grimley et al., 2013; Sato et al., 2017). However, a major limitation of these Cl^- imaging techniques is that they are affected by changes in intracellular pH that are known to fluctuate along with neuronal activity, particularly seizures (Raimondo, Irkle, Wefelmeyer, Newey and Akerman, 2012; Raimondo et al., 2013).

Electrophysiological methods include cell-attached recordings (Tyzio et al., 2008) and perforated patch-clamp recordings (Kyrozis and Reichling, 1995). The main advantage of these techniques is that they are not affected by fluctuations in intracellular pH. Using this technique, E_{GABA} is measured and the $[Cl^-]_i$ subsequently calculated using the Nernst equation (see Equation 1.3). Perforated patch-clamp recordings are the predominant technique used in this thesis to measure $[Cl^-]_i$.

The state of the transmembrane Cl^- gradient can also be manipulated. Traditionally, this has been achieved through genetic or pharmacological manipulation of NKCC2 (Flemmer et al., 2002; Dzhala et al., 2005) or KCC2 function (Hübner et al., 2001; Deisz et al., 2014; Mahadevan and Woodin, 2016; Kelley et al., 2016). However, the more recent development of optogenetic tools has provided a further ability to modulate Cl^- concentration. These include a chloride-specific pump (Raimondo, Kay, Ellender and Akerman, 2012); a chloride-conducting channelrhodopsin (Berndt et al., 2014); an anion-conducting channelrhodopsin (Govorunova et al., 2015) and a Cl^- extruder (Alfonsa et al., 2016).

The development of these advanced techniques has allowed scientists to investigate and manipulate Cl^- to explore its role in both development and disease.

1.2.4 Differential expression of CCCs causes long-term plasticity at the GABA synapse

As explained in Section 1.2.2, $GABA_AR$-mediated signalling can be depolarising or excitatory due to increases in $[Cl^-]_i$. These changes are thought to be driven by changes in the expression patterns of NKCC1 and KCC2 that are relevant in both neurological development and disease (Ben-Ari et al., 2012; Kaila et al., 2014).

In the developing brain, NKCC1 is up-regulated resulting in a higher intracellular concentration of Cl^- (Ben-Ari, 2002). In this state, GABA is depolarising and is thought to be required in order to 'unsilence' glutamatergic synapses through the co-activation of NMDA receptors (Wang and Kriegstein, 2008; van Rheede et al., 2015). However, as neural tissues mature there is a down-regulation of NKCC1 which is accompanied by an up-regulation of KCC2 (Rivera et al., 1999). In this mature state, there is increased Cl^- extrusion which results in a lower $[Cl^-]_i$ and an inhibitory shift in GABA function. This is further illustrated in Figure 1.2.

Figure 1.2 ***(following page)*:** Cation-chloride co-transporters set the transmembrane chloride gradient. The Na^+/K^+ ATPase sets the electrochemical gradient of Na^+ and K^+ across the neuronal membrane. This gradient is then used by the cation-chloride co-transporters, NKCC1 and KCC2, in order to pump chloride in or out of the intracellular space. **A**, In the developing brain, NKCC1 is upregulated allowing for a higher $[Cl^-]_i$ and subsequently more positive E_{GABA} values. In this immature state, $GABA_AR$-mediated signalling is depolarising and can facilitate network excitation. **B**, As neural tissue matures, there is a down regulation of NKCC1 which is accompanied by an upregulation of KCC2. KCC2 uses the K^+ gradient to actively extrude Cl^-. In this state, there is a lower $[Cl^-]_i$, which allows for an inhibitory-shift in $GABA_AR$ function as it becomes hyperpolarising. The relative differences in $[Cl^-]_i$ and corresponding E_{GABA} values are shown here. This figure was adapted from Blaesse et al (2009) and Raimondo et al (2017).

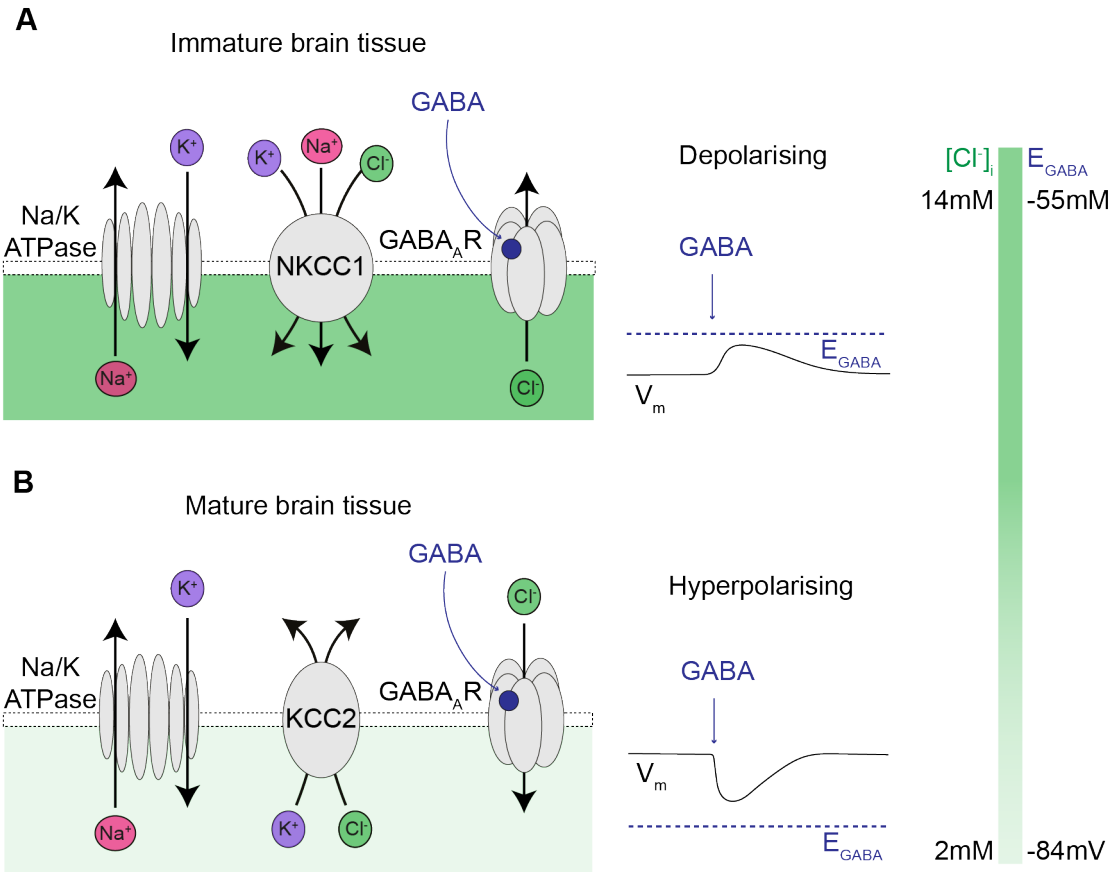
A
Immature brain tissue
GABA
K+
Na+
Cl-
Na/K
ATPase
NKCC1
GABA$_A$R
Na+
Cl-
Depolarising
GABA
E$_{GABA}$
V$_m$
[Cl-]$_i$
E$_{GABA}$
14mM
-55mM
B
Mature brain tissue
GABA
K+
Cl-
Na/K
ATPase
KCC2
GABA$_A$R
Na+
K+
Cl-
Hyperpolarising
GABA
V$_m$
E$_{GABA}$
2mM
-84mV

The role of CCCs has also been implicated in various disease states. Here disease-associated changes in the NKCC1 and/or KCC2 expression profile alter inhibitory signalling and overall network function. CCC-induced changes in $[Cl^-]_i$ has been shown to be involved in the pathophysiology of a growing number of complex disorders (Raimondo et al., 2017). These include autism (Tang et al., 2016), neuropathic pain (Li et al., 2016), schizophrenia (Tao et al., 2012), spasticity (Boulenguez et al., 2010) and, most relevant to this thesis, epilepsy (Huberfeld et al., 2007).

1.2.5 Activity-driven Cl^- plasticity

While CCCs are considered to be a fundamental factor in setting $[Cl^-]_i$, the state of network activity can also significantly alter the state of the transmembrane Cl^- gradient (Raimondo, Kay, Ellender and Akerman, 2012; Raimondo et al., 2017).

During baseline network activity, E_{GABA} is typically negative relative to the resting membrane potential (V_m). When the $GABA_AR$ is activated, the state of the transmembrane gradient favours Cl^- influx causing membrane hyperpolarisation. KCC2 then uses the transmembrane K^+ gradient to extrude Cl^-. In this state, the inhibitory function of the $GABA_AR$ is preserved by maintaining a low $[Cl^-]_i$ (Staley and Mody, 1992) and low $[K^-]_e$ (Kaila et al., 1997).

An increase in network activity causes an increase in synaptic GABA release and greater $GABA_AR$ activation (Staley and Proctor, 1999). This generates more Cl^- influx and a subsequent rise in the $[Cl^-]_i$. The E_{GABA} becomes positive relative to the V_m but typically remains below the action potential threshold. In this state, $GABA_AR$-mediated signalling remains inhibitory by counteracting the net effect of the surrounding influx of

cations through shunting inhibition (as explained in Section 1.2.2). The rise in $[Cl^-]_i$ is met by an increase in KCC2 activity in an attempt to re-establish the transmembrane Cl^- gradient. This is accompanied by increased K^+ extrusion and a rise in the $[K^-]_e$ (Kaila et al., 1997).

If network activity increases further, the combined effect of the rising $[Cl^-]_i$ and $[K^-]_e$ soon overwhelms the Cl^- extrusion capabilities of KCC2. This increased accumulation of Cl^- depolarises E_{GABA} above the action potential threshold. In this state, with subsequent $GABA_AR$ activation, action potentials will be triggered as GABAergic signalling has become excitatory. This short term change in $GABA_AR$ signalling as a function of a change in the transmembrane Cl^- gradient is referred to as short-term ionic plasticity and is further summarised in Figure 1.3.

Figure 1.3 ***(following page)*:** Activity-driven ionic plasticity precipitates a transient excitatory shift in $GABA_AR$-mediated signalling. **A**, At rest, there is a low $[Cl^-]_i$ and E_{GABA} is hyperpolarised relative to the resting membrane potential (V_m). This allows Cl^- influx and membrane hyperpolarisation. The low $[K^-]_e$ allows for efficient KCC2-mediated extrusion of Cl^-. **B**, During states of increased network activity, more GABA is released into the synaptic cleft leading to enhanced $GABA_AR$ activation. This allows for a greater amount of Cl^- influx and rise in the $[Cl^-]_i$, shifting the E_{GABA} to sit above V_m but remain below the AP threshold. This allows GABA to facilitate shunting inhibition. There is also increased KCC2 activity to try and correct the $[Cl^-]_i$ which may lead to an increased $[K^-]_e$. **C**, When hyperexcitability is sustained, E_{GABA} depolarises above the AP threshold and $GABA_AR$ activation becomes excitatory and can trigger APs. The rising $[K^-]_e$ reduces the transmembrane K^+ gradient which impedes KCC2 function and further facilitates the rise in $[Cl^-]_i$. This figure is adapted from Viitanen et al (2010) and Raimondo et al (2017).

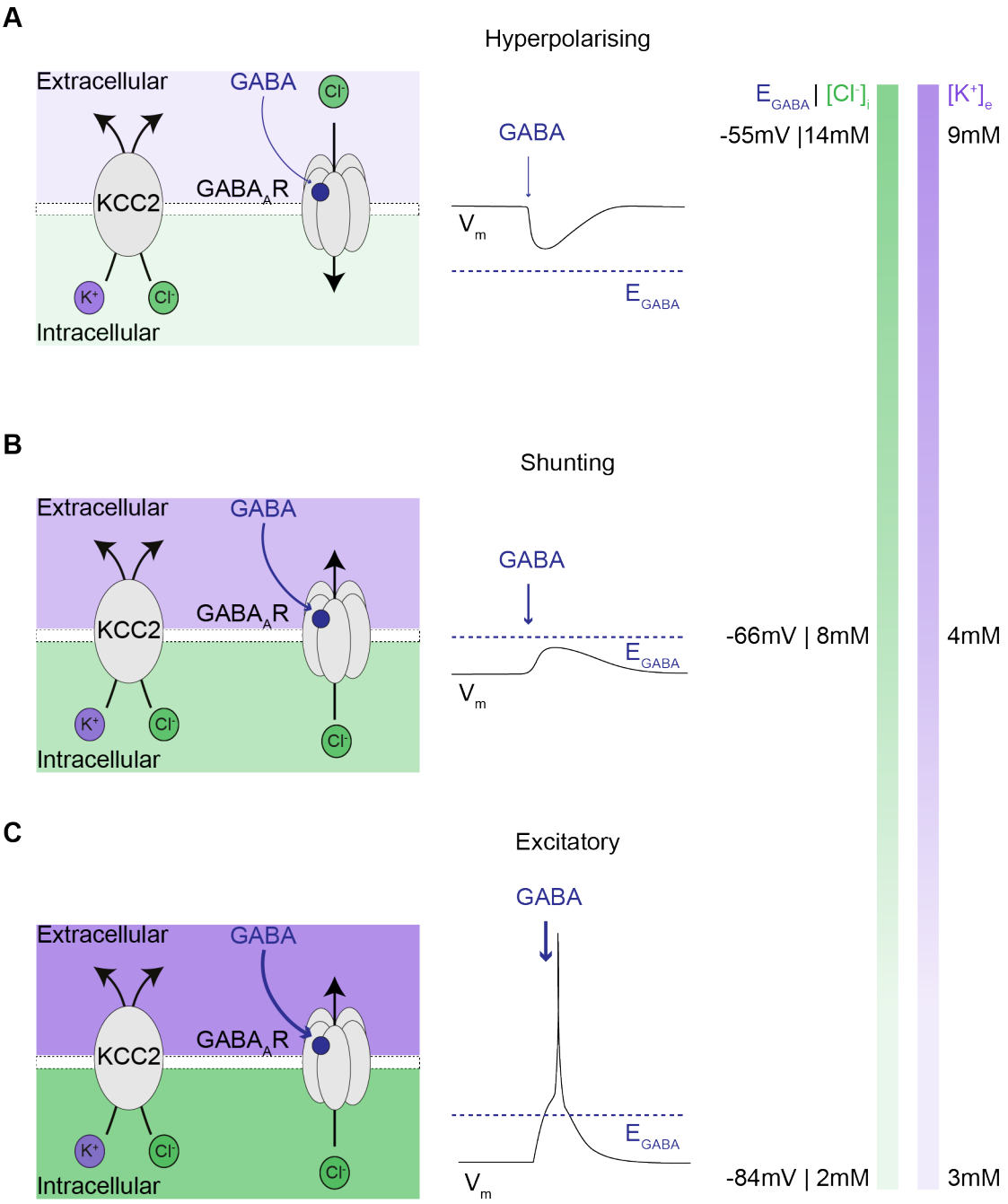
A
Hyperpolarising
Extracellular
GABA
Cl-
KCC2
GABA$_A$R
K+
Cl-
Intracellular
GABA
V_m
E_{GABA}
E_{GABA} | $[Cl^-]_i$
$[K^+]_e$
-55mV |14mM
9mM
B
Shunting
Extracellular
GABA
KCC2
GABA$_A$R
K+
Cl-
Intracellular
Cl-
GABA
E_{GABA}
V_m
-66mV | 8mM
4mM
C
Excitatory
Extracellular
GABA
KCC2
GABA$_A$R
K+
Cl-
Intracellular
Cl-
GABA
E_{GABA}
V_m
-84mV | 2mM
3mM

1.3 Alterations in Cl^- dynamics and $GABA_AR$ signalling during seizures

1.3.1 Seizures: unregulated hypersynchronous hyperexcitability

Normal neuronal processing is typically characterised by asynchronous firing within neural networks. This regulated activity is formed by excitation being broadly matched by inhibition. However, if inhibitory processes are compromised, an unregulated propagation of hyperexcitability may occur. In this state, network firing becomes hypersynchronous and dysfunctional. This type of aberrant electrical activity is understood to underlie what is referred to clinically as an ictus or seizure. Moreover, the process that leads to this seizure activity is known as ictogenesis (Blauwblomme et al., 2014).

Seizures can manifest clinically in a variety of both convulsive and non-convulsive ways (Fisher et al., 2005). Seizure activity can occur following acute disruptions of the brain (i.e. immediately following trauma) or following systemic disturbances (i.e. metabolic dysfunction). If seizure initiation is unprovoked and recurrent, this clinical presentation is referred to as the neurological disorder of epilepsy. Furthermore, the pathological transition that occurs within the brain to generate unprovoked ictal activity is called epileptogenesis (Goldberg and Coulter, 2013).

1.3.2 Epilepsy: a global health burden

Across the world, epilepsy remains a significant health burden (Salomon et al., 2012). Those affected are severely compromised, both by their seizures and from the side effects of their treatment. While epilepsy remains a global problem, the majority of those who suffer from it reside in resource-poor areas where access to care is limited (Ngugi et al., 2011; Newton and Garcia, 2012). There is also a paucity of research describing epilepsy epidemiology and treatment paradigms in this setting (Wilmshurst et al., 2014).

1.3.3 *In vitro* models of epileptic seizures

In vitro models of epileptic seizures provide a useful means for studying mechanisms underlying seizures and for developing new therapeutic interventions. These *in vitro* models typically use brain slices which have been prepared acutely (acute brain slices) or slices which have been cultured over a period of days to weeks (organotypic brain slices) (Pitkänen et al., 2017).

Traditionally, various chemo-convulsant paradigms have been used to induce seizure activity using both the above-mentioned brain slice preparations. Disruptions to $GABA_A$Rs will readily induce seizure activity. This can be achieved by applying $GABA_A$R antagonists such as bicuculline (Griffiths et al., 1983; Borck and Jefferys, 1999) and picrotoxin (Hablitz, 1984) or by removing $[Cl^-]_e$ (Avoli et al., 1990). Other strategies include lowering or elevating the extracellular concentration of various ionic species like Ca^{2+} (Jefferys and Haas, 1982; Yaari et al., 1983), K^+ (Jensen and Yaari, 1988) or Mg^{2+} (Anderson et al., 1986). An advantage of the 0 Mg^{2+} model is that it leaves GABAergic transmission intact. This allows for the study of how the GABA

system might contribute to the evolution and propagation of seizures. This has been demonstrated by Ellender et al (2014) who used a combination of both ionic changes and electrical stimulation to initiate seizure-like events in order to study changes in GABA signalling during seizures.

These *in vitro* models have allowed for an indepth investigation into the ion dynamics that occur during seizure-like events (Raimondo et al., 2015, 2017). This has largely been achieved using advanced electrophysiology including the use of ion-sensitive electrodes (Dreier and Heinemann, 1991) and perforated patch-clamp recordings (Kyrozis and Reichling, 1995). In addition, recent developments in imaging techniques have allowed for fluctuations in Ca^{2+} (Badea et al., 2001) and Cl^- (Raimondo, Irkle, Wefelmeyer, Newey and Akerman, 2012; Sato et al., 2017) to be studied during *in vitro* epileptiform activity using different biosensors and genetic reporters.

These *in vitro* models of seizures do have limitations in terms of accurately representing *in vivo* conditions. However, they have provided an accessible way of studying different aspects of both ictogeneis and epileptogenesis. This includes studying the role GABAergic signalling plays in these processes.

1.3.4 Endogenous anticonvulsant mechanisms

Most seizures are self-limiting in that they stop of their own accord. This is largely due to diverse endogenous anticonvulsant systems that are able to terminate aberrant electrical activity. These systems include sophisticated and potent inhibitory mechanisms that operate at the level of individual neurons and larger networks of neurons (Lado and Moshé, 2008).

The endogenous anticonvulsant mechanisms include pH fluctuations (Chesler and Kaila, 1992) as well as glutamate depletion (Staley et al., 1998) and glutamate buffering (Benarroch, 2005). In addition, during seizures there appears to be release of various inhibitory neuromodulators including adenosine (Takigawa and Alzheimer, 2002; Ilie et al., 2012), endocannabinoids (Lutz, 2004; Wallace et al., 2003), neuropeptide-Y (Deborah Lin et al., 2006) and GABA (Wilson et al., 1996). The mechanisms involving the GABAergic system are of particular relevance to this thesis.

Feed-forward and feedback GABAergic transmission is a major endogenous control mechanism for regulating network excitability. (Trevelyan et al., 2007). This process is mediated by GABA-releasing interneurons that increase their activity and the release of GABA in response to elevated network activity. In so doing, they provide a significant inhibitory barrier to the spread of seizures.

1.4 The relevance of excitatory GABAergic signalling in seizure activity

Changes in intracellular Cl^- dynamics and depolarising GABA have been implicated in the initiation and propagation of seizures. This is summarised in Figure 1.4 and further explained here.

1.4.1 Depolarising GABAergic signalling within the ictal focus is caused by changes in the expression of cation-chloride co-transporters

Within epileptic tissue, there appears to be changes in the expression pattern of CCCs that leads to a depolarising shift in GABAergic signalling. Huberfeld et al (2007) showed this using resected epileptic brain tissue from human patients who had undergone surgery to treat refractory epilepsy. Within this tissue, they noticed that in a significant subset of pyramidal neurons GABAergic signalling was depolarising with this being caused by a down-regulation of KCC2 and a upregulation of NKCC1. This finding suggests that within an epileptic focus, an altered expression of CCCs results in GABAergic signalling becoming permanently depolarising (as illustrated in Figure 1.4, **A**). These changes in CCCs' expression appear to be precipitated by neuronal injury either from ischaemia (Pond et al., 2006), trauma (Nabekura et al., 2002) or following recurrent or prolonged seizure activity (Rivera et al., 2004; Pathak et al., 2007; Lee et al., 2010).

To confirm the contribution of these CCCs to seizure activity, *in vitro* and *in vivo* studies have used a variety of genetic and pharmacological techniques. Dzhala et al (2005) showed that by blocking the function of NKCC1 with bumetanide, they could drive a negative shift in E_{GABA} as well as reduce epileptiform activity within immature brain tissue. Moreover, Kelley et al (2016) have shown that compromising KCC2 function enhanced the development of seizure activity.

What is clear from this body of work is that long-term changes to Cl^- transporters and consequent perturbations of Cl^- homeostasis is likely to contribute to the generation of seizures. However, what is somewhat less well studied is how transient changes in $[Cl^-]_i$ might contribute to the evolution of seizure activity.

1.4.2 Transient Cl^- loading occurs during seizure activity

During individual seizures there is a transient depolarising shift in GABAergic signalling (Ilie et al., 2012). This is likely caused by intense $GABA_AR$ activation, Cl^- influx and a subsequent increase in $[Cl^-]_i$ (Raimondo, Kay, Ellender and Akerman, 2012; Ellender et al., 2014; Sato et al., 2017). A representation of these fluctuations is illustrated in Figure 1.4, **B**. In this state, the activation of the GABAergic interneurons can precipitate after-discharges (Fujiwara-Tsukamoto et al., 2010; Ilie et al., 2012; Ellender et al., 2014). This observation suggests that interneurons may further drive excitation. Importantly, both the $[Cl^-]_i$ and E_{GABA} return to their baseline levels after the seizure activity has terminated with GABAergic signalling resuming its inhibitory function.

Another contributor to this transient, seizure-associated increase in $[Cl^-]_i$ is the activity of KCC2 (Viitanen et al., 2010). Cl^- extrusion is linked to K^+ extrusion, hence KCC2 activity during seizures leads to elevated $[K^+]_e$. This then combines with the effect of increased channel-mediated K^+ efflux to reduce the transmembrane K^+ gradient. In this state KCC2 extrusion is impaired and precipitates further accumulation of Cl^- in the intracellular space.

1.4.3 Implications of depolarising $GABA_AR$ function on seizure dynamics

At the epileptic focus, the above-mentioned changes in CCCs expression and function produce a chronically elevated Cl^- state where $GABA_AR$ activation will remain depolarising (as illustrated in Figure 1.4, **A**). This process is thought to provide a focus for the generation of seizure activity. Surrounding this focus, Cl^- extrusion mechanisms are intact and $[Cl^-]_i$ is maintained at low levels. This helps prevent the propagation

of hyperexctability beyond the seizure focus. However, under certain conditions the compensatory and intense activation of $GABA_AR$ signalling leads to a massive influx of Cl^- into the intracellular space. This can overwhelm otherwise normal Cl^- extrusion mechanisms causing the Cl^- transmembrane gradient to collapse, resulting in a loss of inhibitory function. When this inhibitory restraint is compromised, it allows a seizure to propagate freely (Trevelyan et al., 2006; Schevon et al., 2012). Furthermore, under these conditions it is possible that compromised GABAergic signalling may also exacerbate the propagation of seizures.

Figure 1.4 ***(following page)*****:** Cl^- dynamics during seizure activity. **A**, In healthy mature neuronal tissue KCC2 is responsible for maintaining a low $[Cl^-]_i$. In the epileptic focus KCC2 appears dysfunctional or downregulated while NKCC1 is upregulated. This causes a significant increase in $[Cl^-]_i$. **B**, A recording trace of a whole-cell patch-clamp recording in voltage-clamp mode (-40mV) showing a 0 Mg^{2+}-induced single seizure-like event from a hippocampal organotypic slice culture. These events are characterised by 4 distinct phases. The pre-ictal period shows an increase in network activity. The tonic phase is characterised by a sudden depolarisation of the membrane accompanied by high-frequency and low-amplitude discharges. The clonic phase is marked by rhythmic bursts or discharges. The post-ictal phase marks the recovery period back to baseline activity. Previous experimental data from both perforated patch-clamp and imaging experiments have shown a transient increase in $[Cl^-]_i$ that occurs during these single seizure-like events that then recovers to baseline when activity is terminated. This is matched by fluctuations in $[K^+]_e$ obtained from extracellular K^+-sensitive recordings. **C**, An illustration of how seizure activity is believed to propagate within the cortex. At the ictal focus both the Cl^- and K^+ gradients are perturbed, however in the surrounding penumbra, they are intact. As seizure activity continues, the surrounding ion gradients are compromised leading inhibition to become dysfunctional. This in turn allows the aberrant ictal activity to propagate. Figure adapted from Raimondo et al (2015; 2017).

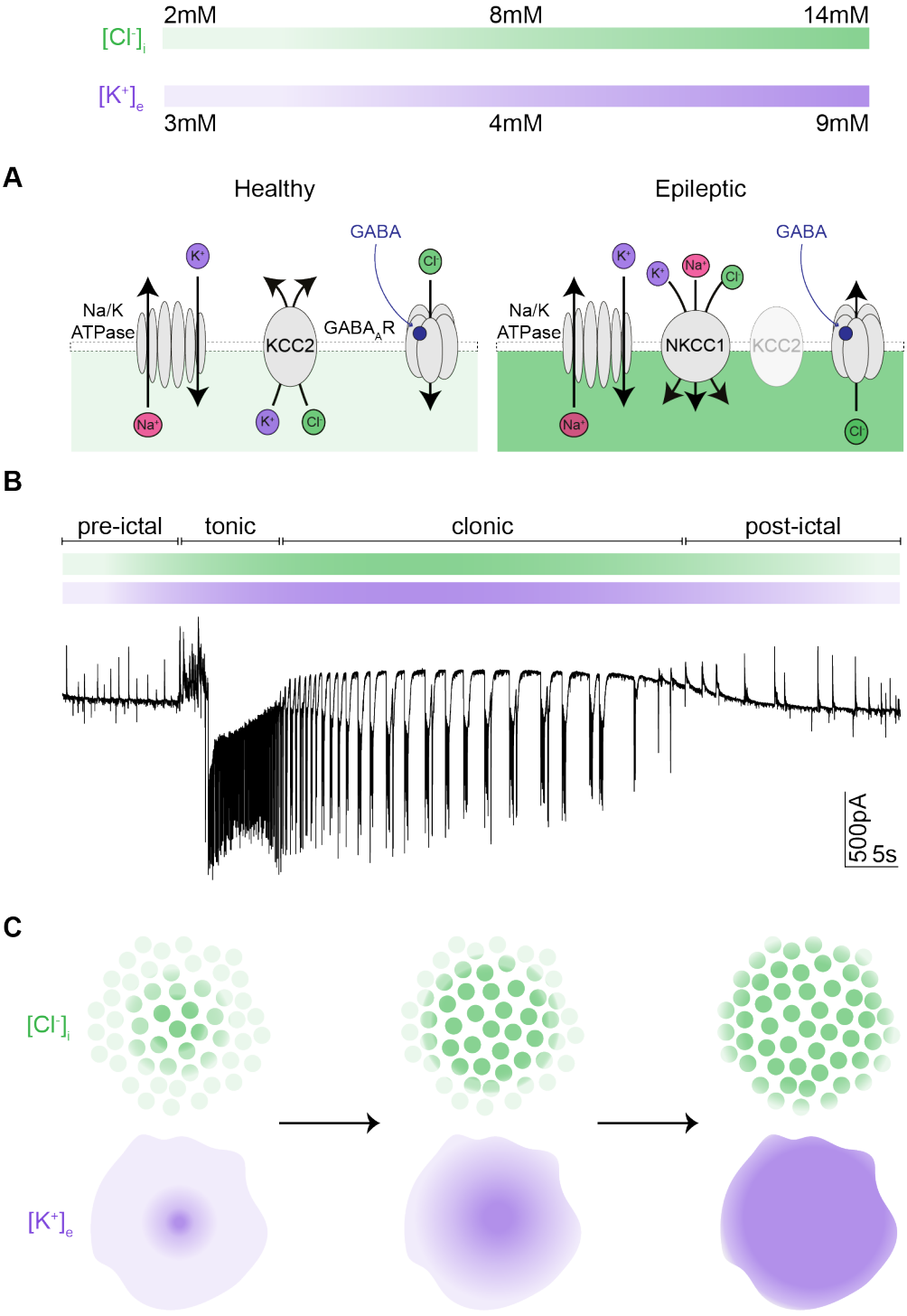
2mM
8mM
14mM
[Cl-]i
[K+]e
3mM
4mM
9mM
A
Healthy
Epileptic
GABA
Na/K ATPase
KCC2
GABAAR
NKCC1
B
pre-ictal
tonic
clonic
post-ictal
500pA
5s
C
[Cl-]i
[K+]e

Another important consideration is the possible effect these perturbed Cl^- dynamics could have on the anticonvulsant efficacy of pharmacological agents which enhance the activity of $GABA_A$Rs, such as the benzodiazepine class of drugs. Previous data from Deeb et al (2013) has shown that the high $[Cl^-]_i$ that accompanies hyperexcitable states decreases the inhibitory effects of diazepam. Glykys et al (2015) then showed that the inhibitory efficacy of diazepam correlates with the state of the transmembrane Cl^- gradient during development. In addition, Sivakumaran and Maguire (2016) show that when NKCC1 is blocked, diazepam is more effective in reducing epileptiform activity in immature tissue.

Therefore, the effect of disrupted neuronal Cl^- on the efficacy of commonly used anticonvulsants which target the $GABA_A$R may be particularly relevant in the context of prolonged seizure states such as status epilepticus.

1.5 Status epilepticus & benzodiazepine resistance

1.5.1 Unremitting & self-perpetuating seizure activity

Seizures are typically self-limiting and arrest within a few minutes in adults (DeLorenzo et al., 1992), but in children individual seizures often last slightly longer (Shinnar et al., 2001; Jenssen et al., 2006). Seizure termination is due to many endogenous anticonvulsant mechanisms that can effectively limit ongoing seizure-activity (as discussed in Section 1.3.4). However, under certain conditions, hyperexcitability within the network persists.

Status epilepticus (SE) is the clinical description of enduring and self-perpetuating seizure activity. The recently revised definition now varies across different semiologies with generalised convulsive SE (CSE) being the most common clinical presentation (Trinka et al., 2015). SE is traditionally defined as a seizure persisting for ≥ 30 minutes. However, it is now appreciated that seizures that do not self-abort within 5 minutes (or recur continuously) are less likely to do so without therapeutic intervention. Therefore, the practical definition of SE is any seizure that is ≥ 5 minutes in duration or multiple discrete seizures between which there is no extended period of recovery between events.

The prolonged aberrant electrical activity of SE is accompanied by significant morbidity and mortality (Betjemann and Lowenstein, 2015). In adults, mortality associated with convulsive SE is estimated at around 20% (DeLorenzo et al., 1995). This is largely determined by the underlying aetiology, with acute cerebrovascular events and tumours being the most lethal. In children, SE appears to occur more frequently with the most common presentation being prolonged febrile seizures (Chin et al., 2006).

1.5.2 Benzodiazepine resistance in status epilepticus

The current treatment guidelines for SE recommend the use of benzodiazepines as the first line-agents (Trinka et al., 2016). These typically include either diazepam, lorazepam or midazolam with them being equal in their anticonvulsant effect (Alldredge et al., 2001). However, in a subset of patients, mostly children, these agents prove to be ineffective (Appleton et al., 2000). When this occurs second-line agents come with a more severe side effect profile (Chin et al., 2008).

The prevalence of benzodiazepine-resistant SE in children has not been described within a South African context. Therefore, an objective of this thesis was to explore this clinical phenomena in our local paediatric cohort (see Objective 1, Section 1.6.1).

Pharmacoresistant SE has previously been studied using *in vitro* models, using notably the Mg^{2+}-free chemoconvulsant model in both acute (Dreier et al., 1998) and organotypic (Albus et al., 2008) brain slices. In these experiments, a Mg-free aCSF solution is used to promote excitation. From the time the Mg^{2+}-free aCSF is washed in, the network shows an evolution from single seizure-like events into a recurrent bursting pattern of activity that has been termed the late recurrent discharge phase (LRD). This LRD phase is thought to be an *in vitro* replica of the unrelenting hyperexcitability underlying SE.

Using this Mg^{2+}-free model, previous data has described a differential effect of benzodiazepines (Zhang et al., 1995; Dreier et al., 1998). Benzodiazepines appear to retain an anticonvulsant effect if introduced early by delaying the onset of seizure-like events. However, if introduced once LRD had been established, the benzodiazepines failed to show an anticonvulsant effect. A major objective of this thesis was to confirm the effect of benzodiazepine on baseline inhibitory GABAergic signalling in brain slices (see Objectives 2, Section 1.6.1). A subsequent objective was to investigate and quantify differential effects of benzodiazepines on epileptiform activity in the 0 Mg^{2+} model of SE (see Objectives 3 and 4, Section 1.6.1).

In trying understand what may underlie benzodiazepine-resistant SE, it is important to consider the role of GABAergic signalling during these prolonged seizure states.

1.5.3 Changes in $GABA_AR$ signalling during status epilepticus

The unremitting aberrant network activity seen in SE is caused by a combination of inhibitory failure as well as the recruitment of processes that facilitate ongoing network excitation (Chen et al., 2007; Betjemann and Lowenstein, 2015). Specifically, changes in $GABA_AR$ transmission are thought to contribute towards SE and will constitute the major focus of this thesis.

Previous data has suggested that after a certain period of ongoing seizure activity, $GABA_A$Rs are internalised (Kapur and Coulter, 1995; Goodkin et al., 2005; Naylor et al., 2005; Goodkin and Kapur, 2009). This would result in a loss of GABAergic inhibitory signalling, which could contribute to both prolonged seizure activity and the loss of benzodiazepine efficacy.

Currently, there is no clear description of how GABAergic signalling might be affected within the early phases of SE. Is GABAergic signalling reduced or does it become excitatory during SE? I will address these question in Objectives 5 and 6 of this thesis (see Section 1.6.1).

1.6 Aims & Objectives

The overall aim of this thesis was to investigate the role of activity-driven excitatory GABAergic signalling on the propagation of prolonged seizures and how this may affect benzodiazepine efficacy.

1.6.1 Objectives

The objectives of this thesis were as follows:

1. To explore the prevalence of benzodiazepine resistance in a local paediatric cohort of patients presenting with SE.
2. To confirm that the anticonvulsant benzodiazepine, diazepam, positively modulates $GABA_A$R-mediated inhibitory signalling.
3. To setup and characterise an established *in vitro* model of SE using Mg^{2+} withdrawal in acute and organotypic brain slices.

4. To study the effects of diazepam when applied at different time points in the 0 Mg^{2+} model of SE.

5. To study changes in GABAergic signalling in the development of prolonged seizure-like states.

6. To investigate activity-driven changes in $[Cl^-]_i$.

Chapter 2

Materials and Methods

2.1 Clinical data

The clinical data I present in this thesis was generated by performing an interim analysis on the data being acquired from an ongoing clinical study.

2.1.1 Study design

A randomised and unblinded clinical trial was setup at the Medical Emergency Unit at Red Cross War Memorial Children's Hospital (RXH) in Cape Town, South Africa. This is an equivalence trial with its main aim being to evaluate the use of two protocols used in the second-line management of paediatric convulsive status epilepticus (CSE). Both protocols (see Appendix A) start with repeated doses of benzodiazepines as first-line management. If the CSE does not terminate after first-line management has been given, patients are then randomised to one of the two second-line management

protocols. The first protocol recommends the use of repeated doses of intravenous (IV) phenobarbitone. The second protocol recommends IV phenytoin followed by an IV midazolam infusion. This study was approved by the University of Cape Town Human Research Ethics Council (UCT HREC 297/2005).

At admission patients are diagnosed with CSE primarily based on the history given by the patient's care-givers (or anyone who witnessed the event) along with what is reported by the managing doctor. The definition of CSE includes any convulsive seizure that extends beyond 5 minutes or multiple recurrent convulsive seizures with no return to cognitive baseline in-between events (Trinka et al., 2015). Once the diagnosis is made, patients are randomised to one of the treatment protocols. Randomisation of protocols was done using the online platform, Research Randomizer (Urbaniak and Plous, 2013). As the pharmacokinetic and side-effect profiles of the agents being compared are distinctly different, it is not possible to blind the managing doctor or study investigators from which intervention the patient has been assigned to. After admission, further clinical information is captured retrospectively by reviewing the patient's hospital folder (obtained from the RXH Medical Records Department).

For this interim analysis, only paediatric patients (under 13 years of age) who presented to the RXH Medical Emergency Department in CSE for the first time were included. Patients readmitted with repeated episodes of CSE were excluded. Furthermore, patients were excluded if they did not meet the clinical definition of CSE, there was a deviation from the treatment protocol or if their clinical records could not be traced.

2.2 Tissue preparation

In my experiments I used brain slices of the hippocampus and entorhinal cortex prepared from transgenic C57BL/6 mice. These brain areas were chosen due to their significant abundance of GABAergic interneurons (Klausberger and Somogyi, 2008; Melzer et al., 2012). Furthermore, both these areas are common epileptogenic foci (Schwartzkroin, 1994; Avoli, 2007; Kumar and Buckmaster, 2006).

Two different preparations of mouse brain tissue were used: organotypic hippocampal slices (organotypic brain slices) and acute hippocampal slices (acute brain slices). The majority of experiments were performed in organotypic brain slices and, where possible, experiments were repeated using acute brain slices. This was done to further validate the results and to limit bias from a single *in vitro* model (Pitkänen et al., 2017). Due to time and technical restraints, it was not possible to replicate all the experiments in acute brain slices.

2.2.1 Animal tissue

The use of transgenic C57BL/6 in this thesis was approved by the University of Cape Town Research Animal Unit Ethics Committee (project number 014/035). All experiments used a crossed mouse strain on a C57BL/6 background. This strain was a cross between mice expressing cre-recombinase in glutamic acid decarboxylase 2 (GAD2) positive interneurons (GAD2-cre) and mice with a loxP-flanked STOP cassette preventing transcription of the red-fluorescent protein tdTomato (a cre-reporter strain). This created the GAD2-cre-tdTomato strain which exposed the cre-recombinase and tdTomato in all GABAergic interneurons as originally described by Taniguchi et al (2011). All mice were purchased from Jackson Laboratory (USA).

All mice used in this thesis were killed by decapitation in accordance with the South African National Standard (SANS10386:2008) and the Veterinary and Paraveterinary Professions Act (Act 19 of 1982). I am a registered member of the South African Veterinary Council (AR14/1327) and am licensed to perform these decapitations. Animal husbandry was provided by the UCT Animal Research Unit.

2.2.2 Organotypic brain slice cultures

Organotypic brain slices were prepared using 7 day old transgenic C57BL/6 mice and followed the protocol originally described by Stoppini et al (1991). Mouse brains were extracted and swiftly placed in cold (4°C) dissection media consisting of Geys Balanced Salt Solution (GBSS #G9779, Sigma-Aldrich, USA) supplemented with D-glucose (#G5767, Sigma-Aldrich, USA). The hemispheres were separated and individual hippocampi were removed and immediately cut into 350 μm slices using a Mcllwain tissue chopper (Mickle, UK). Cold dissection media was used to rinse the slices before placing them onto Millicell-CM membranes (#Z354988, Sigma-Aldrich, USA). Slices were maintained in culture medium consisting of 25% (vol/vol) Earles balanced salt solution (#E2888, Sigma-Aldrich, USA); 49% (vol/vol) minimum essential medium (#M2279, Sigma-Aldrich, USA); 25% (vol/vol) heat-inactivated horse serum (#H1138, Sigma-Aldrich, USA); 1% (vol/vol) B27 (#17504044, Invitrogen, Life Technologies, USA) and 6.2 g/l D-glucose. Slices were incubated in a 5% carbon dioxide (CO2) humidified incubator at between 35 - 37°C.

Recordings were made after 6-14 days in culture. Previous studies have shown that after 7 days in culture (equivalent to postnatal day 14) GABAergic signaling and E_{GABA} has sufficiently developed to a level resembling mature nervous tissue (Streit et al., 1989; Tyzio et al., 2007; Raimondo, Kay, Ellender and Akerman, 2012).

2.2.3 Acute brain slices

Transgenic C57BL/6 mice between 14 to 21 days old were used to prepare acute brain slices. After decapitation, the mouse brain was extracted and quickly placed in a 50% sucrose cutting solution bubbled with carbogen gas (95% oxygen and 5% carbon dioxide). The cutting solution used was composed of (in mM): NaCl (60); KCl (3); NaH2PO4 (1.2); NaHCO3 (23); D-glucose (11); MgCl2 (3); CaCl2 (1) and sucrose (120). pH was adjusted to between 7.38 and 7.42 using 0.1mM NaOH. The mouse brain was then appropriately sectioned using a scalpel blade to ensure that the hippocampus and entorhinal cortex would be sliced in the transverse plane. 400 μm horizontal slices were cut using a vibrating VF-200 Compresstome® (Precisionary Instruments, USA). This method of preparing acute brain slices is similar to that employed by Dreier et al (1991; 1998)

For patch-clamp experiments, slices were then transferred to a submerged chamber which contained standard artificial cerebro-spinal fluid (aCSF) and bubbled with carbogen gas. For local field potential recordings, slices were transferred to a custom-built interface chamber (Krimer and Goldman-Rakic, 1997). The standard aCSF was composed of (in mM): NaCl (120); KCl (3); MgCl2 (2); CaCl2 (2); NaH2PO4 (1.2); NaHCO3 (23); D-Glucose (11) with pH adjusted to be between 7.35-7.40 using 0.1 mM NaOH.

2.2.4 Viral transfection

After 1 day in culture, organotypic brain slices were transfected with adeno-associated vector serotype 1 (AAV1) containing a floxed-STOP channelrhodopsin (ChR2) linked to a yellow fluorescent protein (YFP) tag. The AAV1 has been shown to be effective for viral transfection in organotypic brain slices (Royo et al., 2008).

The AAV1-ChR2-YFP (UNC Vector Core, USA) was then diffusely injected into the organotypic brain slices using a custom-built Openspritzer pressurised ejection device (Forman et al., 2017). 6 days after injection, there was sufficient expression of the ChR2-YFP. Figure 2.1 illustrates this optogenetic paradigm and further highlights how it was used to activate endogenous GABAergic signalling.

Figure 2.1 ***(following page)*:** Using optogenetics to activate endogenous GABAergic signalling. **A**, Organotypic brains slices were prepared from the GAD2-cre-tdTomato mice and transfected with an AAV1 containing a floxed-STOP ChR2-YFP. This allowed for selective expression of ChR2 in all GABAergic interneurons. Confocal images demonstrate how ChR2-YFP (green) is predominately expressed on the membrane of the GAD2-cre-tdTomato expressing interneurons (red). **B**, ChR2 is a cation channel that is activated by blue light. Once activated the channel permits cation influx facilitating membrane depolarisation and the generation of action potentials. **C**, Whole-cell patch-clamp recordings in current-clamp mode from a ChR2-expressing interneuron and a neighbouring pyramidal cell in an organotypic brain slice. Shining blue light (17.1 mW) selectively activates interneurons as shown by how action potentials are generated whenever the light stimulus is present. By contrast, the light stimulus generated hyperpolarsing potentials in the pyramidal cell. These are GABAergic postsynaptic potentials.

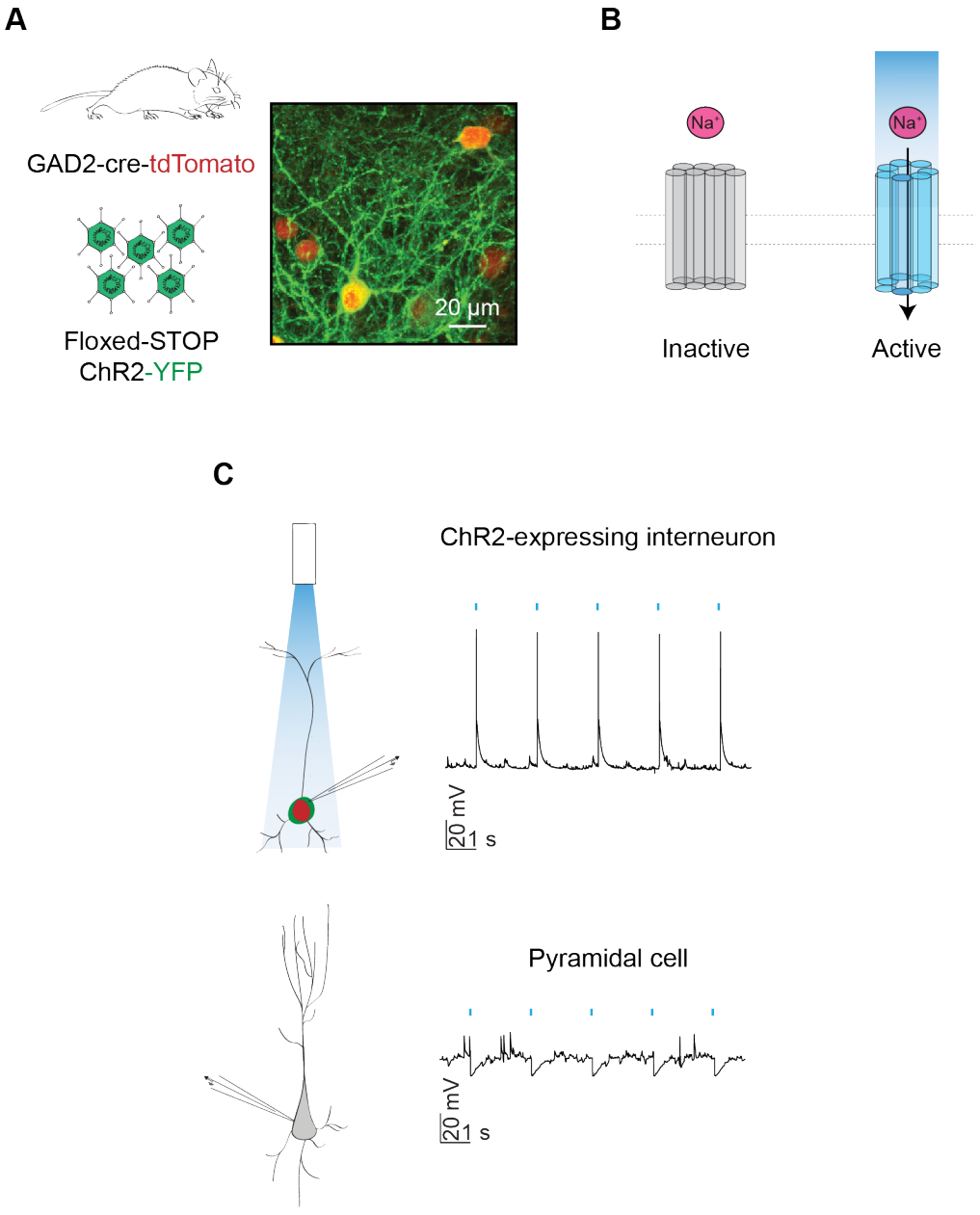
A
GAD2-cre-tdTomato
Floxed-STOP
ChR2-YFP
20 µm
B
Na+
Na+
Inactive
Active
C
ChR2-expressing interneuron
20 mV
1 s
Pyramidal cell
20 mV
1 s

2.3 Imaging

The images presented in this thesis were acquired using a confocal microscope (LSM510 Meta NLO, Car Zeiss, Jena, Germany). To visualise tdTomato expression a 561 nm laser was utilised. To visualise YFP-labelled ChR2 a 488nm laser was utilised. In each case, appropriate band pass filters were employed to collect emitted fluorescence.

2.4 Intracellular recordings

2.4.1 Cell visualisation

Brain slices were transferred to the recording chamber where they were continuously superfused with standard aCSF using peristaltic pumps (400D1, Watson-Marlow, UK). Neurons were visualized using a 20X water-immersion objective (XLUMPCFLN-W 20X, Olympus, Japan) or a 40X water-immersion objective (LUMPLFLN 40X, Olympus, Japan) on either a BX51WI upright microscope (Olympus, Japan) or an Axioskop upright microscope (Zeiss, Germany). Digital images of the slices were obtained using a CCD camera (VX55, TILL Photonics, Germany). In acute brain slices, visualization of pyramidal cells was achieved with infrared differential interference contrast microscopy.

2.4.2 Whole-cell recordings

Micropipettes were prepared from borosilicate glass capillaries with an outer diameter of 1.20mm and inner diameter of 0.69mm (Warner Instruments, USA), using a horizontal puller (Intracell Model P-1000, Sutter, USA). When recording GABAergic synaptic currents, pipettes were filled with a high Cl^- internal solution (Cl^- 141mM) composed of (in mM): KCl (135), NaCl (8.9) and HEPES (10). When recording seizure activity,

pipettes were filled with an internal solution (Cl^- 10mM) composed of (in mM): K-gluconate (120); KCl (10); Na2ATP (4); NaGTP (0.3); Na2-phosphocreatinine (10) and HEPES (10). The pipettes were then placed over a silver wire electrode attached to a CV 203BU head stage (Molecular Devices, USA) which was controlled using motorised micromanipulators (Luigs and Neuman, Germany). Positive pressure was applied and the pipette was lowered onto the surface of the target cell. Once a membrane gigaseal had formed, pipette capacitance was compensated. Break-through was achieved with gentle negative pressure and defined as a drop of access resistance to <20 MΩ. Recordings were made in both current-clamp and voltage-clamp modes using an Axopatch 200B amplifier (Molecular Devices, USA) with data being acquired with either IGOR Pro software (Wavemetrics, USA) or WinWCP (University of Strathclyde, Scotland).

2.4.3 Perforated patch-clamp recordings

To perform gramicidin perforated patch-clamp recordings, I followed the protocol described by Kyrozis and Reichling (1995). The advantage of this recording technique is that it preserves $[Cl^-]_i$. Micropipettes were filled with the high Cl^- (described in Section 2.4.2). The osmolarity of all internal solutions was adjusted to 290 mOsM and the pH adjusted to 7.38 with NaOH. Gramicidin A (90% pure, Sigma, USA) was dissolved in dimethylsulfoxide (DMSO, Sigma, USA) to achieve a stock solution of 4 mg/ml. Before each recording, a working internal solution was prepared by diluting 5μL of Gramicidin stock in 995μL of the high Cl^- internal solution to achieve a final gramicidin concentration of 80μg/ml. The solution was then sonicated and mixed on a rotamixer before being filtered with a 0.45 microm cellulose acetate membrane filter (Merck, USA). Patch pipettes (described in Section 2.4.2) were then back filled with gramicidin working solution. Positive pressure was applied and the pipette was lowered onto the surface of the target cell. Once a membrane gigaseal had formed, pipette capacitance was

compensated. Adequate perforation of the membrane was assessed by monitoring access resistance and was defined when access resistance was <50 MΩ. This usually occurred between 10-45 minute after gigaseal had formed. Recordings were made in both current-clamp and voltage-clamp modes using an Axopatch 200B amplifier (Molecular Devices, USA) with data being acquired with WinWCP (University of Strathclyde, Scotland).

Rupture of the gramicidin patch, referred to as a break through, causes massive influx of the high Cl^- internal solution into the cell. This causes a significant and permanent increase in the E_{GABA} at which time recordings would be discarded.

2.4.4 Calculating $GABA_AR$ parameters

In order to study $GABA_AR$ function, E_{GABA} and g_{GABA} were calculated. This was achieved by activating $GABA_ARs$ either with endogenous or exogenous GABA. Endogenous GABA was released by either stimulating ChR2-expressing interneurons with light (in organotypic brain slices), or by electrically stimulating GAD2-interneurons in the presence of glutamate receptor blockade (in acute brain slices). Light stimulus was typically set at 100ms and LED intensity of 17.1 mW. The electrical stimulus was set at 2pA for 3ms. Alternatively, exogenous GABA (#0344, Torcis Bioscience, United Kingdom) was puffed onto the cell using an Opensprizter device (Forman et al., 2017).

In order to calculate resting E_{GABA} and g_{GABA}, peak $GABA_AR$ currents were elicited at different stepped voltages (a series of 10mV steps above and below a set resting potential of -60mV). Between each recording sweep there was a 10-30s break to allow for adequate recovery of $[Cl^-]_i$. The peak $GABA_AR$ currents at each voltage were then plotted against the holding potential to generate a current-voltage (I-V) curve. Using this

graph the resting E_{GABA} was defined as the x-intercept of the peak $GABA_AR$ currents and holding potential. Applying Equations 1.1 and 1.2, g_{GABA} could be calculated. Furthermore, the $[Cl^-]_i$ could be calculated from E_{GABA} by way of the Nernst Equation (see Equation 1.3).

2.5 Extracellular recordings

2.5.1 Local field potentials

For local field potentials, slices were placed in an interface recording chamber (Krimer and Goldman-Rakic, 1997) perfused with aCSF using a peristaltic pump (Model 205S Watson-Marlow, UK). Temperature was adjusted to ensure the solution in the chamber surrounding the slice was kept between 33 - 35°C.

Single-electrode extracellular recordings were performed using patch pipettes (similar to those described in Section 2.4.2) with their tips broken under microscope visualisation using a VT-II 2147861 microscope (Olympus, Japan). Pipettes were filled with Mg^{2+}-free aCSF and lowered onto brain slices under microscope guidance. For organotypic brain slices, pipettes were placed in the CA1 region while in acute brain slices they were placed in the entorhinal cortex. Adequate contact was defined by visualising the pipette tip breaking the surface of the perfusing solution above the slice.

Recordings were performed using a 1800 2-Channel Microelectrode AC amplifier (A-M Systems, USA) and associated headstages attached to silver-wire electrodes. Data was acquired using the PowerLab 15T hardware (AD Instruments, New Zealand) and LabChart Pro software package (AD Instruments, New Zealand). Recordings were processed using a digital low-pass filter at 140Hz. During analysis an additional digital high-pass filter at 0.1Hz was applied.

2.6 Seizure models

2.6.1 The 0 Mg^{2+} chemo-convulsant model

To elicit *in vitro* epileptiform activity, slices were bathed in Mg^{2+}-free aCSF (Anderson et al., 1986; Mody et al., 1987; Dreier and Heinemann, 1991; Albus et al., 2008). Removing extracellular Mg^{2+} reduces the voltage dependent block of Mg^{2+} on N-methyl-D-aspartic acid (NMDA) receptors. When this occurs, the brain slices become predisposed to developing synchronised and sustained hyperexcitability that initially manifests as single seizure-like events (SLEs). Over time this activity then progresses into recurrent epileptiform discharges referred to as the late recurrent discharge (LRD) phase.

2.6.2 Definitions of *in vitro* seizure activity

SLEs recorded using whole-cell patch-clamp recordings were defined as a significant depolarisation (2 standard deviations above the resting membrane potential) that lasted at least 5 seconds while following the typical tonic-clonic pattern (illustrated in Figure 1.4). These were represented as upward deflections in current-clamp mode and downward deflections in voltage-clamp mode. When using extracellular recordings, SLEs were defined as a change in the local field potential that was at least 2 standard deviations away from the baseline activity and lasted for a period of at least 5 seconds.

The LRD phase was defined as recurrent discharges (termed epileptiform discharges) that persist for at least 2 minutes with no return to baseline. This definition was guided by previous *in vitro* work (Zhang et al., 1995; Dreier and Heinemann, 1991; Dreier et al., 1998). Furthermore, as the LRD aims to model clinical SE, this definition aims to align with the revised clinical definition of SE (Trinka et al., 2015).

Data was excluded from analysis if electrical noise prevented accurate identification of SLEs or LRD. In addition, slices that developed spontaneous seizures prior to being exposed to 0 Mg^{2+} were also excluded. This was done to prevent any potential kindling process whereby prior seizure activity could alter various properties of the neuronal network, specifically in the GABAergic system. These changes could affect SLE and LRD propensity. (Kamphuis et al., 1991; Morimoto et al., 2004)

2.7 Drugs

Here the various drugs used will be described. Their exact application is explained in greater detail with the relevant experiments presented in Chapter 3.

The following drugs were added to the aCSF solution in the course of various experiments: the $GABA_AR$ agonist, diazepam (#2805, Torcis Bioscience, United Kingdom); the benzodiazepine competitive antagonist, flumazenil (#1328, Torcis Bioscience, United Kingdom); the $GABA_BR$ antagonist, CGP-35348 (#1248, Torcis Bioscience, United Kingdom) and the glutamate receptor antagonist, kynurenic acid (#0223, Torcis Bioscience, United Kingdom). Where applicable, the intracellular Na^+ channel blocker QX-314 (#1014, Torcis Bioscience, United Kingdom) was added to the internal solution used to fill patch pipettes.

As diazepam is classified as a schedule 4 restricted substance within South Africa, an import and possession permit was obtained from the South African Medicines Control Council (IMP/123/2016 and Permit No: 033/2016/2017).

2.8 Data analysis

Data analysis was performed using custom written scripts in Matlab (MathWorks, USA). Statistical measurements were performed using GraphPad Prism version 6.0 (GraphPad Software, USA).

For normally distributed numerical data ($p \geq 0.05$, Shapiro-Wilk test), parametric tests were used (i.e. paired or unpaired student's t-tests). Welch correction was added to unpaired data as I could not assume the standard deviations were the same.

If data was found not to be normally distributed ($p < 0.05$, Shapiro-Wilk test), non-parametric tests were used. For unpaired data this included the Mann-Whitney U test (referred to as Mann-Whitney test) while for paired data the Wilcoxon signed-rank test (referred to as Wilcoxon test) was used.

Categorical data was summarised in contingency tables and differences between groups were identified using the Fisher-exact test.

Significance was defined as a p-value <0.05. Data is reported as mean $\pm$ standard error of the mean (SEM) unless otherwise stated.

When comparing the effect of diazepam on various manually measured SLE and LRD parameters, data was randomised and the treatment groups blinded by an independent party. Analysis was then performed not knowing which recordings had diazepam added. Data was unblinded only after the statistical analysis was performed. This was done to eliminate any bias introduced by manual analysis of the recordings.

Chapter 3

Results

3.1 Benzodiazepine-resistant status epilepticus is prevalent in a South African paediatric cohort

To give a clinical context to my experimental research, I sought to determine the local prevalence of benzodiazepine-resistant convulsive status epilepticus (CSE). To achieve this, a sample was taken from a cohort of patients that had been recruited into an ongoing clinical trial. The aim of this clinical study is two-fold: (i) to study the epidemiology of CSE in the local paediatric population and (ii) to assess the response to current, unvalidated treatment protocols. However, for the purpose of this thesis, I performed a limited interim analysis to measure the prevalence of benzodiazepine-resistant CSE in a South African paediatric cohort.

At the time this analysis was performed, 144 entries had been loaded into the study (see Figure 3.1, **A**). 106 (74%) of these had been reviewed while 38 (26%) are still pending review. Moreover, of those patients who's folders had been reviewed, 13 (12%) were excluded from the study. This was done if the patient either did not satisfy the definition of CSE at admission or if the record of their admission was incomplete (as described in Section 2.1.1). Of the remaining eligible patients, I only analysed their first admission into the study.

As shown in Figure 3.1, of the 73 patients included in the interim analysis, 42% did not respond to first-line benzodiazepine agents that included either diazepam, lorazepam or midazolam given either intravenously (IV) or per rectally (PR). In the sample of the cohort used, 52% were female and 48% males. The median age was 24.95 months with an interquartile range of 38.59 months. Furthermore, there was no significant difference in age between the benzodiazepine-sensitive vs benzodiazepine-resistant patients (42.20 $\pm$ 5.64 months vs 33.95 $\pm$ 6.58 months, $p = 0.16$, *Mann-Whitney test*). However, when looking at the time between seizure onset and time to delivery of the first-line agent, this was significantly longer in the benzodiazepine-resistant group (45.93 $\pm$ 5.45 minutes vs 68.29 $\pm$ 8.65 minutes, $p = 0.018$, *Mann-Whitney test*). The median time of seizure duration was 45 minutes with an interquartile range of 52.5 minutes. This suggests that the longer CSE remains untreated the more likely it is to become resistant to benzodiazepines.

This data confirmed that benzodiazepine-resistant CSE is a relevant clinical entity which warrants further investigation into possible cellular mechanisms. This provides the justification for the *in vitro* research using animal models which follows.

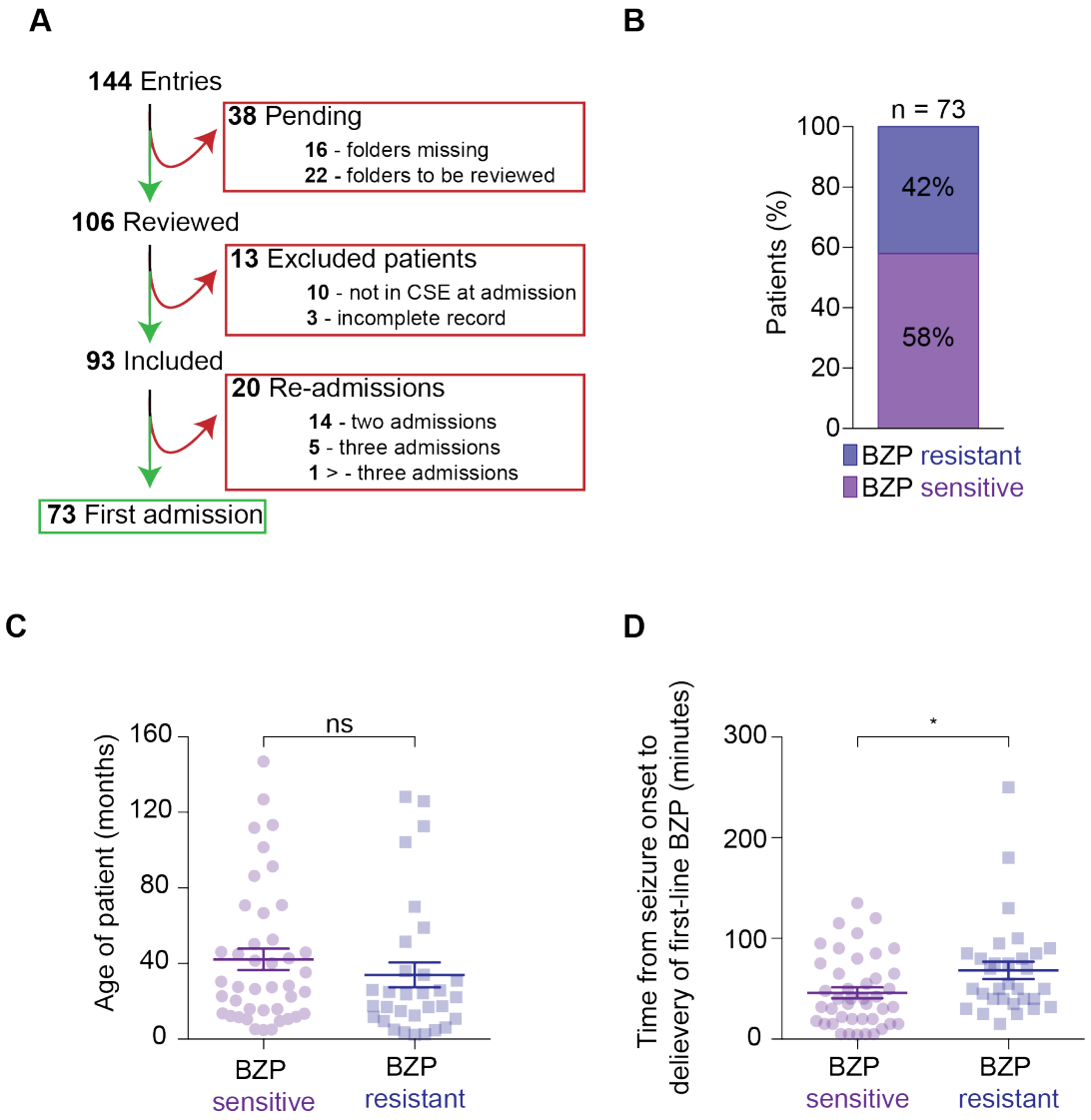

Figure 3.1: Local paediatric prevalence of benzodiazepine-resistant convulsive status epilepticus. **A**, Flow-diagram showing how the data was selected for the interim analysis. **B**, The proportion of the selected patients who are resistant to first-line treatment with benzodiazepines. **C**, There was no significant difference in ages between patients in the two groups. **D**, In the benzodiazepine-resistant group, there was a significantly longer delay from seizure onset to the time the first-line benzodiazepine agent was given. ns = not significant ($p > 0.05$), *$p < 0.05$.

3.2 Diazepam enhances $GABA_AR$ mediated signaling

The aim of these experiments was to confirm that benzodiazepines positively modulate $GABA_AR$-mediated fast synaptic transmission. To achieve this, I performed whole-cell patch-clamp recordings on pyramidal cells whilst eliciting and comparing $GABA_AR$ synaptic currents (GSCs) in the presence of the benzodiazepine, diazepam, and its competitive antagonist, flumazenil. I repeated these experiments using two different experimental paradigms.

In the first experiment, I used organotypic brain slices prepared from GAD2-cre-tdTomato mice (as described in Section 2.2.2 and 2.2.4). At day 1 in culture, I injected AAV1 containing floxed-STOP channelrhodopsin (ChR2) into the slices using a custom built pressure ejection system, Openspritzer (Forman et al., 2017). After several days in culture, ChR2 was progressively and selectively expressed in the GAD2 expressing interneurons. I then performed voltage-clamp recordings on CA1 pyramidal cells after 6-14 days in culture. To elicit GSCs, I used blue light photoactivation (17.1mW, 100ms) of the ChR2-expressing interneurons to trigger endogenous synaptic release of GABA. Pyramidal cells were voltage-clamped at -40mV in order to increase the Cl^- driving force. Moreover, I used a high Cl^- internal solution (141mM) to artificially load the cell with Cl^-. This was done to accentuate $GABA_AR$-mediated signalling. GSCs evoked under these condition generated negative currents that represent Cl^- efflux. In order to prevent the generation of action potentials, I added the intracellular voltage-gated Na^+ channel blocker, QX314 (5μM), to the internal solution. In addition, to block the activation of $GABA_B$ receptors, I added CGP55845 (10μM) to the perfusing aCSF solution.

The recording protocol consisted of 30 x 10 second traces in standard aCSF solution. Light stimulation was triggered 2 seconds into each 10 second trace. I then added 3μM diazepam to the aCSF. A 5 minute delay was set before repeating the stimulation protocol. This was done to allow for full perfusion of the submerged chamber with the diazepam-containing solution. Thereafter, in order to reverse any diazepam effect, I washed in aCSF containing the benzodiazepine competitive antagonist, flumazenil (0.4μM) and repeated the same recording protocol. For the analysis, I measured the mean amplitude and time constant (tau). I then compared these metrics across the different treatment groups.

For the second experiment, I prepared acute brain slices from the GAD2-cre-tdTomato mice on the same day of the experiment (see Section 2.2.3). Coronal brain slices including the entorhinal cortex were prepared and I then performed whole-cell recordings on layer V pyramidal cells. To elicit GSCs in these slices, I electrically stimulated the surrounding GAD2-interneurons in the presence of the glutamate-receptor blocker, kynurenic acid (2μM). The same internal solution, blockers and recording protocol was used as described above.

3.2.1 Diazepam enhances the decay time constant, but not the amplitude of light-induced $GABA_AR$ synaptic currents in organotypic brain slices

In organotypic CA1 pyramidal cells ($n = 8$), diazepam increased the mean amplitude of the light-induced GSCs compared to baseline (297.70 ± 38.74pA vs 315.00 ± 42.96pA, $p = 0.08$, *paired t-test*), however this result was not statistically significant (see Figure 3.2). The application of flumazenil decreased the current size compared to the diazepam group (297.40 ± 38.53pA vs 315.00 ± 42.96pA, $p = 0.09$, *paired t-test*) with it showing no difference compared to the baseline GSCs (297.70 ± 38.74pA vs 297.40 ± 38.53pA, $p = 0.87$, *paired t-test*).

However, diazepam significantly increased the GSC decay time constant (tau) compared to baseline (43 ± 4 ms vs 57 ± 6 ms, $p = 0.004$, *paired t-test*). This was then reversed by the flumazenil (57 ± 6ms vs 40ms ± 4ms, $p = 0.005$, *paired t-test*). There was no difference between the time-constants of the baseline and flumazenil groups (43 ± 4ms vs 40 ± 4ms, $p = 0.50$, *paired t-test*).

Figure 3.2 ***(following page)*:** Diazepam enhances the decay time constant but not the amplitude of light-induced $GABA_AR$ currents in organotypic brain slices. **A**, Whole-cell patch-clamp recordings ($n = 8$) from CA1 pyramidal cells in organotypic brain slices. **B**, During 10s sweeps, $GABA_AR$ synaptic currents (GSCs) were elicited at 2s by photoactivation (17.1mW, 100ms) of ChR2-expressing interneurons. The mean GSC was calculated from 30 traces in each of the different treatment groups: baseline (B, black), diazepam - 3μM (D, red) and flumazenil - 0.4μM (F, purple). **C**, Population data of mean GSC amplitudes in each of the treatment groups showing no significant difference between them. **D**, Deactivation kinetics of $GABA_AR$ could be fitted by a single exponential function (grey line) to allow for the decay time constant (tau) to be calculated. **E**, Population data of taus for each group showing that diazepam significantly increased the taus, with this effect being reversed by the application of flumazenil. ns = not significant ($p > 0.05$), $^{**}p \leq 0.01$. DG - dentate gyrus.

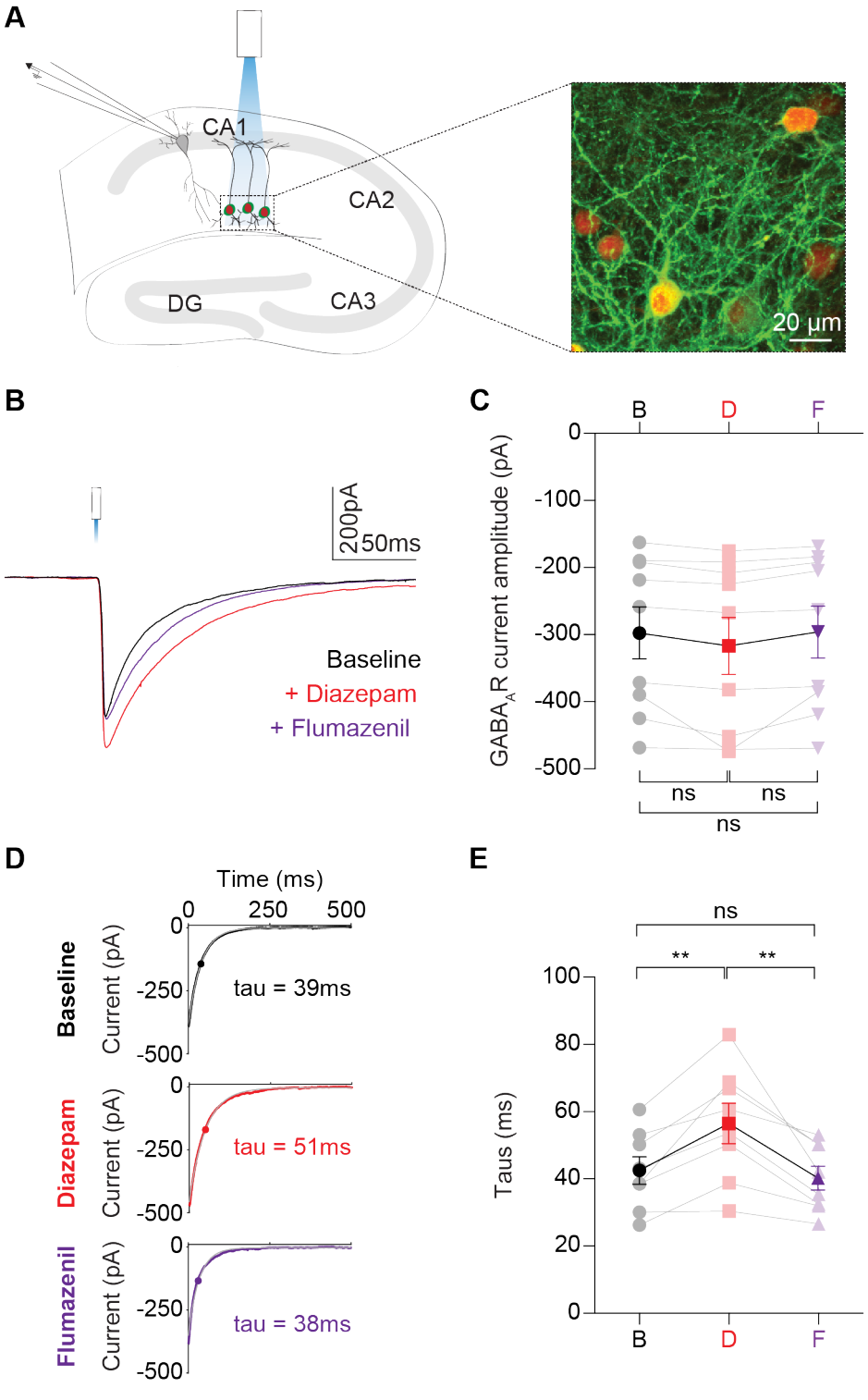
A
CA1
CA2
DG
CA3
20 µm
B
200pA
50ms
Baseline
+ Diazepam
+ Flumazenil
C
B
D
F
0
-100
-200
-300
-400
-500
GABA$_A$R current amplitude (pA)
ns
ns
ns
D
Time (ms)
0
250
500
Baseline
Diazepam
Flumazenil
Current (pA)
0
-250
-500
tau = 39ms
tau = 51ms
tau = 38ms
E
ns
**
**
100
80
60
40
20
0
Taus (ms)
B
D
F

3.2.2 Diazepam enhances both the amplitude and the decay time constant of $GABA_AR$ synaptic currents in acute brain slices

As shown in Figure 3.3, in acute brain slices ($n = 8$), diazepam significantly increased the amplitude of the electrically-evoked GSCs (216.50 ± 33.58pA vs 350.80 ± 56.00pA, $p = 0.003$, *paired t-test*). This was then reversed by the application of flumazenil (350.80 ± 56.00pA vs 215.40 ± 31.64pA, $p = 0.003$, *paired t-test*). There was no difference in amplitude between baseline and flumazenil groups (216.50 ± 33.58pA vs 215.40 ± 31.64pA, $p = 0.94$, *paired t-test*).

In addition, diazepam lengthened the decay time constant compared to baseline (24 ± 2ms vs 32 ± 3ms, $p = 0.001$, *paired t-test*) and flumazenil (32 ± 3ms vs 24 ± 2ms, $p = 0.003$, *paired t-test*). Again, there was no difference between baseline and flumazenil groups (24ms ± 2ms vs vs 24 ± 2ms, $p = 0.84$, *paired t-test*).

Through these experiments, I was able to confirm that diazepam positively modulates $GABA_AR$-mediated synaptic currents in both organotypic and acute brain slice preparations. Furthermore, this effect is reversed by the application of the competitive antagonist, flumazenil.

Figure 3.3 ***(following page)*:** Diazepam enhances the amplitude and decay time constant of $GABA_AR$ currents in acute brain slices. **A**, Whole-cell patch-clamp recordings ($n = 7$) from layer V pyramidal cells in entorhinal cortex in mouse acute brain slices. **B** During 10s sweeps, $GABA_AR$ currents (GSCs) were elicited by electrical stimulation of afferent fibers (2pA, 3ms) in the presence of the glutamate receptor blocker, kynurenic acid (2μM). The mean GSC was calculated from 30 traces in each of the different treatment groups: baseline (B, black), diazepam - 3μM (D, red) and flumazenil - 0.4μMM (F, purple). **C**, Population data of mean GSC amplitudes in each of the treatment groups showing a significant increase in GSC size in the presence of diazepam that was then reversed by flumazenil. **D**, Deactivation kinetics of $GABA_AR$ currents could be fitted by a single exponential function (grey line) to allow for the time constant (tau) to be calculated. **E**, Population data of taus for each group showing diazepam significantly increased taus with this effect being reversed by the application of flumazenil. ns = not significant ($p > 0.05$), $^{**}p \leq 0.01$. S - subiculum, MEnt - medial entorhinal cortex, LEnt - lateral entorhinal cortex, DG - dentate gyrus.

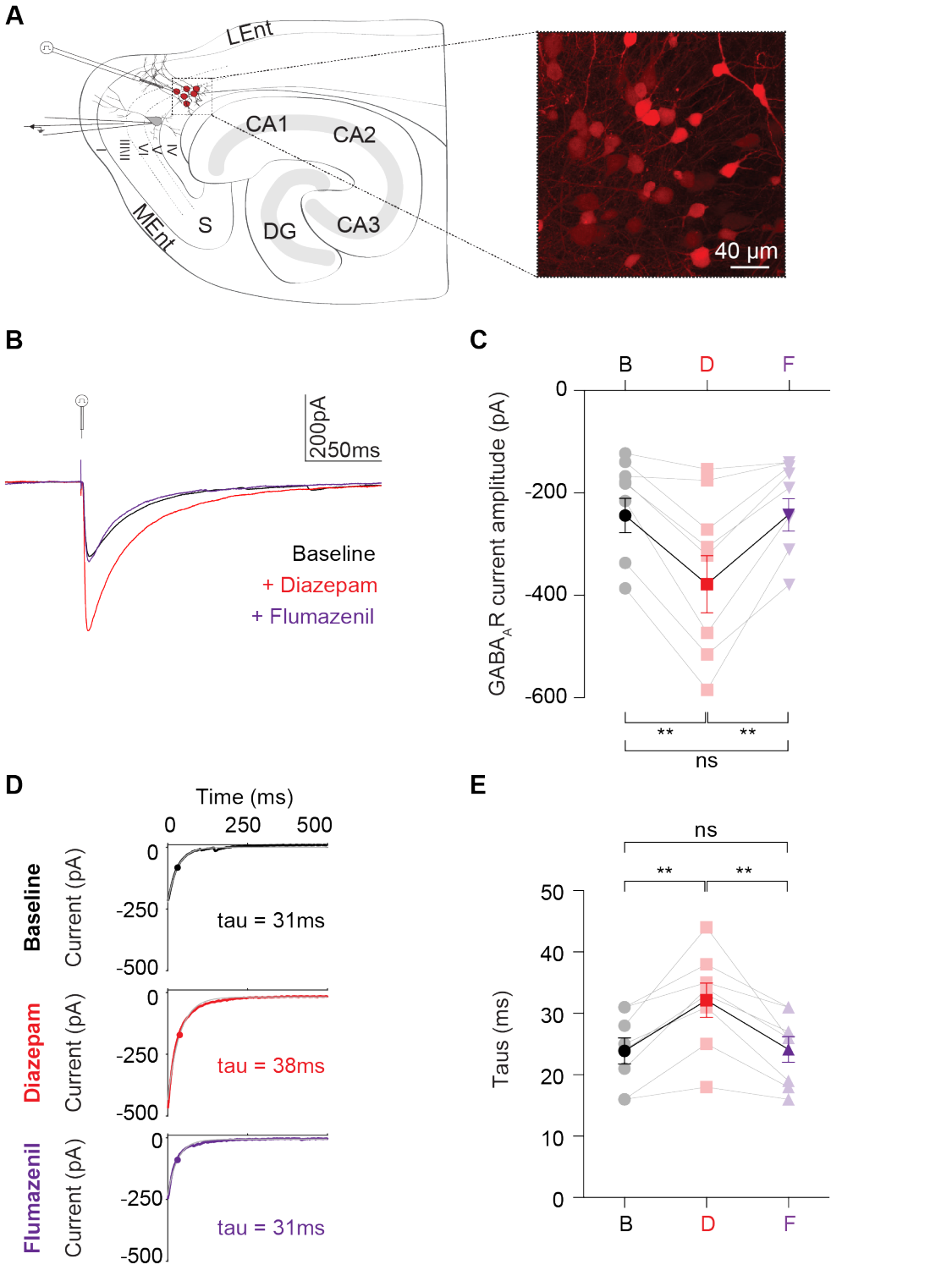
A
LEnt
CA1
CA2
CA3
DG
S
MEnt
40 µm
B
200pA
250ms
Baseline
+ Diazepam
+ Flumazenil
C
B
D
F
GABA$_A$R current amplitude (pA)
0
-200
-400
-600
**
**
ns
D
Time (ms)
0
250
500
Baseline
Current (pA)
tau = 31ms
Diazepam
tau = 38ms
Flumazenil
tau = 31ms
E
ns
**
**
Taus (ms)
50
40
30
20
10
0

3.3 0 Mg^{2+} is a reliable *in vitro* model of status epilepticus

To study the effect of diazepam on prolonged seizure states, I first needed to establish a working *in vitro* model of SE. Previous data suggested that the 0 Mg^{2+} model reliably elicits both single seizure-like events (SLEs) followed by recurrent bursting activity known as the late recurrent discharge (LRD) phase (Zhang et al., 1995; Albus et al., 2008). The LRD phase is thought to be an *in vitro* replica of the ongoing unrelenting epileptiform discharges that occurs during SE.

In these experiments, I performed local field potential recordings in organotypic and acute brain slices using an interface perfusion chamber (see Section 2.5.1). The recording protocol would include a 5-10 minute calibration period in standard aCSF, whereafter I would remove Mg^{2+} from the aCSF (0 Mg^{2+}). I then noted the differences in SLE and LRD propensity between the organotypic and acute brain slices. In addition, the time delay from when 0 Mg^{2+} was washed to the onset of SLE and LRD was calculated.

3.3.1 The 0 Mg^{2+} model elicits prolonged seizure states in both organotypic and acute brain slices

Recordings were made from the CA1 region of organotypic brain slices ($n = 52$) and entorhinal cortex in acute brain slices ($n = 64$) (see Figure 3.4). SLEs were elicited in 79% of the organotypic brain slices ($n = 41$) and 64% of the acute brain slices ($n = 41$). However, of these slices only 54% of the organotypic brain slices ($n = 22$) and 32% of the acute brain slices ($n = 15$) continued into the LRD phase. There was no significant difference in SLE propensity ($p = 0.15$, *Fisher's exact test*) or LRD propensity ($p = 0.18$, *Fisher's exact test*) between the different tissue preparations.

Interestingly, organotypic brain slices appear to have SLEs more rapidly compared to acute brain slices (533.12 ± 30.09s vs 2183s ± 149.70s, p <0.0001, *Mann-Whitney test*). Moreover, organotypic brain slices go into the LRD phase sooner than acute brain slices (1365.23 ± 112.20s vs 5461s ± 403.80s, p <0.0001, *Mann-Whitney test*).

From this data, I was able to confirm that the 0 Mg^{2+} model can reliably elicit prolonged seizure activity *in vitro*. Furthermore, there appear to be differences in SLE and LRD onset times between the organotypic and acute brain slice preparations.

Figure 3.4 *(following page)*: The 0 Mg^{2+} *in vitro* model of status epilepticus. **A**, Local field potential recording from CA1 in an hippocampal organotypic slice on an interface perfusion chamber. The recording starts with a 10 min calibration in standard aCSF (Std, grey) followed by washing in 0 Mg^{2+} (purple). The time from 0 Mg^{2+} wash in to first seizure-like event (SLE, orange) and entry into the late recurrent discharge phase (LRD, blue) are depicted. **B**, A recording from entorhinal cortex in an acute brain slice. **C**, The organotypic brain slices (black outline) tended to have a higher propensity for SLEs and LRD compared to acute brain slices (grey outline), but this was not statistically significant. **D**, Organotypic brain slices have SLEs sooner and more rapidly enter into the LRD phase compared to acute brain slices. ns = not significant ($p > 0.05$), ****$p \leq 0.0001$.

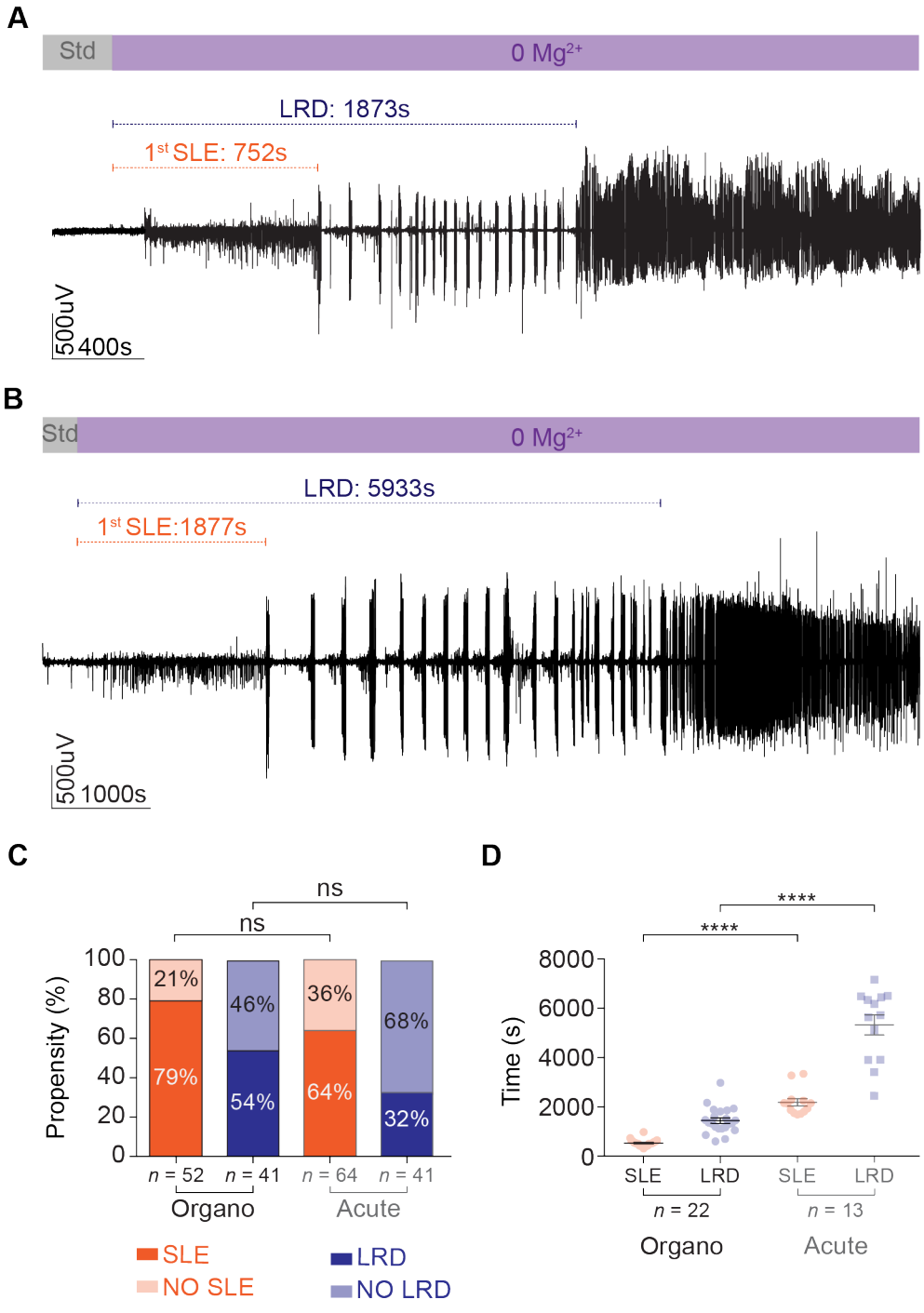
A
Std
0 Mg2+
LRD: 1873s
1st SLE: 752s
500uV
400s
B
Std
0 Mg2+
LRD: 5933s
1st SLE:1877s
500uV
1000s
C
ns
ns
Propensity (%)
100
80
60
40
20
0
21%
79%
46%
54%
36%
64%
68%
32%
n = 52
n = 41
n = 64
n = 41
Organo
Acute
SLE
NO SLE
LRD
NO LRD
D
****
****
Time (s)
8000
6000
4000
2000
0
SLE
LRD
SLE
LRD
n = 22
n = 13
Organo
Acute

3.4 Differential effect of diazepam on the 0 Mg^{2+} *in vitro* model of status epilepticus

Having established a working 0 Mg^{2+} model of SE, I then sought to study the effect of diazepam on these prolonged seizure states. In order to extend data from previous studies (Zhang et al., 1995; Dreier et al., 1998; Albus et al., 2008), the aim of these experiments was to investigate the effect of diazepam on the evolution of seizure activity in the 0 Mg^{2+} model using organotypic brain slices.

To achieve this, I setup three different experimental paradigms (see Figure 3.5). The first was a control group ($n = 13$) where after the 5-10 minute calibration period 0 Mg^{2+} was washed in. The second, the early group ($n = 10$), included washing in diazepam (3μM) with the 0 Mg^{2+}. The third, the late group ($n = 9$), only introduced diazepam after LRD was established. Various properties of epileptiform activity were measured including the time to SLE onset, SLE duration, the frequency of SLEs prior to entry into the LRD phase and the time to the onset of the LRD phase. In addition, a 60 second window of LRD activity was analysed. This window was taken at a standard point across all three groups, exactly 7 minutes after the onset of LRD. This includes the 2 minutes of ongoing bursting activity to confirm entry into the LRD phase (Section 2.6.2). Furthermore, a 5 minute delay was then added to accommodate full perfusion of the interface chamber with a new solution. This was relevant to the late group when diazepam was only introduced after initiation of the LRD phase. Within these 60 second windows, I then measured the discharge duration, frequency and inter-discharge interval.

For the analysis, I only included recordings if they did not have any SLEs during the 5-10 minute calibration period. Furthermore, recording needed to display SLEs followed by LRD. Traces where only SLEs or LRD existed were not included. Importantly, in order to eliminate any possibility of bias introduced during the analysis, the experimental traces were randomised and I was blinded to which treatment group they belonged to (as explained in Section 2.8).

3.4.1 Early application of diazepam has a significant anticonvulsant effect while late application augments bursting activity in the LRD phase

As illustrated in Figures 3.5 and 3.6, when diazepam is introduced early, it significantly delayed the onset of SLEs compared to the control (522.15 ± 45.93s vs 799.73s ± 89.81s, p =0.003, *Mann-Whitney test*) and late groups (548.8 ± 34.46s vs 799.73 ± 89.81s, p =0.008, *Mann-Whitney test*). Moreover, washing diazepam in early significantly decreased SLE duration compared to control (21.04 ± 1.69s vs 14.57 ± 1.66s, p =0.013, *unpaired t-test*) and late groups (27.41 ± 2.72s vs 14.57 ± 1.66s, p =0.001, *unpaired t-test*). Furthermore, there was a significant decline in SLE frequency before entry into the LRD in the early group compared to control (10.85 ± 1.66 vs 5.00 ± 3.06, p =0.01, *unpaired t-test*) and late groups (11.33 ± 1.78 vs 5.00 ± 3.06, p =0.005, *unpaired t-test*). There was no difference between the control and late groups in SLE onset (522.15 ± 45.93s vs 548.8 ± 34.46s, p =0.50, *Mann-Whitney test*), duration (21.04 ± 1.69s vs 27.41 ± 2.72s, p =0.07, *unpaired t-test*) or frequency (10.85 ± 1.66 vs 11.33 ± 1.78, p =0.85, *unpaired t-test*). Taken together this demonstrates that diazepam has a significant anticonvulsant effect on the 0 Mg^{2+} model when it is applied early.

In terms of entry into the LRD phase, in the early group there was a significant delay vs the control (1429 ± 187.1s vs 2623 ± 513.9s, p =0.03, *Mann-Whitney test*) and late groups (1274 ± 169.2s vs 2623 ± 513.9s, p =0.0004, *Mann-Whitney test*). Within the defined 60 second analysis windows, there was a significant increase in discharge duration between both the control versus early (2.4 2± 0.41s vs 4.44 ± 0.68s, p =0.02, *Mann-Whitney test*) and late groups (2.42 ± 0.41s vs 4.72 ± 2.62s, p =0.02, *Mann-Whitney test*). Furthermore, there was a significant decrease in discharge frequency in the 60 second window between control versus the early (12.92 ± 1.77 vs 7.10 ± 1.52, p =0.0005, *Mann-Whitney test*) and late groups (12.92 ± 1.77 vs 7.44 ± 0.99, p =0.01, *Mann-Whitney test*). There was no difference between early and late groups in either discharge duration (4.44 ± 0.68s vs 4.72 ± 2.62s, p =0.81, *unpaired t-test*) or frequency (7.10 ± 1.52 vs 7.44 ± 0.99, p =0.76, *unpaired t-test*). Although it is not shown in Figure 3.6, there was no significant difference in the inter-discharge interval between the control and the early (5.20 ± 0.72 vs 6.00 ± 1.05, p =0.51, *Mann-Whitney test*) or late groups (5.20 ± 0.72 vs 6.56 ± 0.88, p =0.25, *Mann-Whitney test*). These findings suggest that the presence of diazepam once LRD has been established does not reduce epileptiform activity. On the contrary, diazepam increases the duration of discharges without affecting the inter-discharge interval.

From these experiments I have demonstrated that diazepam has a differential effect on evolution of epileptiform activity using the 0 Mg^{2+} model depending on whether it is applied 'early' or 'late'.

Figure 3.5 ***(following page)*:** Differential effect of diazepam on the 0 Mg^{2+} model of status epilepticus in organotypic brain slices. **A**, Control experiment where 0 Mg^{2+} was washed in after a 5-10 minute calibration period. Time to SLE onset (orange) and entry into the LRD phase (blue) are marked. **B**, Early application of diazepam (3μM) introduced when 0 Mg^{2+} is washed in. **C**, Late group where diazepam only washed in after the LRD phase had been established. Windows $t_{1\text{-}3}$ highlight individual SLEs shown in Figure 3.6, **A**. Windows $t_{4\text{-}6}$ highlight 60s of LRD used for analysis as shown in Figure 3.6, **E**.

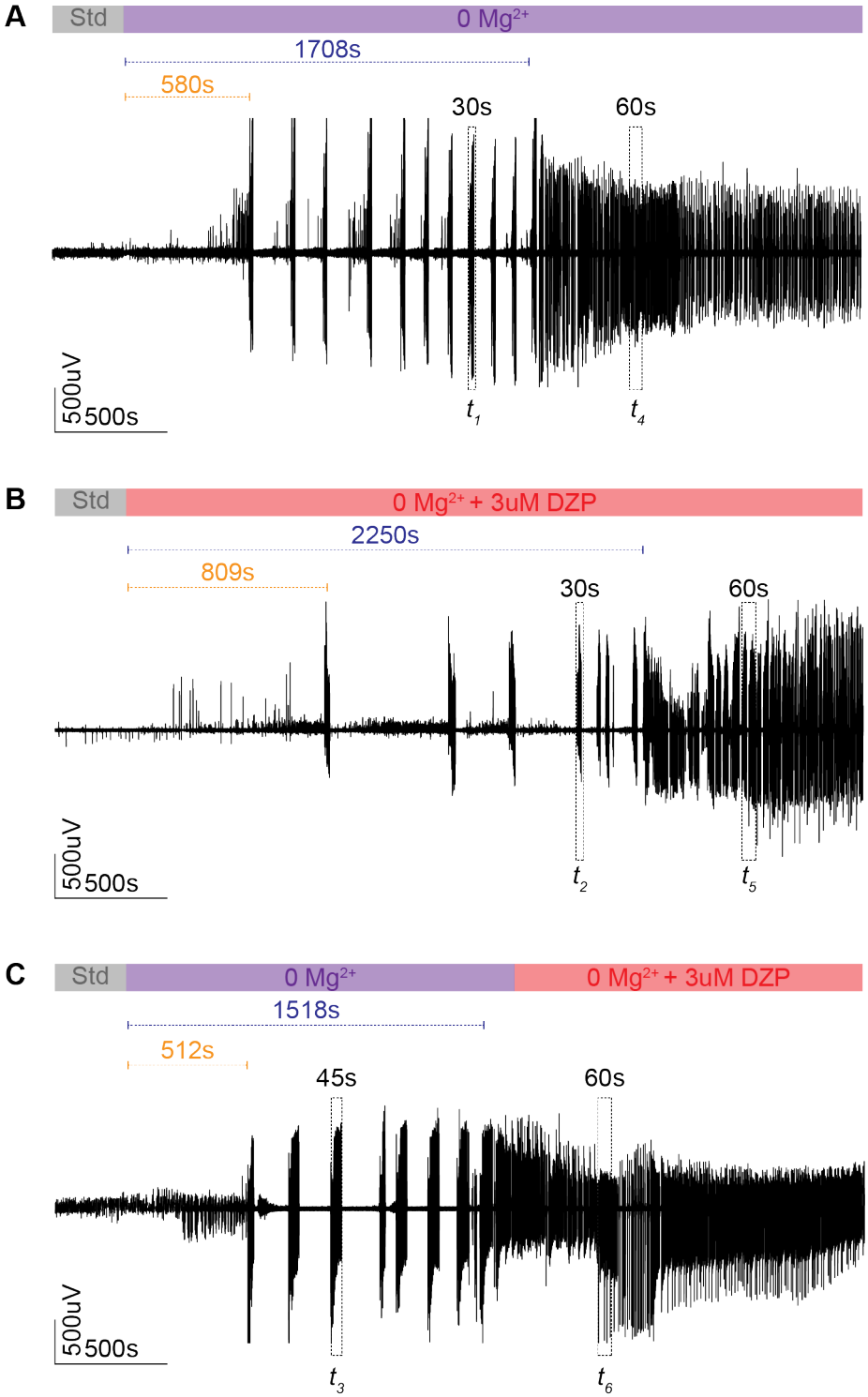
A
Std
0 Mg2+
1708s
580s
30s
60s
500uV
500s
t1
t4
B
Std
0 Mg2+ + 3uM DZP
2250s
809s
30s
60s
500uV
500s
t2
t5
C
Std
0 Mg2+
0 Mg2+ + 3uM DZP
1518s
512s
45s
60s
500uV
500s
t3
t6

Figure 3.6 ***(following page)*:** Population data showing the differential effect of diazepam on the 0 Mg^{2+} model of status epilepticus in organotypic brain slices. The data in this figure follows from the experimental paradigms presented in Figure 3.5. **A**, $t_{1\text{-}3}$ showing individual SLEs from the control (t_1), early (t_2) and late groups (t_3). **B**, Population data showing that early introduction of diazepam delays SLE onset whilst decreasing SLE duration, **C**, and frequency before entry into the LRD phase, **D**. **E**, $t_{4\text{-}6}$ marking the 60 second windows used to analyse LRD activity in the control (t_4), early (t_5) and late groups (t_6). **F**, Population data showing that diazepam delays onset of LRD in the early group. The presence of diazepam in the early and late groups increases discharge duration, **G**, while decreasing discharge frequency, **H**. ns = not significant ($p > 0.05$), * $p \leq 0.05$, ** $p \leq 0.01$, *** $p \leq 0.001$.

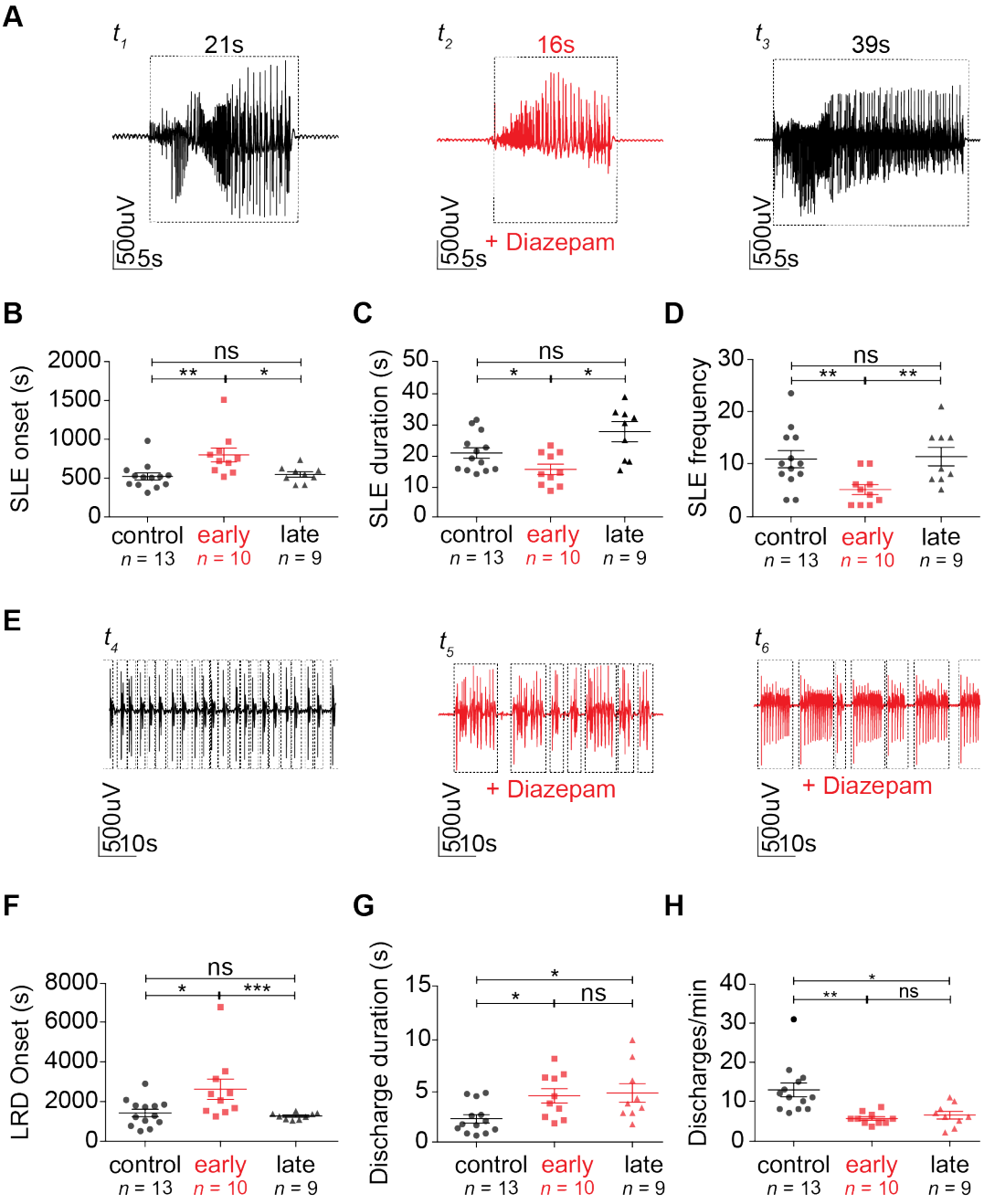
A
t1
21s
500uV
5s
t2
16s
+ Diazepam
t3
39s
B
SLE onset (s)
ns
control
early
late
n = 13
n = 10
n = 9
C
SLE duration (s)
D
SLE frequency
E
t4
t5
t6
10s
F
LRD Onset (s)
G
Discharge duration (s)
H
Discharges/min

3.5 GABAergic signalling is strongly depolarising during the late recurrent discharge phase

Previously in this Chapter (see Section 3.2), I showed that diazepam positively modulates $GABA_AR$-mediated signalling. Having now shown that diazepam has a differential effect on the evolution of *in vitro* SE (see Section 3.4), I then focused on exploring changes in the properties of $GABA_AR$-mediated signalling during these states. While previous work has confirmed a transient excitatory shift in $GABA_AR$ function during single SLEs (Ilie et al., 2012; Ellender et al., 2014), to date there is no data confirming whether this may still be relevant in the LRD phase which models SE.

3.5.1 Optogenetic activation of interneurons drives excitatory signalling in the evolution of prolonged seizure states

Using the same optogenetic paradigm described in Section 3.2, I performed whole cell recordings on CA1 pyramidal cells in organotypic brain slices ($n = 7$). Voltage-clamp was used with cells clamped at -40mV using a standard internal solution (see Section 2.4.2). The ChR2 expressing GAD2-interneurons were then activated every 7s with 100ms of blue-light illumination. After 3 minutes of recording in standard aCSF, 0 Mg^{2+} was washed in and SLEs and LRD allowed to develop. After at least 5 minutes of LRD, I then reintroduced standard aCSF in an attempt to arrest the LRD phase. Only traces with both SLEs and LRD were included in the analysis.

In order to study changes in the light-induced currents, I used a combination of both automated and manual detection methods to measure the size and direction of these currents. Figure 3.7 demonstrates the experimental protocol using current-clamp. Figure 3.8 then shows the same protocol in voltage-clamp with population data highlighting the changes in light-induced currents. The light-induced currents are an unspecified combination of both $GABA_AR$, $GABA_BR$ and possibly disynaptic glutamate receptors.

There was a significant positive shift in the direction of light-induced currents during a single SLE, t_2, vs baseline, t_1 (448.80 ± 70.34pA vs -752 ± 88.67pA, p =0.0002, *paired t-test*). This would recover after the SLE had self-terminated. There was a significant change in the currents during SLE recovery, t_3, versus those seen during the after-discharge phase of the SLE, t_2 (-752.00 ± 88.67pA vs 536.50 ± 134.90pA, p =0.0007, *paired t-test*). Furthermore, light-induced currents during the LRD phase, t_4, were significantly more depolarising compared to recovery after the single SLE, t_3 (536.50 ± 134.90pA vs -894.00 ± 164.80pA, p =0.0018, *paired t-test*). After reintroduction of Mg^{2+}-containing aCSF and termination of LRD, the currents again became significantly hyperpolarising, t_6, compared to those observed during the LRD phase, t_4 (-894.00 ± 164.80pA vs 242.00 ± 21.21pA, p =0.0005, *paired t-test*). There was no significant difference in amplitude between induced currents during SLE, t_2, and LRD, t_4 (-752.00 ± 88.67pA vs -894.00 ± 164.80pA, p =0.18, *paired t-test*). However, the light-induced currents appear significantly smaller after recovery from LRD, t_6, compared to baseline, t_1 (242.00 ± 21.21pA vs 448.80 ± 70.34pA vs, p =0.04, *paired t-test*).

3.5.2 Prolonged seizure activity leads to a significant decrease in light-induced GABAergic conductances

In comparing the amplitude of the light-induced currents before and after seizure activity (see Figure 3.9), there was a significant decrease between baseline (t_1) and recovery (t_6) (448.80 ± 70.34pA vs 242.00 ± 21.21pA, p =0.04, *paired t-test*). Furthermore, step protocols performed before baseline and after recovery (see Figure 3.7) show a significant decrease in conductance in the light-induced currents (17.79 ± 5.93nS vs 12.37 ± 5.18nS, p =0.02, *Wilcoxon test*). Importantly, there was no change in access resistance (15.50 ± 1.87mΩ vs 17.12 ± 5.91mΩ, p =0.13, *paired t-test*) nor in membrane potential (-58.75 ± 2.22mV vs -59.37 ± 2.36mV, p =0.19, *paired t-test*). This confirms that the observed decrease in current amplitude and conductance was not as a consequence of the whole-cell recording deteriorating over time.

Figure 3.7 ***(following page)*:** Transient shifts in the effect of GABAergic interneurons during the evolution of prolonged seizure activity. **A**, Current-clamp recording from a CA1 pyramidal cell in an organotypic slice with photoactivation of ChR2-expressing GAD2 interneurons (100ms every 7s at 17.1mW). After 3 minutes of recording in standard aCSF (Std, grey), 0 Mg^{2+} aCSF (purple) was washed in. After at least 5 minutes of late recurrent discharge (LRD) activity, standard aCSF was washed in. The boxes labelled ($t_{1\text{-}6}$) mark 30 second windows of the trace. **B**, Expanded view of the $t_{1\text{-}6}$ windows. t_1 is taken from baseline, t_2 during the after-discharge phase of a single seizure-like event (SLE), t_3 recovery after single SLE, t_4 cut-out of activity during LRD, t_5 during recovery in standard aCSF showing sudden change in size and direction of light-induced currents and t_6, a cut-out of activity when the slice had fully recovered in standard aCSF.

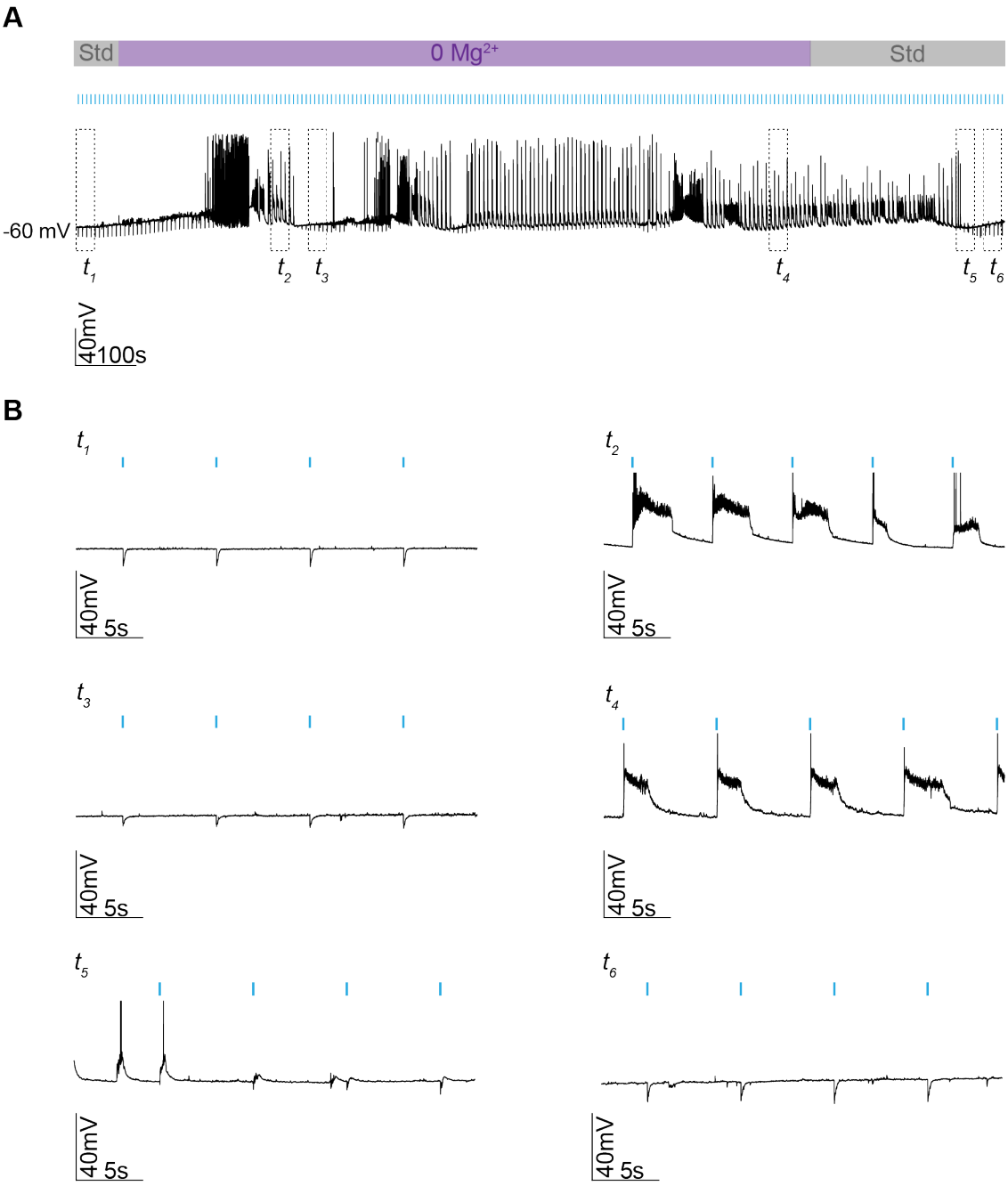
A
Std
0 Mg2+
Std
-60 mV
t1
t2
t3
t4
t5
t6
40mV
100s
B
t1
t2
t3
t4
t5
t6
40mV
5s

Figure 3.8 ***(following page)*:** Activation of GAD2 interneurons results in depolarising currents in pyramidal cells during single and prolonged seizures. **A**, Voltage-clamp recording from a CA1 pyramidal cell in an organotypic slice clamped at -40mV. Photoactivation of ChR2-expressing GAD2 interneurons (17.1mW, 100ms) occurred every 7 seconds. After 3 minutes of recording in standard aCSF (Std, grey), 0 Mg^{2+} aCSF (purple) was washed in. After at least 5 minutes of late recurrent discharge (LRD) activity, standard aCSF was again washed in. The boxes labelled ($t_{1\text{-}6}$) mark 30 second windows of the trace. **B**, Expanded view of the $t_{1\text{-}6}$ windows where t_1 is taken from baseline, t_2 is taken during the after-discharge phase of a single seizure-like event (SLE), t_3 is taken during recovery after single SLE, t_4 is a cut-out of activity during LRD, t_5 is taken during recovery in standard aCSF showing sudden change in size and direction of light-induced currents and t_6 is a cut-out of activity when the slice had fully recovered in standard aCSF. **C**, Population data showing significant changes in current size and direction across the different time intervals $t_{1\text{-}4}$ and t_6. $^{*}p \leq 0.05$), $^{**}p \leq 0.01$, $^{***}p \leq 0.001$.

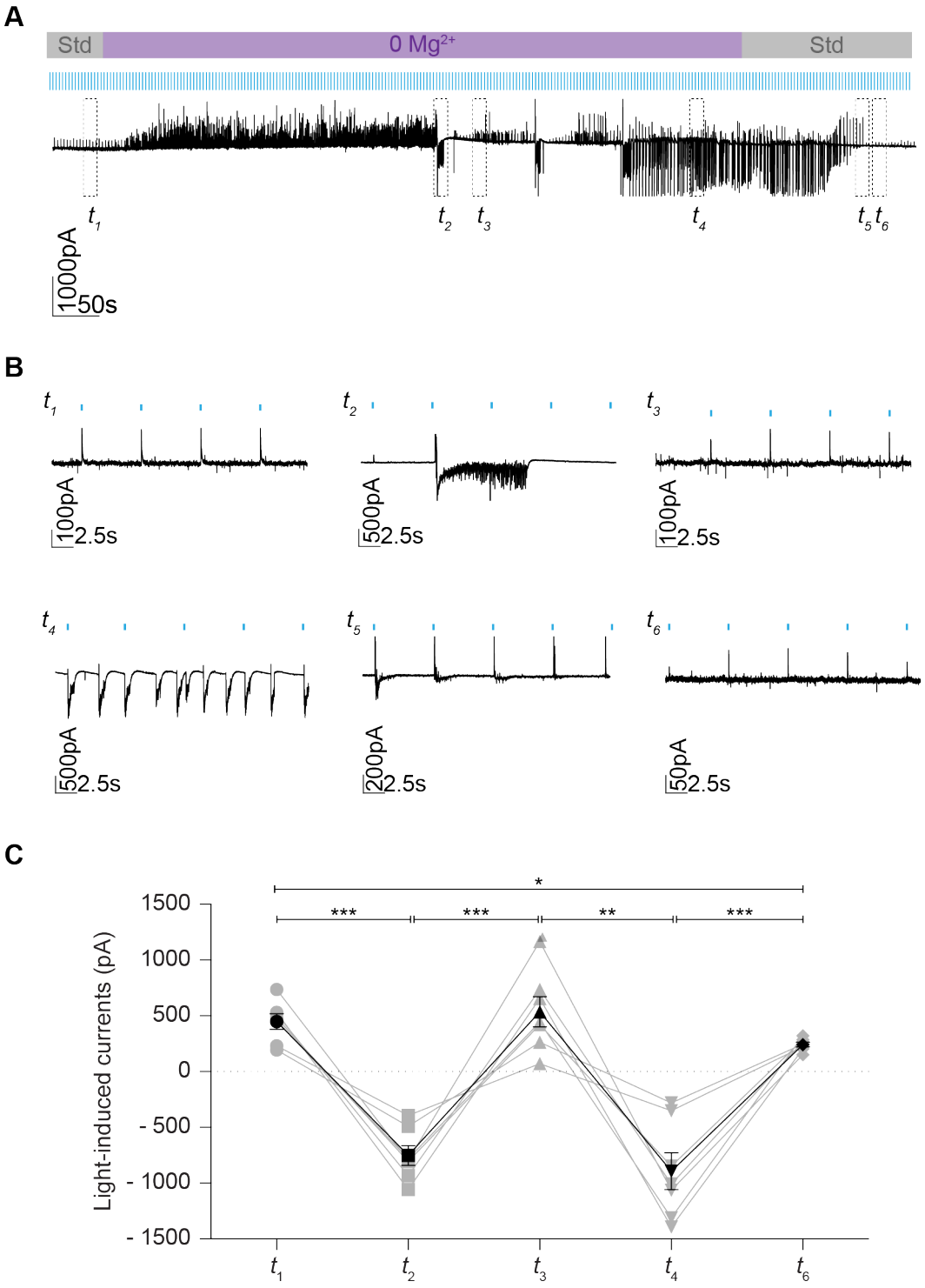
A
Std
0 Mg2+
Std
t1
t2
t3
t4
t5 t6
1000pA
50s
B
t1
100pA
2.5s
t2
500pA
2.5s
t3
100pA
2.5s
t4
500pA
2.5s
t5
200pA
2.5s
t6
50pA
2.5s
C
Light-induced currents (pA)
1500
1000
500
0
- 500
- 1000
- 1500
*
***
***
**
***
t1
t2
t3
t4
t6

Figure 3.9 ***(following page)*:** Changes in baseline GABAergic signalling before and after prolonged seizure activity. **A**, Whole-cell voltage-clamp recording from a CA1 pyramidal cell in an organotypic brain slice clamped at -60mV using an internal solution containing 10mM of Cl^-. A voltage step protocol was followed starting at -100mV and ending at -40mV progressing in 10mV increments. At 1 second after each voltage step, ChR2-expressing GAD2 interneurons were activated with 100ms of blue light (17.1mW). The grey dotted line marks the holding current at each step. The red dotted line marks the GABA currents elicited by photoactivation. The baseline (black) was taken before 0 Mg^{2+} wash in (before t_1 in Figures 3.7 and 3.8). The recovery (blue) was taken after the network had fully recovered from LRD (after t_6 in Figures 3.7 and 3.8). **B**, A current-voltage (IV) plot showing intersection of baseline and light-induced currents at different holding voltages. Reversal potential for the light-induced GABA current E_{GABA} is marked by the black arrow. **C**, Population data showing no difference in E_{GABA} between baseline and recovery. **D**, There was a significant difference in conductance of the light-induced GABA current in the recovery phase compared to baseline. The was no difference in access resistance, **E**, or membrane potential, **F**, between the step protocols in the baseline and recovery groups. ns = not significant ($p > 0.05$), ***$p \leq 0.001$.

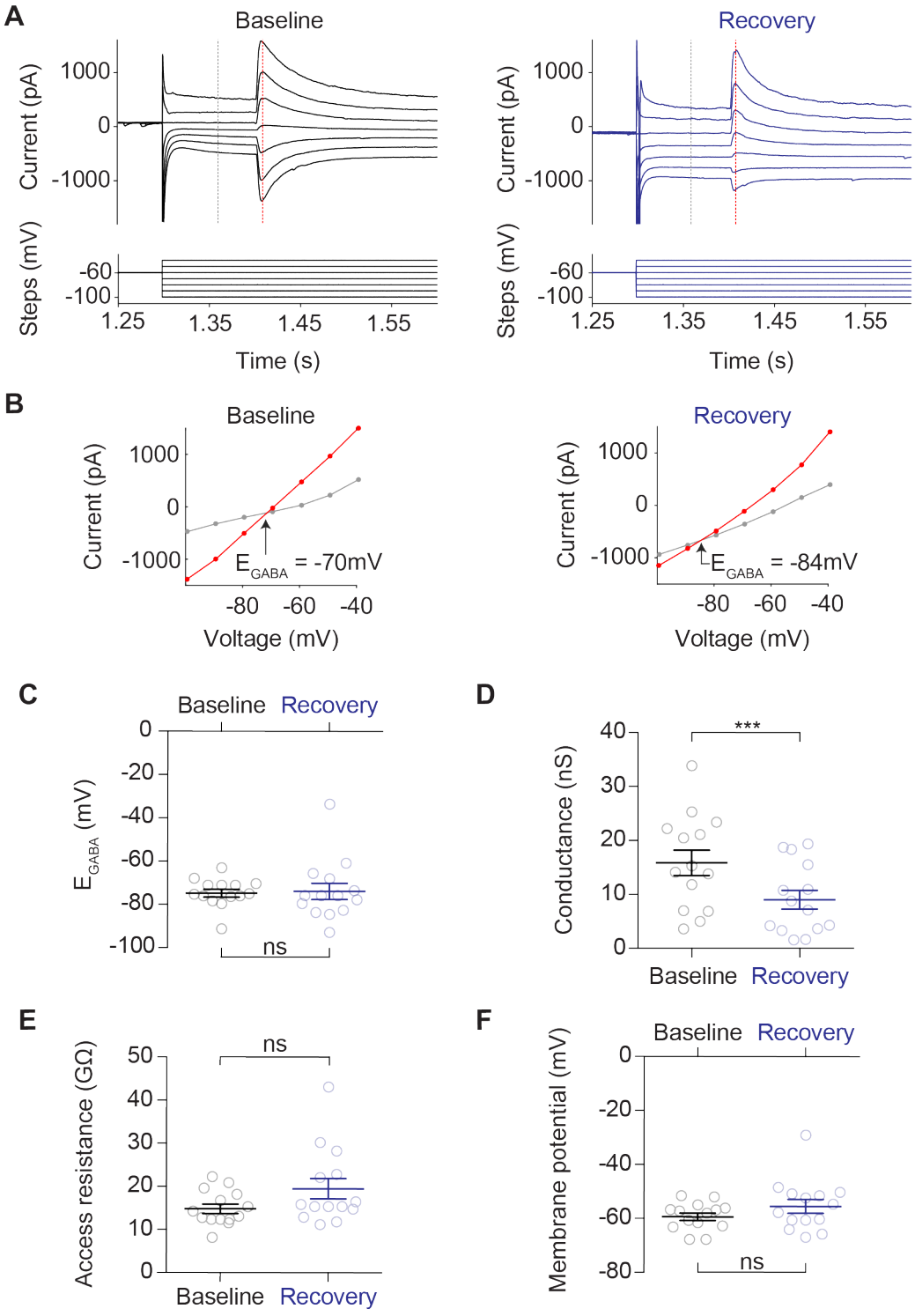
A
Baseline
Recovery
Current (pA)
1000
0
-1000
Steps (mV)
-60
-100
1.25
1.35
1.45
1.55
Time (s)
B
Baseline
Recovery
Current (pA)
E_GABA = -70mV
E_GABA = -84mV
-80
-60
-40
Voltage (mV)
C
Baseline
Recovery
E_GABA (mV)
0
-20
-40
-60
-80
-100
ns
D
Conductance (nS)
40
30
20
10
0
***
Baseline
Recovery
E
Access resistance (GΩ)
50
40
30
20
10
0
ns
Baseline
Recovery
F
Membrane potential (mV)
0
-20
-40
-60
-80
ns
Baseline
Recovery

3.6 Synchronised activation of GAD2 interneurons entrains network activity during the LRD phase through $GABA_AR$ signalling

In previous experiments (see Figures 3.7 and 3.8), I show how photoactivation of GAD2 interneurons drives strongly depolarising currents during the LRD phase. I then noted that the epileptiform discharges that occur during the LRD could be elicited by photoactivation of interneurons (see Figure 3.10). During a 5 minute analysis period taken from the LRD phase, I analysed traces in 7 second frame windows, with light activation occurring 3.5 seconds into the 7 second window. This 7 second window was then divided into smaller 200 millisecond time bins whereby the probability of an epileptiform discharge being initiated could be calculated.

I observed that the probability of eliciting a discharge increased to 0.78 $\pm$ 0.06 during the 200 milliseconds immediately following light application. Furthermore, the probability of the being in a discharge increased for several seconds following light-activation. This suggests that optogenetic activation of GAD2 interneurons entrains the hippocampal network during the LRD phase.

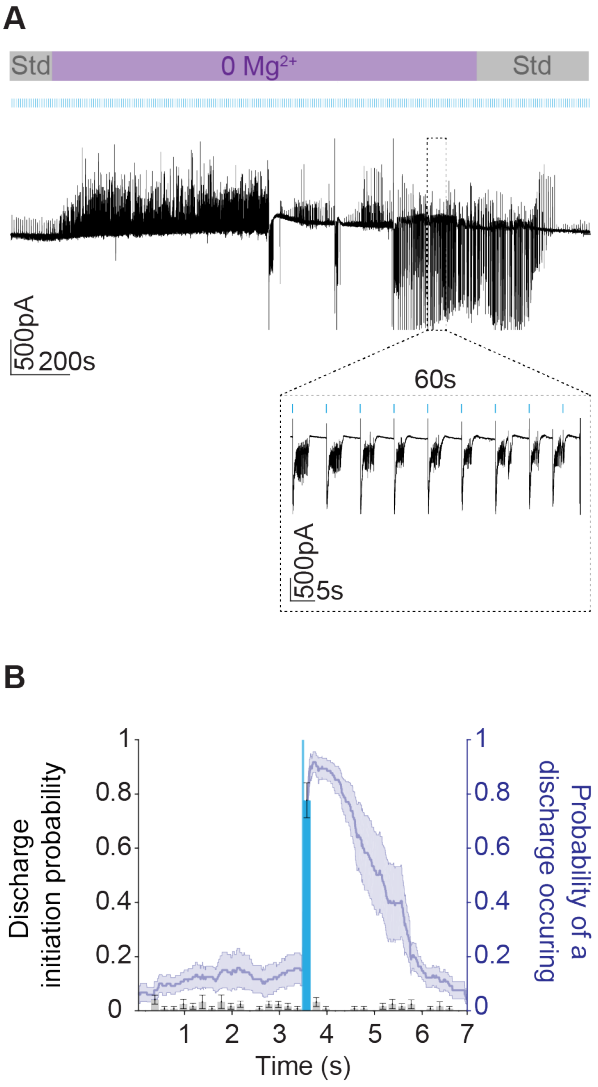

Figure 3.10: Photoactivation of GAD2 interneurons significantly increases discharge probability in the LRD phase. **A**, Whole-cell voltage-clamp recording from a CA1 pyramidal cell in an organotypic slice clamped at -40mV (same trace seen in Figure 3.9). Cut-out is of a 60s window of LRD showing discharges being initiated by photoactivation. **B**, Population data from 7 slices. Left axis (black, histograms with ± SEM) represents the probability of a discharge being initiated in any given 200 millisecond time bin within a 7 second window from a 5 minute LRD analysis period. The right axis (blue, line plot with ± SEM) represents the probability of a discharge being present at the time of photoactivation.

3.6.1 Synchronised activation of GAD2 interneurons is responsible for entraining the hippocampal network during the LRD phase

To provide further evidence to support that this entrainment is indeed due to photoactivation of GAD2 interneurons, I then performed a control experiment to compare discharge probability before and after photoactivation (see Figure 3.11). To do this, I switched on the light only after a minimum of 5 minutes of LRD activity had occurred. The discharge probability at the point the light was switched on significantly increased (0.06 ± 0.02 vs 0.53 ± 0.09, $p = 0.002$, *paired t-test*).

Figure 3.11 ***(following page)*:** Network entrainment follows photoactivation of GAD2 interneurons during the LRD phase. **A**, Whole-cell voltage-clamp recording from a CA1 pyramidal cell in an organotypic brain slice clamped at -40mV. This trace represents a 10 minute window from the onset of LRD. t_1 and t_2 are 60 second windows of activity before and after photoactivation (17.1mW, 100ms) was initiated. **B**, Population data ($n = 7$) from the 5 minute analysis window showing the probability of a discharge initiation in 200 millisecond time bins (black, histograms with ± SEM) as well as the probability of a discharge occurring at any point during the 7 second window (blue, line plot with ± SEM). **C**, Population data showing the mean change in discharge and event probability after photoactivation was initiated. **D**, Graph highlighting how discharge probability significantly increases when the blue light is switched on.

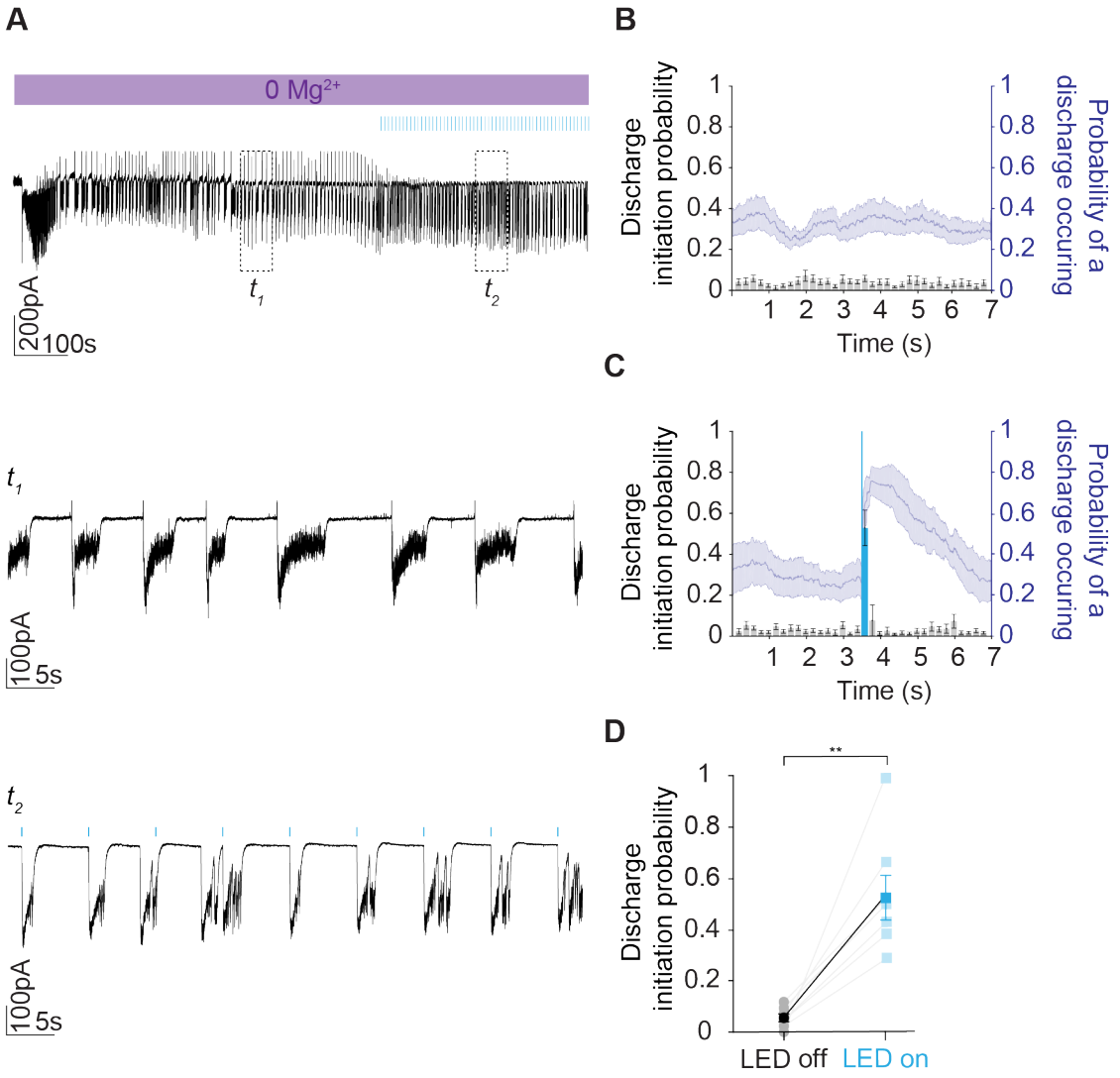
A
0 Mg2+
t1
t2
200pA
100s
t1
100pA
5s
t2
100pA
5s
B
Discharge initiation probability
Probability of a discharge occuring
Time (s)
C
Discharge initiation probability
Probability of a discharge occuring
Time (s)
D
**
Discharge initiation probability
LED off
LED on

3.7 Blocking the $GABA_AR$ reverses network entrainment via optogenetic activation of GAD2 interneurons

Lastly, to test whether excitatory $GABA_AR$ signalling was responsible for these light-induced discharges, I added the $GABA_AR$ blocker, picrotoxin (100uM), to the perfusing aCSF after at least 5 minutes of LRD activity (see Figure 3.12). The picrotoxin did not arrest the LRD activity. However, I did note that the discharge probability following the light stimulus decreased significantly (0.64 ± 0.08 vs 0.08 ± 0.03, p =0.03, *Wilcoxon test*).

Figure 3.12 ***(following page)*:** The $GABA_AR$ antagonist, picrotoxin, decreased network entrainment by photoactivation of GAD2 interneurons. **A**, A whole-cell voltage-clamp recording from a CA1 pyramidal cell in an organotypic brain slice clamped at -40mV. This trace is a 10 minute window from the onset of LRD with light-stimulus (100ms) every 7 seconds. After at least 5 minutes of LRD activity, picrotoxin (100μM) was washed in. t_1 and t_2 are 60a windows of activity before and after picrotoxin (orange) was washed in. **B**, Combined graph of population data ($n = 6$) from the 5 minute analysis window showing the probability that photoactivation initiates a discharge (black, histograms with $\pm$ SEM) and the probability of a discharge bring present is shown in blue (line plot with $\pm$ SEM). **C**, Population data showing the mean change in discharge and event probability after picrotoxin was washed in. **D**, Graph highlighting how discharge probability significantly decreased in the time bin following when the blue light was switched on in 0 Mg^{2+} versus when picrotoxin had been added (orange). $^{**}p \leq 0.01$.

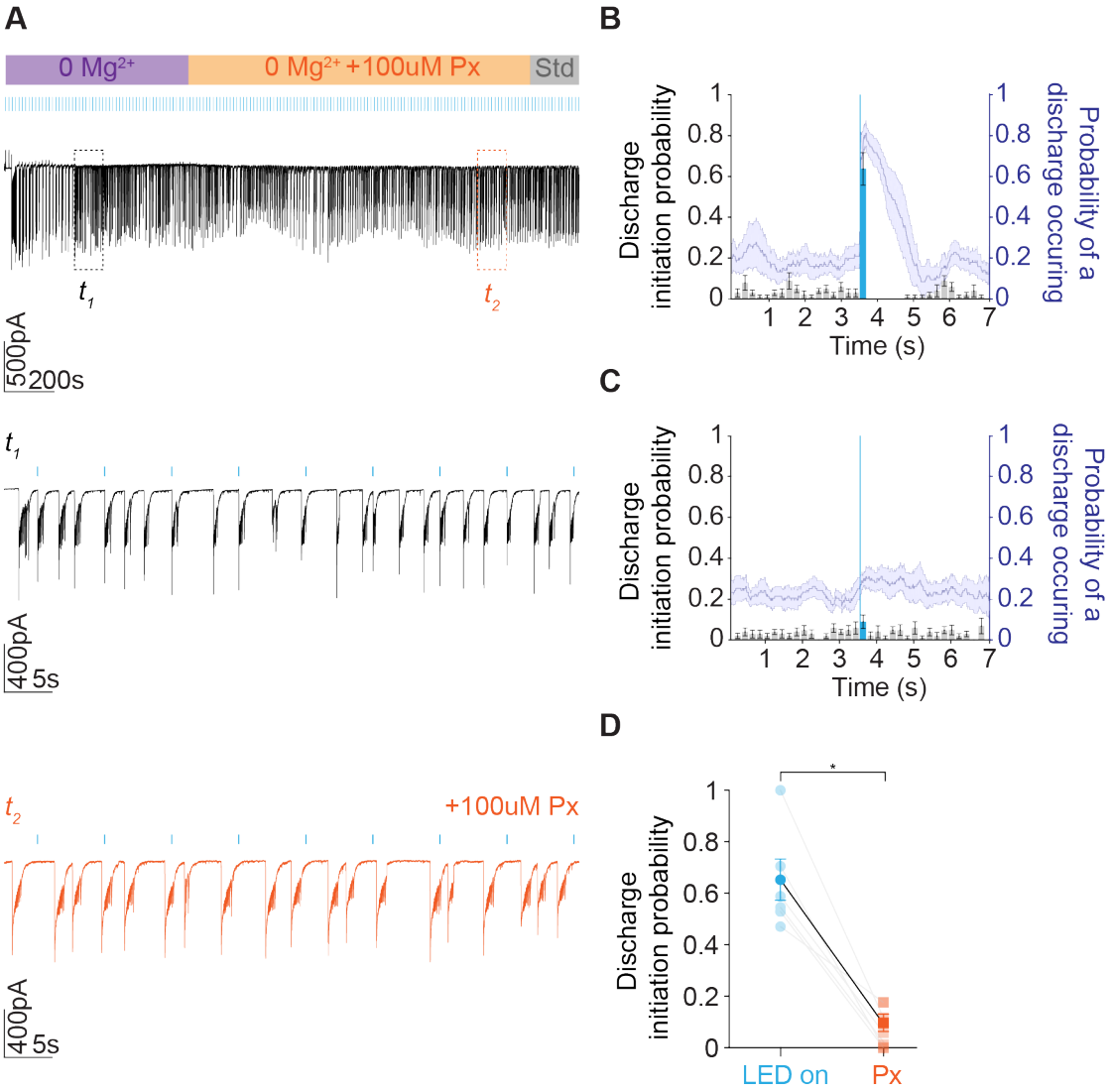
A
0 Mg2+
0 Mg2+ +100uM Px
Std
t1
t2
500pA
200s
t1
400pA
5s
t2
+100uM Px
400pA
5s
B
Discharge initiation probability
Probability of a discharge occuring
Time (s)
C
Discharge initiation probability
Probability of a discharge occuring
Time (s)
D
Discharge initiation probability
*
LED on
Px

3.7.1 The frequency of epileptiform discharges during the LRD phase is affected by synchronised activation of GAD2 interneurons

In the previous experiments (see Figures 3.10, 3.11 and 3.12), I showed how photoactivation GAD2 interneurons can entrain the hippocampal network. I then noted that this entrainment could affect the frequency of epileptiform discharges. This is illustrated in Figure 3.13 (**A**) where it appears that within a 5 minute analysis period, whenever photoactivation occurs ('LED on'), 30% of the discharges follow the frequency at which the light stimulus is activated (0.14 Hz). In comparison, if the light is off ('LED off') or picrotoxin is present (Px) there is a wider distribution of frequencies at which the discharges occur.

This was then confirmed by calculating the difference between the frequency at which the light was activated and the frequency of discharges within the 5 minute analysis window (see Figures 3.13, **B**). This difference is smaller in the 'LED on' group compared to the 'LED off' group (0.04 ± 0.02 vs 0.12 ± 0.03, $p = 0.03$, *Mann-Whitney test*) and Px (0.04 ± 0.02 vs 0.12 ± 0.02, $p = 0.04$, *Mann-Whitney test*) groups. Taken together, this suggests that the frequency at which the recurrent epileptiform discharges occur during the LRD phase can be mediated by optogenetic activation of GABAergic signalling.

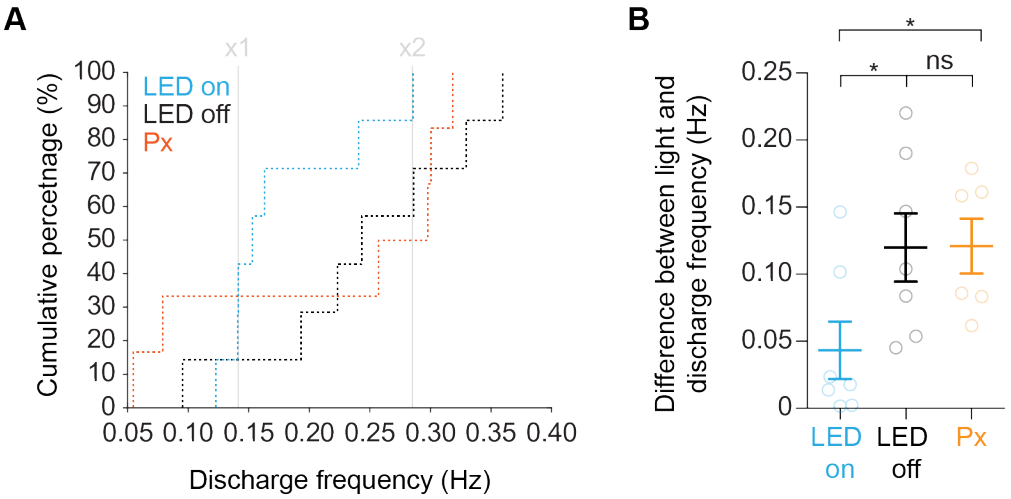

Figure 3.13: Synchronised photoactivation of GAD2 interneurons and blocking of the $GABA_AR$ affects epileptiform discharge frequency during the LRD phase. **A**, Cumulative percentage plot showing the distribution of discharge frequencies across the three groups, control with no photoactivation (LED off, $n = 7$), photoactivation (LED on, $n = 7$) and photoactivation with 100μM picrotoxin washed in (Px , $n = 6$). Grey lines mark x1 and x2 the frequency of the light stimulus (0.14Hz and 0.28Hz). **B**, Population data showing the difference between frequency of photoactivation (x1 grey line in A) and the observed frequency of discharges within a 5 minute analysis window. In the LED on group, this difference is significantly smaller when compared to the LED off and Px groups. ns = not significant, $^*p \leq 0.05$.

3.8 Studying activity-driven changes in intracellular Cl^- concentration

As $GABA_A$Rs are largely permeable to Cl^-, I used the gramicidin perforated patch-clamp technique to measure the E_{GABA} without perturbing the $[Cl^-]_i$ (see Section 2.4.3 and 2.4.4). Once a gigaseal has been achieved, gramicidin perforates the cell membrane with cation-specific pores. While this gives electrical access to the cell, the gramicidin does not permit the passage of Cl^- and thereby maintains the transmembrane Cl^- gradient.

In order to measure E_{GABA}, I activated the $GABA_A$R in one of two ways (see Section 2.4.4). First, GABA (100μM) was puffed on the soma using a pressure ejection system. Alternatively, ChR2-expressing GAD2 interneurons where stimulated with blue light to trigger the release of endogenous GABA. A voltage step protocol similar to that seen in Figure 3.9 was then used to generate IV plots. These were then used to calculate the E_{GABA}. I then used the Nernst Equation (Equation 1.3) to calculate the $[Cl^-]_i$. The $[Cl^-]_e$ I used for solving the Nernst equation was the Cl^- of the standard aCSF solution (123mM).

3.8.1 Both endogenous and exogenous GABA application can be used to determine the intracellular concentration of Cl^- in organotypic brain slices

As illustrated in Figure 3.14, by combining the data from the puffed and light-stimulated GABA ($n = 16$), I was able to calculate a mean E_{GABA} of -80.80 $\pm$ 2.39mV from which I was able to calculate a mean $[Cl^-]_i$ of 5.65 $\pm$ 0.53mM.

It is worth noting that the [Cl^-] in the internal solution was 141 mM which is much higher that the calculated $[Cl^-]_i$. This indicates that it is likely that the integrity of the gramicidin perforated patches were well maintained. Furthermore, there was no difference in conductance of the GABA currents elicited by exogenous ($n = 10$) vs endogenous ($n = 6$) GABA stimulation (11.39 ± 2.28nS vs 7.07 ± 0.69nS, p =0.0.7, *Wilcoxon test*). Although not shown in the Figure 3.14, I observed no difference in membrane potential (-70.65 ± 1.91mV vs -63.74 ± 3.12mV, p =0.21, *Wilcoxon test*) or access resistance (65.09 ± 4.67Ω vs 48.77 ± 7.66Ω, p =0.07, *Wilcoxon test*) between the two different methods.

Figure 3.14 *(following page)*: Exogenous application of GABA versus optogenetic stimulated GAD2-interneurons to determine intracellular concentration of Cl^- in organotypic brain slices. **A**, Gramicidin perforated patch voltage-clamp recordings from CA1 pyramidal cells clamped at -60mV. The recording protocol included voltage steps in increments of 10mV above and below -60mV. During each voltage step, either exogenous GABA (100μM) was puffed onto the soma or ChR2-expressing GAD2 interneurons were stimulated with a light impulse (100ms, 17.1mW). Grey line marks the holding current for each step while the red line marks the current elicited by either the exogenous application or endogenous release of GABA. **B**, Current-voltage (IV) plots showing GABA current reversal potential (E_{GABA}) calculated at the point where the GABA current and the holding current intersect. **C**, Population data of E_{GABA} values obtained using both methods. **D**, Estimated $[Cl^-]_i$ concentrations calculated from E_{GABA} values using the Nernst equation (Equation 1.3). **E**, There was no difference in GABA current conductance elicited by exogenous GABA or ChR2-activated interneurons. ns = not significant.

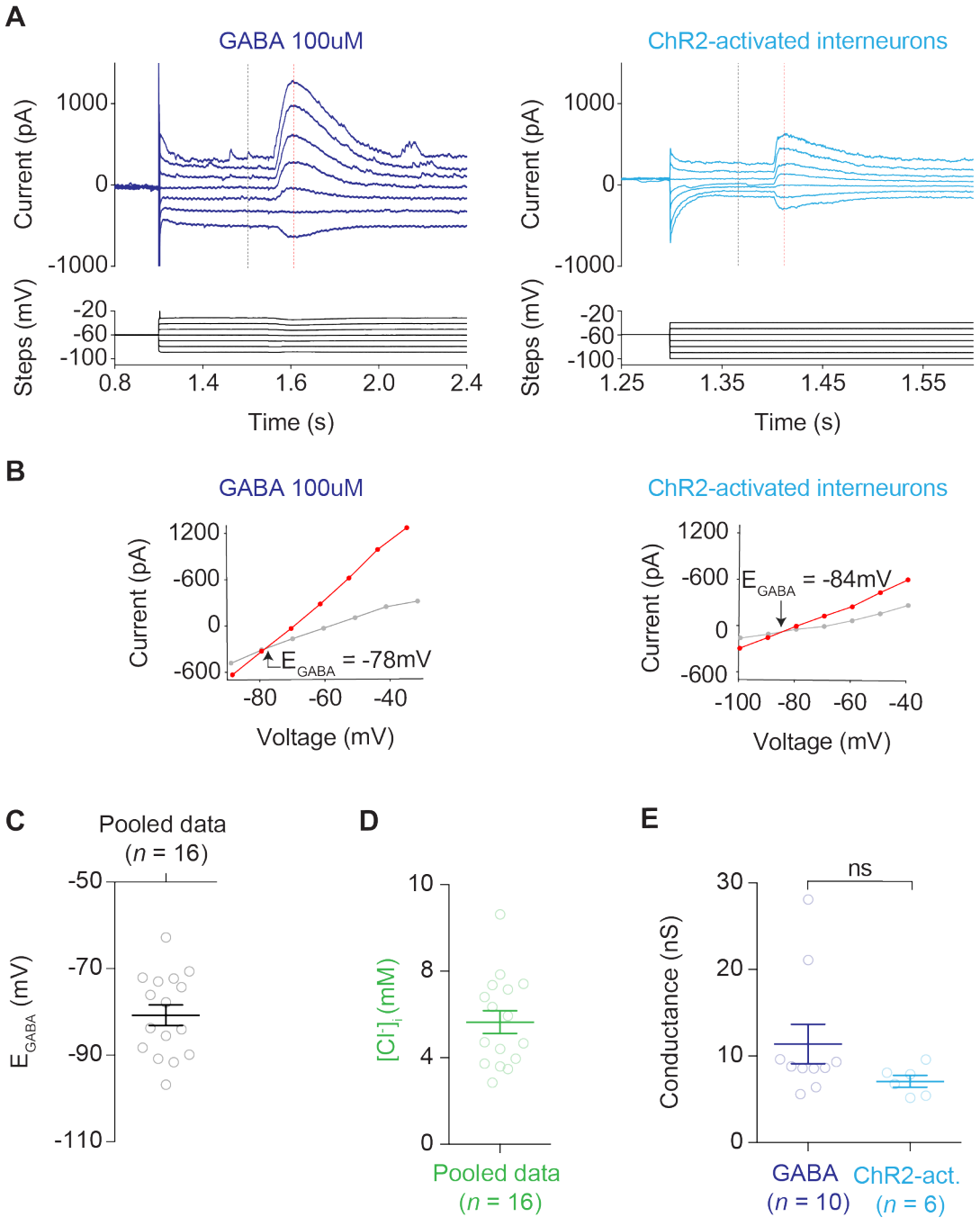
A
GABA 100uM
ChR2-activated interneurons
Current (pA)
Steps (mV)
Time (s)
B
GABA 100uM
ChR2-activated interneurons
Current (pA)
Voltage (mV)
E_GABA = -78mV
E_GABA = -84mV
C
Pooled data
(n = 16)
E_GABA (mV)
D
[Cl-]i (mM)
Pooled data
(n = 16)
E
ns
Conductance (nS)
GABA
(n = 10)
ChR2-act.
(n = 6)

3.8.2 Transient, activity-driven changes in intracellular Cl^- occur during single seizure-like events

In this final experiment, I aimed to confirm the transient, activity-driven changes in $[Cl^-]_i$ that were observed during single SLEs as previously described by Ellender et al (2014). As illustrated in Figure 3.15, I performed a perforated patch-clamp recording in a CA1 pyramidal cell from an organotypic brain slice. The recording protocol alternated between current and voltage-clamp modes. In voltage-clamp a ramp protocol would then start starting at -90mV and continuing until -20mV. The ramps were repeated twice within 1.5 seconds. During the second ramp a GABA conductance was elicited by exogenous puffs of GABA on the soma in order to determine E_{GABA} at that point.

Seizures were elicited using the 0 Mg^{2+} model. At the start of a single SLE standard aCSF containing 2mM Mg^{2+} was washed in. This was done to terminate the seizure and allow for accurate measurement of the E_{GABA} that would otherwise be compromised by ongoing spiking activity during the after-discharge phase. From the ramp protocols, IV plots could be drawn and the estimated E_{GABA} and $[Cl^-]_i$ calculated.

Before the onset of a SLE (t_1), I measured the E_{GABA} to be -65.81mV equating to a $[Cl^-]_i$ of 9.50mM. However, during the afterdischarge phase of the SLE (t_2), both the E_{GABA} and $[Cl^-]_i$ rose to -36.22mV and 30.04mM respectively. Once the cell had recovered (t_3), the E_{GABA} and $[Cl^-]_i$ returned to pre-SLE values (-65.24mV and 9.71mM). This is in keeping with what had been reported by Ellender et al (2014).

Figure 3.15 ***(following page)*****:** Transient Cl^- loading occurs during a single seizure-like event. **A**, Using a gramicidin perforated patch-clamp recording, the E_{GABA} was measured at different stages of a single seizure-like event (SLE). During recording the mode was rapidly switched between current-clamp (CC - 8 seconds) and voltage-clamp (VC - 1.5 seconds). In voltage-clamp, two ramp protocols were applied in quick succession of each other. During the second ramp, GABA (100μM) was puffed onto the cell soma. **B**, Representative trace from a CA1 pyramidal cell from a hippocampal organotypic slice. SLEs were elicited using the 0 Mg^{2+} model. At SLE onset, 2mM Mg^{2+} aCSF was washed in to block ongoing spiking activity. E_{GABA} measurements are marked by blue circles and were sampled prior to SLE onset (t_1), during the after-discharge phase (t_2) and at recovery (t_3). **C**, Ramp protocols taken each of the time points, $t_{(1\text{-}3)}$. **D**, IV plots were drawn and extrapolated to estimate E_{GABA} values. The $[Cl^-]_i$ was then calculated using the Nernst equation (Equation 1.3)

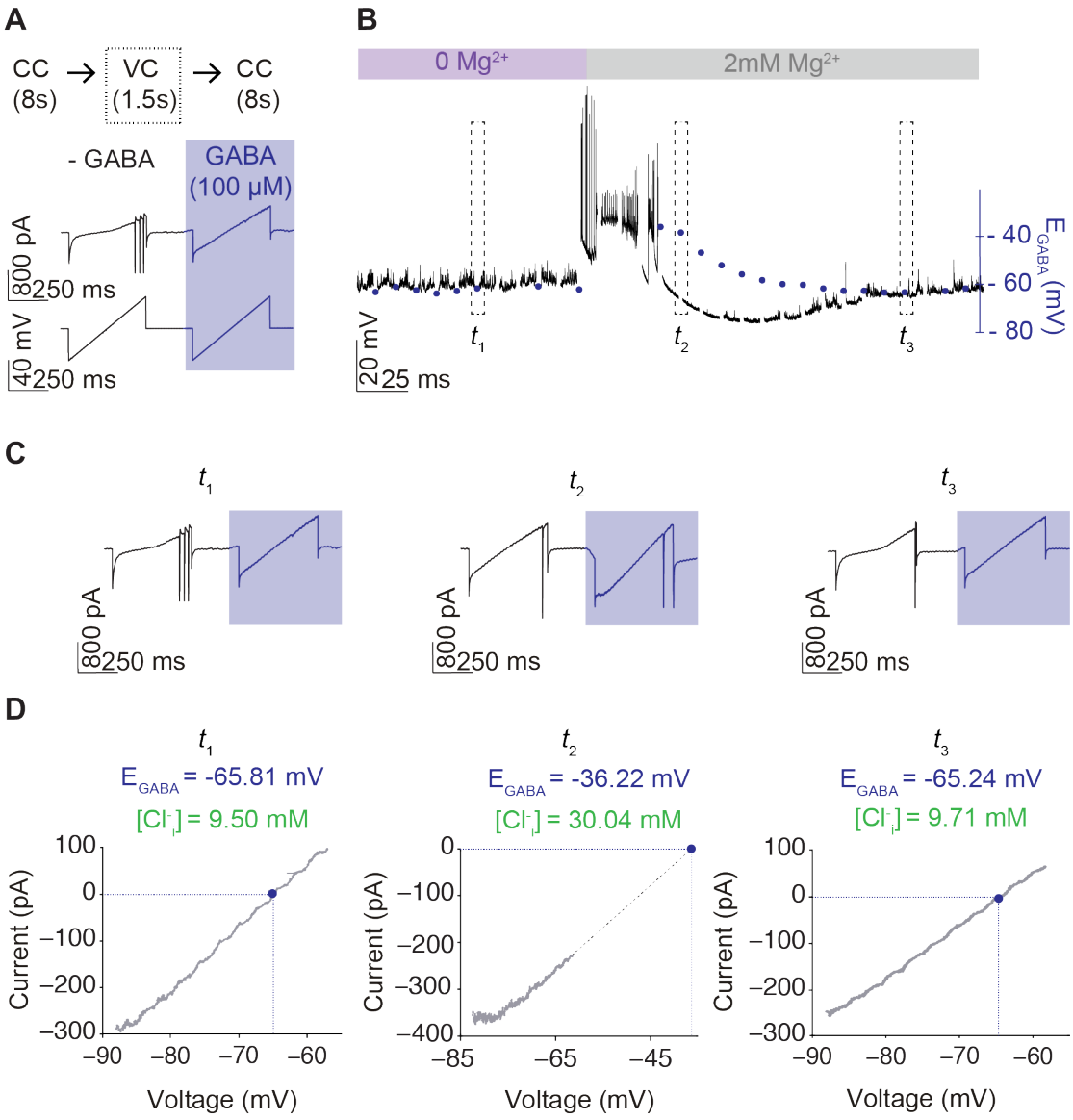
A
CC (8s)
VC (1.5s)
CC (8s)
- GABA
GABA (100 µM)
800 pA
250 ms
40 mV
250 ms
B
0 Mg2+
2mM Mg2+
20 mV
25 ms
t1
t2
t3
- 40
- 60
- 80
EGABA (mV)
C
t1
t2
t3
800 pA
250 ms
D
t1
EGABA = -65.81 mV
[Cl-i] = 9.50 mM
t2
EGABA = -36.22 mV
[Cl-i] = 30.04 mM
t3
EGABA = -65.24 mV
[Cl-i] = 9.71 mM
Current (pA)
Voltage (mV)

Chapter 4

Discussion

In this final chapter I will discuss the relevance of the major clinical and experimental findings that have been presented in this thesis. Where appropriate, I will highlight shortcomings in the methodology and propose avenues for future research.

4.1 Benzodiazepine-resistant status epilepticus is prevalent within our local paediatric population

The clinical data I have presented in this thesis (see Section 3.1), confirms that within our local paediatric cohort, 42% of patients who present in CSE do not respond to first-line treatment with benzodiazepines. I then noticed, that this group of patients appear to have significantly longer episodes of CSE before receiving treatment.

These findings are similar to what has been reported in a larger British study by Chin et al (2008). In their cohort, 187 patients received benzodiazepines as first-line intervention, with 35% not responding to this treatment. Furthermore, they showed that patients who require more than 2 doses of benzodiazepines have a significantly higher risk of going into respiratory depression, a life-threatening complication of benzodiazepine treatment. This suggests that failure to respond to first-line treatment with benzodiazepines is associated with increased morbidity in paediatric patients.

A major limitation of the clinical data presented in this thesis is that it is incomplete. It represents an interim analysis of an ongoing clinical study. A more in-depth analysis is still to be performed in order to identify potential characteristics that may separate out the benzodiazepine-resistant group. This will include studying differences in past medical history, underlying aetiology, semiology, pre-hospital treatment as well as immediate and long-term outcomes.

Despite this clinical data being limited, it was ultimately successful in achieving its modest objective. I was able to confirm that benzodiazepine-resistant SE is a relevant clinical entity within our paediatric population. This has provided a suitable introduction to my experimental investigation into how changes in GABAergic signalling may be relevant to benzodiazepine resistance in SE.

4.2 Diazepam modulates $GABA_AR$ synaptic currents during normal network activity

In Figures 3.2 and 3.3, I showed how diazepam positively modulates $GABA_AR$ synaptic currents (GSCs). I then demonstrated how this can be reversed using the competitive antagonist, flumazenil. These findings are similar to what has been described by Deeb et al (2013) who used dissociated cell cultures and elicited GSCs using exogenous application of the $GABA_AR$ agonist, muscimol.

Interestingly, my data seems to suggest that there is a difference in the effect of diazepam on GSCs between the organotypic and acute brain slices. In the organotypic brain slices diazepam has a more subtle effect by only affecting the decay constant and not the amplitude of the GSCs. By contrast, in the acute brain slices diazepam the effect is more impressive, affecting both the amplitude and decay constant of the GSCs.

This finding may be explained by inherent differences between the two brain slice preparations. In organotypic brain slices, previous work by Mckinney et al (1997) has shown that during the preparation of these slices there is significant damage to the structural integrity of the neural network, mainly in the form of axonal injury. When these neurons are maintained in culture, axonal sprouting occurs that leads to recurrent connections being formed between neurons. This causes an overall increase in network excitability (Dyhrfjeld-Johnsen et al., 2010). The full extent of how this aberrant network activity affects synaptic transmission, and specifically the distribution and configuration of $GABA_ARs$, is still unknown. Future experiments may aim to provide further insight into this by studying $GABA_AR$ subunits in the organotypic brain slices using various antibody-labelling and advanced imaging techniques.

Other important technical differences to consider include the method of activating $GABA_AAR$ signalling as well as the brain area recorded from. Ideally, I would have preferred using optogenetics in both slice preparations. However, due to technical limitations this was not possible in acute brain slices. Moreover, it is also unknown if GABAergic signalling is different between the CA1 (organotypic) and layer 5 of entorhinal cortex (acute). For this reason, these experiments should be repeated in equivalent cell populations in both slice preparations.

Lastly, another limitation was that only one benzodiazepine (diazepam) at one dose (3μM), was studied. This dose was chosen as it had previously been shown to be effective by Deeb et al (2013). Future experiments could aim to study the effect of different types and doses of benzodiazepines on GSCs.

4.3 The 0 Mg^{2+} model provides a reliable *in vitro* replica of status epilepticus

Using the Mg^{2+} model, I demonstrated how SE-like activity could be induced in both organotypic and acute brain slices (see Figure 3.4). In both tissue preparations, the introduction of the Mg^{2+} solution precipitated an increase in slice activity that then progressed first into single SLEs followed by entry into a phase of recurrent epileptiform discharges, known as the LRD phase. These findings are consistent with previous *in vitro* studies (Dreier and Heinemann, 1991; Zhang et al., 1995; Dreier et al., 1998; Pal et al., 1999; Deshpande et al., 2008; Albus et al., 2008; Kelley et al., 2016). Therefore, I have furthered validated that this a reliable model in which to study the evolution of prolonged seizure activity *in vitro*.

Interestingly, there appear to be a significant difference in the SE-like activity between the different tissue preparations. While there was no significant difference in SLE or LRD propensity, in the organotypic brain slices SLE and entry into LRD appears to occur sooner compared to the acute brain slices.

Organotypic brain slices, by themselves, are considered to be a model of post-traumatic epileptogenesis and have been shown to generate spontaneous seizure activity while in culture (Dyhrfjeld-Johnsen et al., 2010). The trauma caused by the slicing procedure in combination with keeping them in culture causes aberrations within the neural circuitry, as well as widespread cell death (Coltman et al., 1995; Simoni et al., 2003; Berdichevsky et al., 2012). The consequence is sustained hyperexcitability within these slices which may explain why there is faster onset of seizure activity in the organotypic brain slices compared to acute brain slices.

A limitation of my data set is that I only studied a single pro-convulsant model. There is a difference in patterns of seizure activity between the various *in vitro* seizure models, and this may prove to be relevant when studying SE-like activity. For example, Albus et al (2008) describe distinct differences in the types of seizures generated by the 0 Mg^{2+} model compared to using the K^{+} channel blocker, 4-aminopyridine (4-AP), to elicit seizure activity. Furthermore, Kelley et al (2016) have demonstrated that the 4-AP model generates repeated SLEs, but never enters into the LRD phase. These differences between models need to be appreciated as they may significantly alter the reproducibility of results. Furthermore, these differences may bias the understanding of underlying ictogenesis as well as the observed sensitivity to anticonvulsants.

4.4 Diazepam has a differential and time-dependent effect on *in vitro* status epilepticus

Having setup the 0 Mg^{2+} model in organotypic brain slices, I then showed how diazepam affects the development and progression of prolonged seizure activity (see Figures 3.5 and 3.6).

When introduced early, diazepam appears to delay the onset of SLEs while also making them shorter and occur less frequently. However, it did not seem to prevent the progression into the LRD phase nor was it able to ablate SE-like activity. Interestingly, I then noticed that the presence of diazepam in the early part of the LRD phase appears to positively modulate the recurrent epileptiform discharges. Notably, diazepam increased the duration of discharges without affecting the inter-discharge duration. The results from these experiments demonstrate how in the 0 Mg^{+} model, diazepam is first anticonvulsant and then progresses to enhancing epileptiform activity.

Albus et al (2008) show a comprehensive study of the effect of various anticonvulsants on organotypic brain slices using the 0 Mg^{2+} model and therefore provide a useful reference to compare findings. Interestingly, their use of diazepam (at higher doses of 5μM and 35μM) also failed to prevent SLE onset and shortened SLEs. However, their data was not statistically significant nor did they look at the effect of diazepam on other LRD parameters like discharge duration and frequency.

A limitation of my results is the particular analysis approach used. Currently, the analysis of LRD activity was limited to discrete 60 second window at a predefined time point early in the LRD period (7 minute after onset). A more accurate method of assessing the effect of diazepam on the LRD activity would be to employ a fully automated approach whereby the individual discharges are detected and analysed across

a much longer time window. In addition, the effect of diazepam on the amplitude and power (using a fast fourier transform) should be performed (Glykys and Staley, 2015). Moreover, future experiments could analyse the effect of diazepam on LRD activity at different time intervals to identify if and when the activity becomes truly pharmacoresistant and can no longer be positively modulated by benzodiazepines.

Another limitation is that these experiments have only been conducted in organotypic brain slices. Therefore, to increase the validity of these results the experiments should be repeated in acute brain slices. Given the impressive effect of diazepam on baseline $GABA_AR$ signalling (as shown in Figure 3.3), it will be interesting to see how diazepam may affect seizure activity in this preparation.

Despite these limitations, taken together with my data showing how diazepam positively modulates the $GABA_AR$ (see Section 4.2), these findings suggest that enhancing this receptor's function during the LRD phase positively modulates the epileptiform discharges. This implies that the $GABA_AR$-signalling may participate in SE-like activity.

4.5 GABAergic signalling drives epileptiform discharges during *in vitro* status epilepticus

4.5.1 GABAergic signalling is excitatory in both single seizures and SE-like activity

In the development of prolonged seizure states, I have shown how GABAergic signalling shifts between being inhibitory and excitatory (see Figures 3.7 and 3.8). This extends previous *in vitro* work by showing that excitatory GABAergic signalling is also present during the LRD phase (Ilie et al., 2012; Ellender et al., 2014).

My findings appear to contrast what has been proposed by Ledri et al (2014) as they had previously shown that the activation of GAD2 interneurons is able to suppress SLEs. However, there are important differences in methodology that may explain this. Importantly, there is a significant difference in the stimulation protocol they used as they found the most significant suppressant effect to occur when the light was activated for prolonged periods of at least 5 seconds. When they only stimulated for 1 millisecond, this suppressant effect was lost, which is consistent with what I found when I only stimulated for 100 milliseconds. Taken together, a possible explanation is that prolonged activation of the interneurons, which are believed to be excitatory during the seizure, may push them into a period of depolarising block whereby they are no longer able to participate in the propagation epileptiform activity.

In this work I activated the entire interneuronal population by using ChR2 expression driven by the GAD2 promoter. However, it may be interesting to determine how the different subpopulations of interneurons might contribute to SE-like activity. For example, a recent study by Khoshkhoo et al (2017) has shown that the various classes of interneurons contribute differently to the initiation and propagation of seizures. Specifically, using an *in vivo* model of induced seizures, they show that the parvalbumin (PV) and somatostatin (SS) interneurons appear to contribute towards maintaining seizure activity. This is consistent with my own data and with what is proposed by Ellender et al (2014), who have shown that synchronised activation of PV interneurons can trigger afterdischarges during individual SLEs. Interestingly, Khoshkhoo et al (2017) also show that vasoactive intestinal-peptide (VIP) interneurons are involved in curtailing seizure activity. As these interneurons primarily target the other two interneuronal subpopulations, they could be viewed as silencing the excitatory activity of PV and SS interneurons.

4.5.2 GABAergic signalling is reduced after prolonged seizure activity

After showing that excitatory GABAergic signalling plays an active role in SE-like activity, I then showed that there is a significant reduction in the conductance of the light-activated GABAergic signalling before and after these prolonged seizures (see Figure 3.9). This finding is consistent with previous data that shows how SE-like activity causes an internalisation of the $GABA_AR$ leading to a decrease in its inhibitory function (Goodkin et al., 2005; Naylor et al., 2005).

Taken together with the data I have shown in Figures 3.5 and 3.6, this suggests that the integrity of GABAergic signalling changes as the LRD phase is allowed to progress. Early in this SE-like activity, $GABA_ARs$ may remain intact which would explain how diazepam is able to modulate the duration of epileptiform discharges. However, over time the prolonged seizure activity drives endocytosis and recycling of $GABA_ARs$ (Goodkin et al., 2005), and may reduce their ability to contribute towards seizure activity. It is therefore assumed that at a certain point the epileptiform discharges will no longer be sensitive to diazepam. In order to confirm this, further research is needed into how diazepam affects LRD activity at different time points (as proposed in Section 4.4).

4.5.3 Photoactivation of GABAergic signalling entrains SE-like activity through the $GABA_AR$

After demonstrating that GABAergic signalling is excitatory during the LRD phase, I then showed that by controlling GABAergic signalling I am able to alter the probability of when the recurrent epileptiform discharges occur (Figure 3.10). Furthermore, if a discharge was not elicited by the activation of the GAD2 interneurons, I found that the network was more likely to already be within a discharge and therefore refractory to subsequent activation.

I then confirmed this observation by showing a significant difference between before and after photoactivation was initiated (Figure 3.11). Thereafter, I showed how this entrainment of the LRD activity is mediated by the $GABA_AR$ as washing in picrotoxin was able to disrupt this effect (see Figure 3.12). Interestingly, the $GABA_AR$ antagonist was not able to ablate epileptiform discharges, which suggests that they can be generated by alternate mechanisms, most likely glutamatergic signalling.

In Figure 3.13, I then showed that by modifying GABAergic signalling, I was able to alter the frequency of epileptiform discharges during the LRD phase. With synchronised activation of the GABAergic interneurons I was able to entrain the frequency of the discharges around the frequency of the light stimulus. By contrast, when the light is off or the $GABA_AR$ is blocked, there is a wider distribution of discharge frequencies.

Taken together, these results suggest that GABAergic interneurons and specifically $GABA_AR$ signalling can precipitate epileptiform discharges during SE-like activity. However, $GABA_AR$ signalling is not solely responsible for generating epileptiform discharges.

Interestingly, previous work confirms that GABAergic signalling is involved in the LRD phase, however in an opposing way. Dreier et al (1991) have shown that washing in picrotoxin accelerates the frequency of discharges during the LRD phase. When the picrotoxin was then accompanied with the $GABA_BR$ agonist, baclofen, they noticed a marked decrease in discharge frequency. By contrast, Albus et al (2008) report that washing in muscimol during the LRD phase reduces the seizure activity which seems to suggest that $GABA_AR$-mediated signalling is inhibitory. These experiments used somewhat crude pharmacological manipulation of the GABAergic system during SE. Nonetheless, this lack of consensus justifies further research into investigating how $GABA_AR$-mediated signalling participates in generating and maintaining the epileptiform discharges during the LRD phase.

4.6 Seizure-induced changes in Cl^-

4.6.1 Using optogenetics to elicit GABAergic inhibitory signalling

While performing perforated patch-clamp recordings, I was able to demonstrate that using optogenetic activation of GABAergic interneurons is an effective way of eliciting GSCs in order to measure $[Cl^-]_i$ (see Figure 3.14). This complements previous work by Raimondo et al (2012) and further shows how optogenetics can be used to study synaptic inhibition as well as to study $[Cl^-]_i$ dynamics.

4.6.2 Transient, activity-driven changes in intracellular Cl^- during single-seizures

In my final experiment (see Figure 3.15), I successfully replicated the results of Ellender et al (2014). Indeed, I showed that GABAergic signalling does become excitatory during the after-discharge phase of single SLEs and this is related to an increase in $[Cl^-]_i$. Furthermore, these seizure-induced Cl^- dynamics have also been imaged using advanced Cl^- genetic reporters (Raimondo, Irkle, Wefelmeyer, Newey and Akerman, 2012; Sato et al., 2017).

This suggests that maintaining Cl^- homeostasis is important in limiting seizure activity. Alfonsa et al (2015) have demonstrated that by inducing Cl^- loads using the light-activated Cl^- pump, halorhodopsin, they were able to increase network excitability. Furthermore, Alfonsa et al (2016) then developed a novel optogenetic Cl^- extruder, Cl-out, that is able to remove Cl^- from the intracellular space and in doing so, delay the propagation of ictal activity.

While the role of these Cl^- dynamics have been shown to occur during single seizures, their relevance during SE-like activity is still to be confirmed.

4.7 General discussion

In this final section, I will broadly conceptualise how changes in $GABA_AR$ function and structure are responsible for benzodiazepine resistance. I do this by situating the findings of my thesis within the context of existing literature. I have further summarised these thoughts in Figure 4.1.

The main finding of my thesis is that excitatory $GABA_AR$-mediated signalling plays an active part in positively modulating the recurrent epileptiform discharges that characterise an *in vitro* replica of SE-like activity. Having confirmed that during single SLEs, this excitatory GABAergic signalling is linked to a transient increase in $[Cl^-]_i$, I postulate that this short-term ionic plasticity may also be present during prolonged seizure activity (see Figure 4.1, **A**). If this is proved to be true, benzodiazepines would be an ineffective anticonvulsant to treat SE and by enhancing excitatory GABAergic signalling, may further propel this unrelenting seizure activity.

In order to confirm this link, further research is needed to study Cl^- dynamics during the LRD using either perforated patch-clamp recordings or Cl^- imaging techniques. Another way of confirming this would be to try and reduce $[Cl^-]_i$ during the LRD phase using the optogenetic Cl^- extruder, Cl-out (Alfonsa et al., 2016). It would be interesting to see if this would be able to reverse the excitatory shift in GABAergic signalling, as well as rescue the anticonvulsant effect of benzodiazepines.

Impaired KCC2 function has also been implicated in prolonged seizure activity (see Figure 4.1, **B**). Kelley et al (2016) showed that by blocking KCC2 with VU0463271 or knocking it out (using the S940A point-mutant mouse) they were able to accelerate entry into the LRD phase. It is postulated that the increased $[Cl^-]_i$ that results from poor KCC2-mediated Cl^- extrusion would drive excitatory GABAergic signalling and render benzodiazepines ineffective.

Finally, SE-driven $GABA_AR$ trafficking and remodeling needs to be considered (see Figure 4.1, **C**). As already discussed (see Section 1.5.3), during SE the $GABA_AR$ undergoes a endocytosis-mediated internalisation. Once internalised, there can be a reconfiguration of $GABA_AR$ subunits which typically involves a replacement of the α_1 and γ_2 subunits (needed to form the benzodiazepine binding-site) with α_5 and δ subunits (Friedman et al., 1994; Rice et al., 1996). This reconfigured $GABA_AR$ no longer possesses a benzodiazepine binding-site, and instead is preferentially re-expressed in the extrasynaptic space. This is likely to represent a more long-term effect (hours to days) which could also explain benzodiazepine resistance to SE.

In summary, changes in Cl^- dynamics and $GABA_AR$ expression may provide an explanation for how the seizure activity becomes resistant to benzodiazepines. Understanding how these mechanisms relate to each other is a fertile ground for future study.

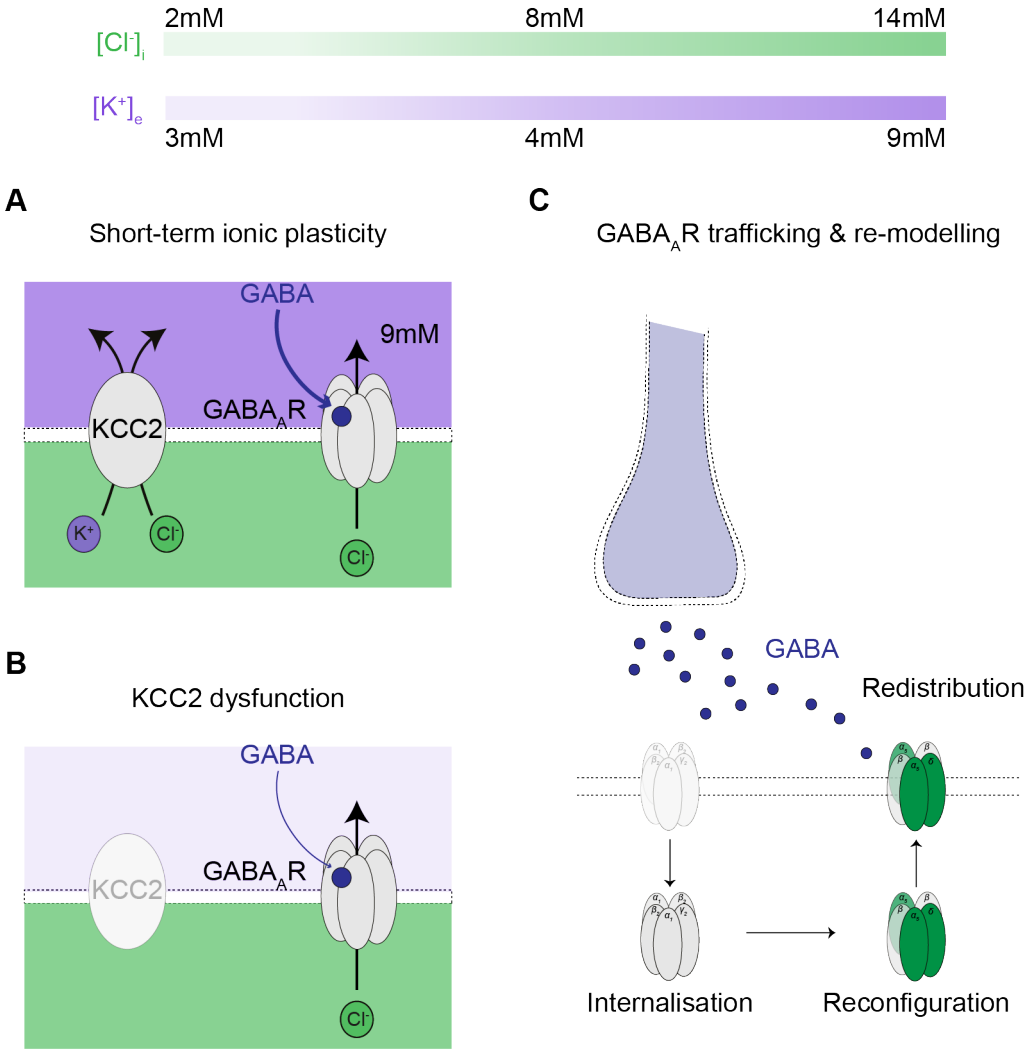

Figure 4.1: Disruptions to $GABA_AR$ structure and function may be responsible for benzodiazepine-resistant status epilepticus. **A**, Activity-driven intracellular accumulation of Cl^- and extracellular K^+ (short-term ionic plasticity). **B**, Long-term or short-term KCC2 dysfunction allow for $[Cl^-]_i$ to rise, leading to an excitatory shift in $GABA_AR$ function. **C**, During SE, the $GABA_AR$ undergoes an endocytosis-mediated internalisation. Once in the intracellular space the subunits are reconfigured with subunits insensitive to benzodiazepines. The refurbished $GABA_AR$ is preferentially redistributed outside the synaptic cleft.

4.8 Concluding remarks

In the course of this thesis I have demonstrated that benzodiazepine-resistant SE is prevalent within our South African paediatric population. I have showed how benzodiazepines have a differential and time dependent effect on an *in vitro* model of SE. My data also demonstrates that excitatory GABAergic signalling plays an active role in driving epileptiform activity during SE and is likely to represent part of the explanation for benzodiazepine resistance in SE. Relating my findings to dynamic changes to the transmembrane Cl^- gradient during SE is a pertinent topic for future research.

Taken together the work presented in this thesis may inform the design and choice of optimum pharmacological strategies for treating SE.

Bibliography

Albus, K., Wahab, A. and Heinemann, U. (2008), 'Standard antiepileptic drugs fail to block epileptiform activity in rat organotypic hippocampal slice cultures', *British Journal of Pharmacology* **154**(3), 709–733.

Alfonsa, H., Lakey, J. H., Lightowlers, R. N. and Trevelyan, A. J. (2016), 'Cl-out is a novel cooperative optogenetic tool for extruding chloride from neurons', *Nature Communications* **7**(1), 1–9.

Alfonsa, H., Merricks, E. M., Codadu, N. K., Cunningham, M. O., Deisseroth, K., Racca, C. and Trevelyan, A. J. (2015), 'The contribution of raised intraneuronal chloride to epileptic network activity', *Journal of Neuroscience* **35**(20), 7715–7726.

Alldredge, B. K., Gelb, A. M., Isaacs, S. M., Corry, M. D., Allen, F., Ulrich, S., Gottwald, M. D., O'Neil, N., Neuhaus, J. M., Segal, M. R. and Lowenstein, D. H. (2001), 'A comparison of lorazepam, diazepam, and placebo for the treatment of out-of-hospital status epilepticus', *New England Journal of Medicine* **345**(9), 631–637.

Anderson, W. W., Lewis, D. V., Swartzwelder, H. S. and Wilson, W. A. (1986), 'Magnesium-free medium activates seizure-like events in the rat hippocampal slice', *Brain Research* **398**(1), 215–219.

Appleton, R., Choonara, I., Martland, T., Phillips, B., Scott, R. and Whitehouse, W. (2000), 'The treatment of convulsive status epilepticus in children. the status epilepticus working party, members of the status epilepticus working party', *Archives of Disease in Childhood* **83**(5), 415–424.

Avoli, M. (2007), 'The epileptic hippocampus revisited: back to the future', *Epilepsy Currents* **7**(4), 116–118.

Avoli, M., Drapeau, C., Perreault, P., Louvel, J. and Pumain, R. (1990), 'Epileptiform activity induced by low chloride medium in the ca1 subfield of the hippocampal slice', *Journal of Neurophysiology* **64**(6), 1747–1757.

Badea, T., Goldberg, J., Mao, B. and Yuste, R. (2001), 'Calcium imaging of epileptiform events with single-cell resolution', *Developmental Neurobiology* **48**(3), 215–227.

Bak, L. K., Schousboe, A. and Waagepetersen, H. S. (2006), 'The glutamate/gaba-glutamine cycle: aspects of transport, neurotransmitter homeostasis and ammonia transfer', *Journal of Neurochemistry* **98**(3), 641–653.

Ben-Ari, Y. (2002), 'Excitatory actions of gaba during development: the nature of the nurture', *Nature Reviews Neuroscience* **3**(9), 728–739.

Ben-Ari, Y., Khalilov, I., Kahle, K. T. and Cherubini, E. (2012), 'The gaba excitatory/inhibitory shift in brain maturation and neurological disorders', *The Neuroscientist* **18**(5), 467–486.

Benarroch, E. E. (2005), 'Neuron-astrocyte interactions: partnership for normal function and disease in the central nervous system', *Mayo Clinic Proceedings* **80**(1), 1326–1338.

Berdichevsky, Y., Dzhala, V., Mail, M. and Staley, K. J. (2012), 'Interictal spikes, seizures and ictal cell death are not necessary for post-traumatic epileptogenesis in vitro', *Neurobiology of Disease* **45**(2), 774–785.

Berndt, A., Lee, S. Y., Ramakrishnan, C. and Deisseroth, K. (2014), 'Structure-guided transformation of channelrhodopsin into a light-activated chloride channel', *Science* **344**(6182), 420–424.

Betjemann, J. P. and Lowenstein, D. H. (2015), 'Status epilepticus in adults', *The Lancet Neurology* **14**(6), 615–624.

Blaesse, P., Airaksinen, M. S., Rivera, C. and Kaila, K. (2009), 'Cation-chloride cotransporters and neuronal function', *Neuron* **61**(6), 820–838.

Blauwblomme, T., Jiruska, P. and Huberfeld, G. (2014), 'Mechanisms of ictogenesis', *International Review of Neurobiology* **114**(1), 155–185.

Borck, C. and Jefferys, J. G. (1999), 'Seizure-like events in disinhibited ventral slices of adult rat hippocampus', *Journal of Neurophysiology* **82**(5), 2130–2142.

Bormann, J. (2000), 'The 'abc' of gaba receptors', *Trends Pharmacol Sci* **21**(1), 16–25.

Boulenguez, P., Liabeuf, S., Bos, R., Bras, H., Jean-Xavier, C., Brocard, C., Stil, A., Darbon, P., Cattaert, D., Delpire, E. et al. (2010), 'Down-regulation of the potassium-chloride cotransporter kcc2 contributes to spasticity after spinal cord injury', *Nature Medicine* **16**(3), 302–307.

Bowery, N. G. and Smart, T. G. (2006), 'Gaba and glycine as neurotransmitters: a brief history', *British Journal of Pharmacology* **147**(1), 109–119.

Boyden, E. S., Zhang, F., Bamberg, E., Nagel, G. and Deisseroth, K. (2005), 'Millisecond-timescale, genetically targeted optical control of neural activity', *Nature Neuroscience* **8**(9), 1263–8.

Chen, J., Naylor, D. and Wasterlain, C. (2007), 'Advances in the pathophysiology of status epilepticus', *Acta Neurologica Scandinavica* **115**(186), 7–15.

Chesler, M. and Kaila, K. (1992), 'Modulation of ph by neuronal activity', *Trends in Neurosciences* **15**(10), 396–402.

Chin, R. F. M., Neville, B. G. R., Peckham, C., Wade, A., Bedford, H. and Scott, R. C. (2008), 'Treatment of community-onset, childhood convulsive status epilepticus: a prospective, population-based study', *The Lancet Neurology* **7**(8), 696–703.

Chin, R. F., Neville, B. G., Peckham, C., Bedford, H., Wade, A., Scott, R. C. et al. (2006), 'Incidence, cause, and short-term outcome of convulsive status epilepticus in childhood: prospective population-based study', *The Lancet* **368**(9531), 222–229.

Christian, C. A., Herbert, A. G., Holt, R. L., Peng, K., Sherwood, K. D., Pangratz-Fuehrer, S., Rudolph, U. and Huguenard, J. R. (2013), 'Endogenous positive allosteric modulation of gaba a receptors by diazepam binding inhibitor', *Neuron* **78**(6), 1063–1074.

Christian, C. A. and Huguenard, J. R. (2013), 'Astrocytes potentiate gabaergic transmission in the thalamic reticular nucleus via endozepine signaling', *Proceedings of the National Academy of Sciences of the United States of America* **110**(50), 20278–20283.

Coltman, B., Earley, E., Shahar, A., Dudek, F. and Ide, C. (1995), 'Factors influencing mossy fiber collateral sprouting in organotypic slice cultures of neonatal mouse hippocampus', *Journal of Comparative Neurology* **362**(2), 209–222.

Costa, E. and Guidotti, A. (1985), 'Endogenous ligands for benzodiazepine recognition sites', *Biochemical Pharmacology* **34**(19), 3399–403.

Deborah Lin, E.-J., Young, D., Baer, K., Herzog, H. and During, M. J. (2006), 'Differential actions of npy on seizure modulation via y1 and y2 receptors: evidence from receptor knockout mice', *Epilepsia* **47**(4), 773–780.

Deeb, T. Z., Nakamura, Y., Frost, G. D., Davies, P. A. and Moss, S. J. (2013), 'Disrupted cl- homeostasis contributes to reductions in the inhibitory efficacy of diazepam during hyperexcited states', *European Journal of Neuroscience* **38**(3), 2453–2467.

Deisz, R. A., Wierschke, S., Schneider, U. C. and Dehnicke, C. (2014), 'Effects of vu0240551, a novel kcc2 antagonist, and dids on chloride homeostasis of neocortical neurons from rats and humans', *Neuroscience* **277**(1), 831–841.

DeLorenzo, R. J., Pellock, J. M., Towne, A. R. and Boggs, J. G. (1995), 'Epidemiology of status epilepticus.', *Journal of Clinical Neurophysiology* **12**(4), 316–325.

DeLorenzo, R. J., Towne, A. R., Pellock, J. M. and Ko, D. (1992), 'Status epilepticus in children, adults, and the elderly', *Epilepsia* **33**(4), 15–25.

Deshpande, L. S., Lou, J. K., Mian, A., Blair, R. E., Sombati, S., Attkisson, E. and DeLorenzo, R. J. (2008), 'Time course and mechanism of hippocampal neuronal death in an in vitro model of status epilepticus: role of nmda receptor activation and nmda dependent calcium entry', *European Journal of Pharmacology* **583**(1), 73–83.

Dreier, J. and Heinemann, U. (1991), 'Regional and time dependent variations of low mg 2+ induced epileptiform activity in rat temporal cortex slices', *Experimental Brain Research* **87**(3), 581–596.

Dreier, J. P., Zhang, C. L. and Heinemann, U. (1998), 'Phenytoin, phenobarbital, and midazolam fail to stop status epilepticus-like activity induced by low magnesium in rat entorhinal slices, but can prevent its development', *Acta Neurologica Scandinavica* **98**(3), 154–160.

Duncalfe, L. L. and Dunn, S. M. (1996), 'Mapping of gaba a receptor sites that are photoaffinity-labelled by [3 h] flunitrazepam and [3 h] ro 15-4513', *European Journal of Pharmacology* **298**(3), 313–319.

Dyhrfjeld-Johnsen, J., Berdichevsky, Y., Swiercz, W., Sabolek, H. and Staley, K. (2010), 'Interictal spikes precede ictal discharges in an organotypic hippocampal slice culture model of epileptogenesis', *Journal of Clinical Neurophysiology* **27**(6), 418–424.

Dzhala, V. I., Talos, D. M., Sdrulla, D. A., Brumback, A. C., Mathews, G. C., Benke, T. A., Delpire, E., Jensen, F. E. and Staley, K. J. (2005), 'Nkcc1 transporter facilitates seizures in the developing brain', *Nature Medicine* **11**(11), 1205–1213.

Ellender, T. J., Raimondo, J. V., Irkle, A., Lamsa, K. P. and Akerman, C. J. (2014), 'Excitatory effects of parvalbumin-expressing interneurons maintain hippocampal epileptiform activity via synchronous afterdischarges', *The Journal of Neuroscience* **34**(46), 15208–15222.

English, D. F., Ibanez-Sandoval, O., Stark, E., Tecuapetla, F., Buzsáki, G., Deisseroth, K., Tepper, J. M. and Koos, T. (2012), 'Gabaergic circuits mediate the reinforcement-related signals of striatal cholinergic interneurons', *Nature neuroscience* **15**(1), 123–130.

Farzampour, Z., Reimer, R. J. and Huguenard, J. (2015), 'Endozepines', *Advances in Pharmacology* **72**, 147–164.

Fisher, R. S., Boas, W. v. E., Blume, W., Elger, C., Genton, P., Lee, P. and Engel, J. (2005), 'Epileptic seizures and epilepsy: definitions proposed by the international league against epilepsy (ilae) and the international bureau for epilepsy (ibe)', *Epilepsia* **46**(4), 470–472.

Flemmer, A. W., Gimenez, I., Dowd, B. F. X., Darman, R. B. and Forbush, B. (2002), 'Activation of the na-k-cl cotransporter nkcc1 detected with a phospho-specific antibody', *The Journal of Biological Chemistry* **277**(40), 37551–37558.

Forman, C. J., Tomes, H., Mbobo, B., Burman, R. J., Jacobs, M., Baden, T. and Raimondo, J. V. (2017), 'Openspritzer: an open hardware pressure ejection system for reliably delivering picolitre volumes', *Scientific reports* **7**(1), 2188–2198.

Friedman, L. K., Pellegrini-Giampietro, D. E., Sperber, E. F., Bennett, M., Moshe, S. L. and Zukin, R. S. (1994), 'Kainate-induced status epilepticus alters glutamate and gabaa receptor gene expression in adult rat hippocampus: an in situ hybridization study', *Journal of Neuroscience* **14**(5), 2697–2707.

Fujiwara-Tsukamoto, Y., Isomura, Y., Imanishi, M., Ninomiya, T., Tsukada, M., Yanagawa, Y., Fukai, T. and Takada, M. (2010), 'Prototypic seizure activity driven by mature hippocampal fast-spiking interneurons', *Journal of Neuroscience* **30**(41), 13679–13689.

Ge, S., Goh, E. L. K., Sailor, K. A., Kitabatake, Y., Ming, G.-l. and Song, H. (2006), 'Gaba regulates synaptic integration of newly generated neurons in the adult brain', *Nature* **439**(7076), 589–593.

Glykys, J. and Staley, K. J. (2015), 'Diazepam effect during early neonatal development correlates with neuronal cl-', *Annals of Clinical and Translational Neurology* **2**(12), 1055–1070.

Goldberg, E. M. and Coulter, D. A. (2013), 'Mechanisms of epileptogenesis: a convergence on neural circuit dysfunction', *Nature reviews Neuroscience* **14**(5), 337–346.

Goodkin, H. P. and Kapur, J. (2009), 'The impact of diazepam's discovery on the treatment and understanding of status epilepticus', *Epilepsia* **50**(9), 2011–2018.

Goodkin, H. P., Yeh, J.-L. and Kapur, J. (2005), 'Status epilepticus increases the intracellular accumulation of gabaa receptors', *The Journal of Neuroscience* **25**(23), 5511–5520.

Govorunova, E. G., Sineshchekov, O. A., Janz, R., Liu, X. and Spudich, J. L. (2015), 'Neuroscience. natural light-gated anion channels: A family of microbial rhodopsins for advanced optogenetics', *Science* **349**(6248), 647–650.

Griffiths, T., Evans, M. C. and Meldrum, B. S. (1983), 'Intracellular calcium accumulation in rat hippocampus during seizures induced by bicuculline or l-allylglycine', *Neuroscience* **10**(2), 385–395.

Grimley, J. S., Li, L., Wang, W., Wen, L., Beese, L. S., Hellinga, H. W. and Augustine, G. J. (2013), 'Visualization of synaptic inhibition with an optogenetic sensor developed by cell-free protein engineering automation', *The Journal of Neuroscience* **33**(41), 16297–16309.

Hablitz, J. J. (1984), 'Picrotoxin-induced epileptiform activity in hippocampus: role of endogenous versus synaptic factors', *Journal of Neurophysiology* **51**(5), 1011–1027.

Haefely, W. E., Martin, J. R., Richards, J. G. and Schoch, P. (1993), 'The multiplicity of actions of benzodiazepine receptor ligands', *Canadian Journal of Psychiatry* **38**(4), 102–108.

Haefely, W., Kulcsár, A. and Möhler, H. (1975), 'Possible involvement of gaba in the central actions of benzodiazepines', *Psychopharmacology Bulletin* **11**(4), 58–59.

Huberfeld, G., Wittner, L., Clemenceau, S., Baulac, M., Kaila, K., Miles, R. and Rivera, C. (2007), 'Perturbed chloride homeostasis and gabaergic signaling in human temporal lobe epilepsy', *Journal of Neuroscience* **27**(37), 9866–9873.

Hübner, C. A., Stein, V., Hermans-Borgmeyer, I., Meyer, T., Ballanyi, K. and Jentsch, T. J. (2001), 'Disruption of kcc2 reveals an essential role of k-cl cotransport already in early synaptic inhibition', *Neuron* **30**(2), 515–524.

Ilie, A., Raimondo, J. V. and Akerman, C. J. (2012), 'Adenosine release during seizures attenuates gabaa receptor-mediated depolarization', *J Neurosci* **32**(15), 5321–5332.

Jefferys, J. and Haas, H. (1982), 'Synchronized bursting of ca1 hippocampal pyramidal cells in the absence of synaptic transmission', *Nature* **300**(5891), 448–450.

Jensen, M. S. and Yaari, Y. (1988), 'The relationship between interictal and ictal paroxysms in an in vitro model of focal hippocampal epilepsy', *Annals of Neurology* **24**(5), 591–598.

Jenssen, S., Gracely, E. J. and Sperling, M. R. (2006), 'How long do most seizures last? a systematic comparison of seizures recorded in the epilepsy monitoring unit', *Epilepsia* **47**(9), 1499–1503.

Johnston, D. and Wu, S. M.-S. (1995), *Foundations of Cellular Neurophysiology*, 1 edn, MIT press.

Kaila, K. (1994), 'Ionic basis of gaba a receptor channel function in the nervous system', *Progress in Neurobiology* **42**(4), 489–537.

Kaila, K., Lamsa, K., Smirnov, S., Taira, T. and Voipio, J. (1997), 'Long-lasting gaba-mediated depolarization evoked by high-frequency stimulation in pyramidal neurons of rat hippocampal slice is attributable to a network-driven, bicarbonate-dependent k+ transient', *Journal of Neuroscience* **17**(20), 7662–7672.

Kaila, K., Pasternack, M., Saarikoski, J. and Voipio, J. (1989), 'Influence of gaba-gated bicarbonate conductance on potential, current and intracellular chloride in crayfish muscle fibres', *The Journal of Physiology* **416**, 161–181.

Kaila, K., Price, T. J., Payne, J. A., Puskarjov, M. and Voipio, J. (2014), 'Cation-chloride cotransporters in neuronal development, plasticity and disease', *Nature Reviews Neuroscience* **15**(10), 637–644.

Kaila, K. and Voipio, J. (1987), 'Postsynaptic fall in intracellular ph induced by gaba-activated bicarbonate conductance', *Nature* **330**(6144-6149), 163–165.

Kamphuis, W., Huisman, E., Veerman, M. and da Silva, F. L. (1991), 'Development of changes in endogenous gaba release during kindling epileptogenesis in rat hippocampus', *Brain Research* **545**(1), 33–40.

Kapur, J. and Coulter, D. A. (1995), 'Experimental status epilepticus alters gamma-aminobutyric acid type a receptor function in ca1 pyramidal neurons', *Annals of Neurology* **38**(6), 893–900.

Kelley, M. R., Deeb, T. Z., Brandon, N. J., Dunlop, J., Davies, P. A. and Moss, S. J. (2016), 'Compromising kcc2 transporter activity enhances the development of continuous seizure activity', *Neuropharmacology* **108**, 103–110.

Khoshkhoo, S., Vogt, D. and Sohal, V. S. (2017), 'Dynamic, cell-type-specific roles for gabaergic interneurons in a mouse model of optogenetically inducible seizures', *Neuron* **93**(2), 291–298.

Klausberger, T. and Somogyi, P. (2008), 'Neuronal diversity and temporal dynamics: the unity of hippocampal circuit operations', *Science* **321**(5885), 53–57.

Kovalchuk, Y. and Garaschuk, O. (2012), 'Two-photon chloride imaging using mqae in vitro and in vivo', *Cold Spring Harbor Protocols* **2012**(7), 778–785.

Krimer, L. S. and Goldman-Rakic, P. S. (1997), 'An interface holding chamber for anatomical and physiological studies of living brain slices', *Journal of Neuroscience Methods* **75**(1), 55–58.

Krnjević, K. (1974), 'Chemical nature of synaptic transmission in vertebrates', *Physiological Reviews* **54**(2), 418–540.

Krogsgaard-Larsen, P., Frølund, B., Jørgensen, F. S. and Schousboe, A. (1994), 'Gabaa receptor agonists, partial agonists, and antagonists. design and therapeutic prospects', *Journal of Medicinal Chemistry* **37**(16), 2489–2505.

Kumar, S. S. and Buckmaster, P. S. (2006), 'Hyperexcitability, interneurons, and loss of gabaergic synapses in entorhinal cortex in a model of temporal lobe epilepsy', *Journal of Neuroscience* **26**(17), 4613–4623.

Kyrozis, A. and Reichling, D. B. (1995), 'Perforated-patch recording with gramicidin avoids artifactual changes in intracellular chloride concentration', *Journal of Neuroscience Methods* **57**(1), 27–35.

Lado, F. A. and Moshé, S. L. (2008), 'How do seizures stop?', *Epilepsia* **49**(10), 1651–1664.

Ledri, M., Madsen, M. G., Nikitidou, L., Kirik, D. and Kokaia, M. (2014), 'Global optogenetic activation of inhibitory interneurons during epileptiform activity', *The Journal of Neuroscience* **34**(9), 3364–3377.

Lee, H. H., Jurd, R. and Moss, S. J. (2010), 'Tyrosine phosphorylation regulates the membrane trafficking of the potassium chloride co-transporter kcc2', *Molecular and Cellular Neuroscience* **45**(2), 173–179.

Li, L., Chen, S.-R., Chen, H., Wen, L., Hittelman, W. N., Xie, J.-D. and Pan, H.-L. (2016), 'Chloride homeostasis critically regulates synaptic nmda receptor activity in neuropathic pain', *Cell reports* **15**(7), 1376–1383.

Lutz, B. (2004), 'On-demand activation of the endocannabinoid system in the control of neuronal excitability and epileptiform seizures', *Biochemical Pharmacology* **68**(9), 1691–1698.

Mahadevan, V. and Woodin, M. A. (2016), 'Regulation of neuronal chloride homeostasis by neuromodulators', *The Journal of Physiology* **594**(10), 2593–2605.

Markram, H., Toledo-Rodriguez, M., Wang, Y., Gupta, A., Silberberg, G. and Wu, C. (2004), 'Interneurons of the neocortical inhibitory system', *Nature Reviews Neuroscience* **5**(10), 793–807.

Mckinney, R. A., Debanne, D., Gähwiler, B. H. and Thompson, S. M. (1997), 'Lesion-induced axonal sprouting and hyperexcitability in the hippocampus in vitro: implications for the genesis of posttraumatic epilepsy', *Nature Medicine* **3**(9), 990–996.

Melzer, S., Michael, M., Caputi, A., Eliava, M., Fuchs, E. C., Whittington, M. A. and Monyer, H. (2012), 'Long-range–projecting gabaergic neurons modulate inhibition in hippocampus and entorhinal cortex', *Science* **335**(6075), 1506–1510.

Mody, I., Lambert, J. and Heinemann, U. (1987), 'Low extracellular magnesium induces epileptiform activity and spreading depression in rat hippocampal slices', *Journal of Neurophysiology* **57**(3), 869–888.

Morimoto, K., Fahnestock, M. and Racine, R. J. (2004), 'Kindling and status epilepticus models of epilepsy: rewiring the brain', *Progress in Neurobiology* **73**(1), 1–6.

Müller, W. and Wollert, U. (1973), 'Characterization of the binding of benzodiazepines to human serum albumin', *Archives of Pharmacology* **280**(3), 229–237.

Nabekura, J., Ueno, T., Okabe, A., Furuta, A., Iwaki, T., Shimizu-Okabe, C., Fukuda, A. and Akaike, N. (2002), 'Reduction of kcc2 expression and gabaareceptor-mediated excitation after in vivo axonal injury', *Journal of Neuroscience* **22**(11), 4412–4417.

Naylor, D. E., Liu, H. and Wasterlain, C. G. (2005), 'Trafficking of gabaa receptors, loss of inhibition, and a mechanism for pharmacoresistance in status epilepticus', *Journal of Neuroscience* **25**(34), 7724–7733.

Newton, C. R. and Garcia, H. H. (2012), 'Epilepsy in poor regions of the world', *The Lancet* **380**(9848), 1193–1201.

Ngugi, A. K., Kariuki, S., Bottomley, C., Kleinschmidt, I., Sander, J. and Newton, C. (2011), 'Incidence of epilepsy a systematic review and meta-analysis', *Neurology* **77**(10), 1005–1012.

Olsen, R. W. and Sieghart, W. (2009), 'Gaba a receptors: subtypes provide diversity of function and pharmacology', *Neuropharmacology* **56**(1), 141–148.

Pal, S., Sombati, S., Limbrick, D. D. and DeLorenzo, R. J. (1999), 'In vitro status epilepticus causes sustained elevation of intracellular calcium levels in hippocampal neurons', *Brain Research* **851**(1), 20–31.

Pathak, H. R., Weissinger, F., Terunuma, M., Carlson, G. C., Hsu, F.-C., Moss, S. J. and Coulter, D. A. (2007), 'Disrupted dentate granule cell chloride regulation enhances synaptic excitability during development of temporal lobe epilepsy', *Journal of Neuroscience* **27**(51), 14012–14022.

Pitkänen, A., Schwartzkroin, P. A. and Moshé, S. L. (2017), *Models of seizures and epilepsy*, 2nd edn, Academic Press.

Pond, B. B., Berglund, K., Kuner, T., Feng, G., Augustine, G. J. and Schwartz-Bloom, R. D. (2006), 'The chloride transporter na+-k+-cl- cotransporter isoform-1 contributes to intracellular chloride increases after in vitro ischemia', *Journal of Neuroscience* **26**(5), 1396–1406.

Raimondo, J. V., Burman, R. J., Katz, A. A. and Akerman, C. J. (2015), 'Ion dynamics during seizures', *Frontiers in Cellular Neuroscience* **9**(21), 419–433.

Raimondo, J. V., Irkle, A., Wefelmeyer, W., Newey, S. E. and Akerman, C. J. (2012), 'Genetically encoded proton sensors reveal activity-dependent ph changes in neurons', *Frontiers in Molecular Neuroscience* **5-17**.

Raimondo, J. V., Joyce, B., Kay, L., Schlagheck, T., Newey, S. E., Srinivas, S. and Akerman, C. J. (2013), 'A genetically-encoded chloride and ph sensor for dissociating ion dynamics in the nervous system', *Frontiers in Cellular Neuroscience* **202-209**.

Raimondo, J. V., Kay, L., Ellender, T. J. and Akerman, C. J. (2012), 'Optogenetic silencing strategies differ in their effects on inhibitory synaptic transmission', *Nature Neuroscience* **15**(8), 1102–1104.

Raimondo, J. V., Richards, B. A. and Woodin, M. A. (2017), 'Neuronal chloride and excitability - the big impact of small changes', *Current Opinion in Neurobiology* **43**, 35–42.

Rice, A., Rafiq, A., Shapiro, S. M., Jakoi, E. R., Coulter, D. A. and DeLorenzo, R. J. (1996), 'Long-lasting reduction of inhibitory function and gamma-aminobutyric acid type a receptor subunit mrna expression in a model of temporal lobe epilepsy', *Proceedings of the National Academy of Sciences* **93**(18), 9665–9669.

Rivera, C., Voipio, J., Payne, J. A., Ruusuvuori, E. et al. (1999), 'The k+/cl-co-transporter kcc2 renders gaba hyperpolarizing during neuronal maturation', *Nature* **397**(6716), 251–256.

Rivera, C., Voipio, J., Thomas-Crusells, J., Li, H., Emri, Z., Sipilä, S., Payne, J. A., Minichiello, L., Saarma, M. and Kaila, K. (2004), 'Mechanism of activity-dependent downregulation of the neuron-specific k-cl cotransporter kcc2', *Journal of Neuroscience* **24**(19), 4683–4691.

Royo, N. C., Vandenberghe, L. H., Ma, J.-Y., Hauspurg, A., Yu, L., Maronski, M., Johnston, J., Dichter, M. A., Wilson, J. M. and Watson, D. J. (2008), 'Specific aav serotypes stably transduce primary hippocampal and cortical cultures with high efficiency and low toxicity', *Brain Research* **1190**, 15–22.

Salomon, J. A., Vos, T., Hogan, D. R., Gagnon, M., Naghavi, M., Mokdad, A., Begum, N., Shah, R., Karyana, M., Kosen, S. et al. (2012), 'Common values in assessing health outcomes from disease and injury: disability weights measurement study for the global burden of disease study 2010', *The Lancet* **380**(9859), 2129–2143.

Sato, S. S., Artoni, P., Landi, S., Cozzolino, O., Parra, R., Pracucci, E., Trovato, F., Szczurkowska, J., Luin, S., Arosio, D. et al. (2017), 'Simultaneous two-photon imaging of intracellular chloride concentration and ph in mouse pyramidal neurons in vivo', *Proceedings of the National Academy of Sciences* **114**(41), 8770–8779.

Schevon, C. A., Weiss, S. A., McKhann Jr, G., Goodman, R. R., Yuste, R., Emerson, R. G. and Trevelyan, A. J. (2012), 'Evidence of an inhibitory restraint of seizure activity in humans', *Nature Communications* **3**(1), 1060–1070.

Schwartzkroin, P. A. (1994), 'Role of the hippocampus in epilepsy', *Hippocampus* **4**(3), 239–242.

Shepherd, G. M. (2003), *The synaptic organization of the brain*, 5 edn, Oxford University Press.

Shinnar, S., Berg, A. T., Moshe, S. L. and Shinnar, R. (2001), 'How long do new-onset seizures in children last?', *Annals of Neurology* **49**(5), 659–664.

Simoni, A., Griesinger, C. B. and Edwards, F. A. (2003), 'Development of rat ca1 neurones in acute versus organotypic slices: role of experience in synaptic morphology and activity', *The Journal of Physiology* **550**(1), 135–147.

Sivakumaran, S. and Maguire, J. (2016), 'Bumetanide reduces seizure progression and the development of pharmacoresistant status epilepticus', *Epilepsia* **57**(2), 222–232.

Staley, K. J., Longacher, M., Bains, J. S. and Yee, A. (1998), 'Presynaptic modulation of ca3 network activity.', *Nature Neuroscience* **1**(3), 201–209.

Staley, K. J. and Mody, I. (1992), 'Shunting of excitatory input to dentate gyrus granule cells by a depolarizing gabaa receptor-mediated postsynaptic conductance', *Journal of Neurophysiology* **68**(1), 197–212.

Staley, K. J. and Proctor, W. R. (1999), 'Modulation of mammalian dendritic gabaa receptor function by the kinetics of cl- and hco3- transport', *The Journal of Physiology* **519**(3), 693–712.

Staley, K. J., Soldo, B. L., Proctor, W. R. et al. (1995), 'Ionic mechanisms of neuronal excitation by inhibitory gabaa receptors', *Science* **269**(5226), 977–981.

Stoppini, L., Buchs, P.-A. and Muller, D. (1991), 'A simple method for organotypic cultures of nervous tissue', *Journal of Neuroscience Methods* **37**(2), 173–182.

Streit, P., Thompson, S. M. and Gähwiler, B. H. (1989), 'Anatomical and physiological properties of gabaergic neurotransmission in organotypic slice cultures of rat hippocampus', *European Journal of Neuroscience* **1**(6), 603–615.

Takigawa, T. and Alzheimer, C. (2002), 'Phasic and tonic attenuation of epsps by inward rectifier k+ channels in rat hippocampal pyramidal cells', *The Journal of Physiology* **539**(1), 67–75.

Tang, X., Kim, J., Zhou, L., Wengert, E., Zhang, L., Wu, Z., Carromeu, C., Muotri, A. R., Marchetto, M. C., Gage, F. H. et al. (2016), 'Kcc2 rescues functional deficits in human neurons derived from patients with rett syndrome', *Proceedings of the National Academy of Sciences* **113**(3), 751–756.

Taniguchi, H., He, M., Wu, P., Kim, S., Paik, R., Sugino, K., Kvitsani, D., Fu, Y., Lu, J., Lin, Y. et al. (2011), 'A resource of cre driver lines for genetic targeting of gabaergic neurons in cerebral cortex', *Neuron* **71**(6), 995–1013.

Tao, R., Li, C., Newburn, E. N., Ye, T., Lipska, B. K., Herman, M. M., Weinberger, D. R., Kleinman, J. E. and Hyde, T. M. (2012), 'Transcript-specific associations of slc12a5 (kcc2) in human prefrontal cortex with development, schizophrenia, and affective disorders', *Journal of Neuroscience* **32**(15), 5216–5222.

Trevelyan, A. J., Sussillo, D., Watson, B. O. and Yuste, R. (2006), 'Modular propagation of epileptiform activity: evidence for an inhibitory veto in neocortex', *Journal of Neuroscience* **26**(48), 12447–12455.

Trevelyan, A. J., Sussillo, D. and Yuste, R. (2007), 'Feedforward inhibition contributes to the control of epileptiform propagation speed', *Journal of Neuroscience* **27**(13), 3383–3387.

Trinka, E., Cock, H., Hesdorffer, D., Rossetti, A. O., Scheffer, I. E., Shinnar, S., Shorvon, S. and Lowenstein, D. H. (2015), 'A definition and classification of status epilepticus–report of the ilae task force on classification of status epilepticus', *Epilepsia* **56**(10), 1515–1523.

Trinka, E., Höfler, J., Leitinger, M., Rohracher, A., Kalss, G. and Brigo, F. (2016), 'Pharmacologic treatment of status epilepticus', *Expert Opinion on Pharmacotherapy* **17**(4), 513–534.

Tyzio, R., Holmes, G. L., Ben-Ari, Y. and Khazipov, R. (2007), 'Timing of the developmental switch in gabaa mediated signaling from excitation to inhibition in ca3 rat hippocampus using gramicidin perforated patch and extracellular recordings', *Epilepsia* **48**(5), 96–105.

Tyzio, R., Minlebaev, M., Rheims, S., Ivanov, A., Jorquera, I., Holmes, G. L., Zilberter, Y., Ben-Ari, Y. and Khazipov, R. (2008), 'Postnatal changes in somatic γ-aminobutyric acid signalling in the rat hippocampus', *European Journal of Neuroscience* **27**(10), 2515–2528.

Urbaniak, G. and Plous, S. (2013), 'Research randomizer'.
URL: *http://www.randomizer.org/*

van Rheede, J. J., Richards, B. A. and Akerman, C. J. (2015), 'Sensory-evoked spiking behavior emerges via an experience-dependent plasticity mechanism', *Neuron* **87**(5), 1050–1062.

Viitanen, T., Ruusuvuori, E., Kaila, K. and Voipio, J. (2010), 'The k+–cl- cotransporter kcc2 promotes gabaergic excitation in the mature rat hippocampus', *The Journal of Physiology* **588**(9), 1527–1540.

Wallace, M. J., Blair, R. E., Falenski, K. W., Martin, B. R. and DeLorenzo, R. J. (2003), 'The endogenous cannabinoid system regulates seizure frequency and duration in a model of temporal lobe epilepsy', *Journal of Pharmacology and Experimental Therapeutics* **307**(1), 129–137.

Wang, D. D. and Kriegstein, A. R. (2008), 'Gaba regulates excitatory synapse formation in the neocortex via nmda receptor activation', *J Neurosci* **28**(21), 5547–58.

Wieland, H. A., Lüddens, H. and Seeburg, P. H. (1992), 'A single histidine in gabaa receptors is essential for benzodiazepine agonist binding', *The Journal of Biological Chemistry* **267**(3), 1426–1429.

Wilmshurst, J. M., Kakooza-Mwesige, A. and Newton, C. R. (2014), 'The challenges of managing children with epilepsy in africa', *Seminars in Pediatric Neurology* **21**(1), 36–41.

Wilson, C. L., Maidment, N. T., Shomer, M. H., Behnke, E. J., Ackerson, L., Fried, I. and Engel, J. (1996), 'Comparison of seizure related amino acid release in human epileptic hippocampus versus a chronic, kainate rat model of hippocampal epilepsy', *Epilepsy research* **26**(1), 245–254.

Wright, R., Raimondo, J. and Akerman, C. (2011), 'Spatial and temporal dynamics in the ionic driving force for gabaa receptors', *Neural plasticity* **2011**(1), 1–10.

Yaari, Y., Konnerth, A. and Heinemann, U. (1983), 'Spontaneous epileptiform activity of ca1 hippocampal neurons in low extracellular calcium solutions', *Experimental Brain Research* **51**(1), 153–156.

Zhang, C. L., Dreier, J. P. and Heinemann, U. (1995), 'Paroxysmal epileptiform discharges in temporal lobe slices after prolonged exposure to low magnesium are resistant to clinically used anticonvulsants', *Epilepsy Research* **20**(2), 105–11.

Appendix A

Appendix

A.1 Protocols for treating paediatric status epilepticus

Included here are the management protocols used by Medical Emergency Unit at Red Cross War Memorial Children's Hospital for the treatment of paediatric status epilepticus (SE). Patients recruited into the above-mentioned clinical study are randomly allocated to one of the two protocols.

Both protocols use repeated doses of benzodiazepines as first-line management. Thereafter, in one protocol a patient will then receive repeated doses of phenobarbitone. This is the preferred clinical practice, however, the use of phenobarbitone for paediatric SE is not recognised by the Medicines Control Council (MCC) of South Africa. By contrast, if allocated to the other protocol, after not responding to the benzodiazepines the patient will receive phenytoin followed by a midazolam infusion. This is the current recognised practice for managing paediatric SE in South Africa.

PATIENT RECRUITMENT FORM

PHENOBARBITONE

Project: Childhood Convulsive Status Epilepticus – in search of optimal drug treatment

UCT HREC #: 297/2005

In managing this patient's status epilepticus, please strictly follow treatment protocol illustrated below and complete the required form that follows.

AIRWAY; OXYGEN; CHECK GLUCOSE; MONITOR BP, HR & SATS

↓

IV / IO ACCESS

YES | NO

STEP I
**IV Lorazepam preferred intervention*

YES: LORAZEPAM 0.1mg/kg IV *or* MIDAZOLAM 0.25mg/kg IV *or* DIAZEPAM 0.25mg/kg IV

NO: LORAZEPAM 0.1mg/kg IMI *or* MIDAZOLAM 0.2mg/kg IMI *or* DIAZEPAM 0.5mg/kg PR

↓ *Still convulsing after 5 - 10 minutes*

STEP II

LORAZEPAM 0.1mg/kg IV *or* MIDAZOLAM 0.25mg/kg IV *or* DIAZEPAM 0.25mg/kg IV

LORAZEPAM 0.1mg/kg IMI *or* MIDAZOLAM 0.2mg/kg IMI *or* DIAZEPAM 0.5mg/kg PR

Still convulsing after 5 - 10 minutes — ** insert IV / IO line*

↓

STEP III

PHENOBARBITONE 20mg/kg IV
(flush line afterwards)

↓ *Still convulsing after 5 - 10 minutes*

STEP IV

PHENOBARBITONE 10mg/kg IV
(flush line afterwards)

↓ *Still convulsing after 5 - 10 minutes*

STEP V

PHENOBARBITONE 10mg/kg IV
(flush line afterwards)

↓ *Still convulsing after 5 - 10 minutes*

STEP VI

Discuss management with senior / ICU
Recheck glucose & consider antibiotics
Additional work-up and management of underlying cause / complications as per standard practice for the individual child

If patient has a high fever:
Sponge child with room temperature water
Do not give oral medication until the convulsion has been controlled

Directions for administering rectal Diazepam
Draw up dose into 1ml syringe and remove the needle
Place child in the recovery position
Insert the syringe 4 - 5cm into the rectum and inject the solution
Hold buttocks together for a few minutes

Please stick patient sticker here

PATIENT RECRUITMENT FORM PHENYTOIN & MIDAZOLAM

Project: Childhood Convulsive Status Epilepticus – in search of optimal drug treatment

UCT HREC #: 297/2005

In managing this patient's status epilepticus, please strictly follow treatment protocol illustrated below and complete the required form that follows.

AIRWAY; OXYGEN; CHECK GLUCOSE; MONITOR BP, HR & SATS

↓

IV / IO ACCESS

YES | NO

STEP I
**IV Lorazepam preferred intervention*

YES: LORAZEPAM 0.1mg/kg IV *or* MIDAZOLAM 0.25mg/kg IV *or* DIAZEPAM 0.25mg/kg IV

NO: LORAZEPAM 0.1mg/kg IMI *or* MIDAZOLAM 0.2mg/kg IMI *or* DIAZEPAM 0.5mg/kg PR

↓ *Still convulsing after 5 - 10 minutes* ↓

STEP II

LORAZEPAM 0.1mg/kg IV *or* MIDAZOLAM 0.25mg/kg IV *or* DIAZEPAM 0.25mg/kg IV

LORAZEPAM 0.1mg/kg IMI *or* MIDAZOLAM 0.2mg/kg IMI *or* DIAZEPAM 0.5mg/kg PR

Still convulsing after 5 - 10 minutes — ** insert IV / IO line*

↓

STEP III

PHENYTOIN
20mg/kg IV slowly over 30min
(Mix in 50 ml NORMAL SALINE only)
ECG monitoring

↓ *Still convulsing after 5 - 10 minutes*

STEP IV

MIDAZOLAM
0.2 mg/kg IV load followed by infusion 3 mg/kg into 50ml 5% DW at 1 - 4 ml/hour (= 1 - 4 mcg/kg/min)
(start at 1 ml/hr, increment 15 min intervals of 1 ml/hr. Max 8 ml/hr (= 8 mcg/kg/min)

↓ *Still convulsing after 5 - 10 minutes*

STEP V

Discuss management with senior / ICU
Recheck glucose & consider antibiotics
Additional work-up and management of underlying cause / complications as per standard practice for the individual child

If patient has a high fever:
Sponge child with room temperature water
Do not give oral medication until the convulsion has been controlled

Directions for administering rectal Diazepam
Draw up dose into 1ml syringe and remove the needle
Place child in the recovery position
Insert the syringe 4 - 5cm into the rectum and inject the solution
Hold buttocks together for a few minutes

Please stick patient sticker here